UNIVERSITÀ DELLA CALABRIA

**UNIVERSITA' DELLA CALABRIA**

Dipartimento di Ingegneria Informatica, Modellistica, Elettronica e Sistemistica

## Scuola di Dottorato Life Sciences

**Indirizzo Ambiente, salute e processi eco-sostenibili**

**CICLO XXVIII**

# DESIGN AND DEVELOPMENT OF MEMBRANES FOR $CO_2/CH_4$ SEPARATION

**Settore Scientifico Disciplinare ING-IND/24**

**Direttore:** Ch.mo Prof. Marcello Canonaco

Firma _____

**Supervisore**: Ch.mo Prof. Stefano Curcio

Firma _____

**Supervisore**: Dott. Johannes Carolus Jansen

Firma _____

**Dottoranda**: Dott./ssa Elisa Esposito

Firma _____

Ai miei genitori

# Index

# List of Figures

# List of Tables

# Symbols and abbreviations

| Symbol | Quantity | Common units |
|---|---|---|
| $R$ | Universal gas costant | J / mol × K |
| $T$ | Temperature | K |
| $d$ | Diameter of molecule | m |
| $r_p$ | Pore radius | m |
| $J$ | Permeate flux | L/h $m^2$ |
| $C_1$ | Concentration at feed side | mol/L |
| $C_2$ | Concentration at permeate side | mol/L |
| $D$ | Diffusion coefficient | $cm^2$/sec |
| $S$ | Solubility coefficient | $cm^3/cm^3$ bar |
| $\ell$ | Membrane thickness | cm |
| $K_d$ | Henry's costant | mol/atm·L |
| $f$ | Gas fugacity | bar |
| $C_H$ | Gas concentration in microvoids | mol/L |
| $MW$ | Molecular weight | g/mol |
| $K_d$ | Kinetic diameter | Å |
| $P_{eff}$ | Effective permeability | Barrer |
| $P_d$ | Permeability of discontinuous phase | Barrer |
| $P_c$ | Permeability of continuous phase | Barrer |
| $P_{MMM}$ | Effective permeability of the mixed matrix membrane | Barrer |
| G' | G prime | Pa |
| G'' | G double prime | Pa |
| $Jw$ | Water flux | L/h $m^2$ |
| $V_p$ | Permeate volume | $cm^3$ |
| $t$ | time | sec |
| $A$ | Membrane areae | $cm^2$ |
| $P_w$ | Water permeance | L/h $m^2$ bar |
| $Q_p$ | Permeate flow rate | $cm^3$/sec |
| $Pe$ | Permeance | $m^3/m^2$ h bar |

| | | |
|---|---|---|
| $P$ | Permeability | $m^3$ m/$m^2$ h ba |
| $a$ | Activity | - |
| $p$ | Pressure | bar |
| $p_0$ | Saturated vapour pressure | bar |
| $p_t$ | Permeate pressure | bar |
| $p_f$ | Feed pressure | bar |
| $L_{eff}$ | Effective thickness | µm |
| $C_{gas}$ | Gas concentration | mol/$dm^3$ |
| $z$ | Vertical position in the solvent | m |
| $H_{gas}$ | Henry's costant in the solvent | bar |

**Greek**

| **symbol** | **Quantity** | **Common units** |
|---|---|---|
| $\alpha$ | Selectivity | - |
| $\lambda$ | Knudsen Flux | L/h $m^2$ |
| $\Theta$ | Time lag | s |
| $\Delta p$ | Pressure difference | bar |
| $\Phi$ | Volume fraction | - |
| tan(δ) | Loss angle | - |
| $\eta$ | Viscosity | cP |
| $\pi$ | Gas vapour permeance | $m^3$/$m^2$ h bar |
| $\rho$ | Density | g/$cm^3$ |

| **Abbreviation** | **Full name** |
|---|---|
| PAN | Polyacrilonitrile |
| PVP | Polyvinylpyrrolidone |
| DMF | Dimethylformamide |
| PEO | Polythyleneoxide |
| EtOH | Ethanol |
| EO | Ethylenoxide |
| PEI | Polyetherimide |
| PDMS | Polydimethylsiloxane |
| PTMSP | Poly(1-trimethylsilyl propyne) |

| | |
|---|---|
| PMP | Poly(4-methyl-2-pentyne) |
| Pfs | Polysulfone |
| PPO | Polyphenyleneoxide |
| SLMs | Supported liquid membranes |
| FCMs | Fixed carrier membranes |
| MCMs | Mobile carrier membranes |
| MMMs | Mixed Matrix membranes |
| CMS | Carbon molecular sieves |
| CNTs | Carbon nanotubes |
| COFs | Covalent organic framework |
| MOFs | Metal-organic frameworks |
| SEM | Scanning electron microscopy |
| FTIR | Infrared spectroscopy |
| ANN | Artificial Neural Network |
| MLP | Multilayer perception |
| [EMIM][$BF_4$] | 1-Ethyl-3-Methylimidazolium Tetrafluoroborate |
| [EMIM][$NTf_2$] | 1-ethyl-3-methylimidazolium bis(trifluoromethylsulfonyl)imide) |
| [EMIM][dca] | 1-ethyl-3-methylimidazolium dicyanimide |
| [BMIM][$PF_6$] | 1-Butyl-3-methylimidazolium hexafluorophosphate |
| [BMIM][$NTf_2$] | 1-Butyl-3-methylimidazolium bis(trifluoromethanesulfonyl)imide |
| [BMIM][OTf] | 1-Butyl-3-methylimidazolium trifluoromethansulfonate |
| CA | Carbonic anhydrase enzyme |
| FV | Feed volume |
| AC | Absorption compartment |
| PIM-1 | Polymer of intrinsic microporosity 1, a polymer of 5,5,6,6-tetrahydroxy-3,3,3,3-tetramethyl-1,1-spirobisindane and tetrafluoroterephtalonitrile |
| ZIF-8 | zeolitic imidazolate framework |
| ED-MIL-101 | Ethylene diamine Cr-terephthalate based metal–organic frameworks |
| UiO-66 | Zr-terephthalate based metal–organic frameworks |
| UiO-66-$(COOH)_2$ | Oxalic acid Zr-terephthalate based metal–organic frameworks |
| UiO-66-$(NH_2)$ | Amino Zr-terephthalate based metal–organic frameworks |

# Abstract

The objective of this work is to compare different membrane materials and different operation modes for the separation of $CO_2$ from $CH_4$. In this context, the working principles in terms of gas transport properties will be evaluated for three different systems. The discussion concerns: (1) poly(ether-*b*-amide) (PEBAX®1657)/polyacrylonitrile (PAN) composite hollow fibre membranes, (2) $CO_2$-selective facilitated transport membranes, and (3) mixed matrix membranes based on Polymers of Intrinsic Microporosity (PIMs).

The Pebax/PAN hollow fibre membranes were prepared by a new continuous coating method based on cross flow-filtration of a PEBAX solution. This allows simultaneous internal coating of a large number of the porous hollow fibres with a thin selective dense layer of PEBAX®, directly inside the module. The membrane preparation was optimized by modulating different parameters, such as coating time, polymer concentration and viscosity. The second approach discusses the potential use of ionic liquids as a vehicle for facilitated $CO_2$ transport in membrane contactors for $CO_2/CH_4$ separation. The increase of the $CO_2$ absorption in the ionic liquid [BMIM][OTf] by the use of the enzyme Carbonic Anhydrase (CA) was evaluated. The third approach analyzes the effect of Metal Organic Frameworks (MOFs) on the performance PIM-1 based mixed matrix membranes, provided by the School of Chemistry, University of Manchester (UK). Single gas permeation measurements were carried out to determine the gas separation performance of the membranes. In conclusion, the different types of membranes for $CO_2/CH_4$ separation will be compared, discussing the limitations and the advantages of all membranes and methods.

# Riassunto

L'obiettivo di questo lavoro è comparare differenti materiali e processi a membrana per la separazione di $CO_2$ dal metano. Le proprietà di trasporto dei gas e i principi di funzionamento dei processi di separazione per le differenti tipologie di membrane sono stati valutati. Tre differenti tipologie di membrane sono state studiate: membrane composite a fibre cave a base di poli(etere-b-ammide) (PEBAX®1657)/poliacrilonitrile (PAN), membrane con trasporto selettivo-facilitato per la $CO_2$, e membrane a matrice mista preparate disperdendo fillers con struttura metallo-organica (MOFs) in un polimero a elevata microporosità intrinseca (PIMs). Le membrane composite a fibra cava di Pebax/PAN sono state preparate con un nuovo metodo di

"coating" che si basa sulla permeazione in flusso trasversale di una soluzione di PEBAX attraverso supporti porosi in PAN. L'innovativo processo di ricoprimento permette la preparazione simultanea di un gran numero di membrane composite a fibra cava, direttamente quando i supporti porosi sono stati già alloggiati all'interno del modulo. Il processo di preparazione è stato ottimizzato cambiando diversi parametri, come il tempo di rivestimento, concentrazione del polimero e la viscosità. Il secondo approccio discute il potenziale uso di contattori a membrana per il trasporto facilitato di $CO_2$ in liquido ionico. Il trasporto della $CO_2$ sarà facilitato dalla presenza nel liquido ionico dell'enzima anidrasi carbonica. L'anidrasi carbonica catalizza la reazione di idratazione della $CO_2$, permettendo un trasporto facilitato della $CO_2$ in forma di ione bicarbonato. Nel terzo approccio è valutato l'effetto dell'aggiunta di fillers in membrane a base di PIM-1, sulle proprietà di trasporto della coppia di gas $CH_4$ e $CO_2$. Misure di permeazione per i gas puri sono state effettuate in modo da studiare le prestazioni di ogni tipologia di membrane nei processi di separazione $CO_2/CH_4$. Limiti e vantaggi per ogni tipologia di membrana e il loro potenziale utilizzo in processi di *upgrading* sono stati valutati.

# Preface

Nowadays energy systems play an important role in economic and social development and in the quality of the people's life. The energy demand is continuously increasing and the energy supply plays an important role in the world economy. The global environmental issues could significantly affect patterns of energy use around the world. Some new governmental policies have been adopted to encourage the introduction of energy efficiency measures, via technological changes and via the use of renewable and sustainable energy. In this context, waste biomass is one of the most promising alternative sources of energy. It is possible to obtain from biomass by anaerobic digestion a mixture of gases, commonly called biogas. Biogas is an example of a gaseous biofuel containing energy in the form of methane that can be exploited as hear or as fuel for vehicles, for other engines or for energy production.

Biogas typically contains saturated water vapour, 50-65% of methane, 30-40% of $CO_2$, traces of hydrogen sulphide, oxygen, nitrogen, ammonia, siloxanes and volatile organic compounds. The heating value of biogas is proportional to the methane concentration and for a higher efficiency, the removal of $CO_2$ and other impurities is required. Furthermore, these components can cause corrosion and freezing problems in pipes and connections. Cleaning and upgrading of biogas can be carried out either by conventional separation techniques, such as pressure swing adsorption, water scrubbing and absorption with organic solvents, or by innovative techniques, such as separation and purification of biomethane by membrane processes. The membrane process presents various advantages with respect to the traditional techniques, such as low energy consumption, ease of operation and low environmental impact. One of the most important aspects in the biogas treatment with membrane processes is the separation of $CH_4$ and $CO_2$, which are the gases present at the highest concentrations. Over the past decades, research groups and commercial companies active in gas separation processes by membranes have dedicated major attention to this field, aiming at a good outcome in this kind of separation. Different membranes have been designed and developed for the $CO_2/CH_4$ separation

The aim of the present thesis was to study and further develop different types of membranes for $CO_2/CH_4$ separation, and to compare the limitations and the advantages of all membranes and methods suitable for this use.

# Chapter 1. Biogas as an alternative and renewable energy source

## 1.1 Fossil Fuels

Today the energy supply in the world still depends for the about 90% on traditional sources and the use of renewable energy has not yet had a strong development (Figure 1.1). Carbon and petroleum are currently the main fuels used. In the world, 25% of electricity is produced in coal-fired plants. Instead, 35% of fossil fuel is represented by petroleum and the daily consumption is about 87 million barrels. The enormous fossil fuels consumption has various environmental consequences. In the last several years, carbon has been recognized a one of the most polluting energy sources, because during the extraction and combustion process, it emits a lot of $CO_2$, sulfur dioxide and in addition heavy metals. The impact of petroleum in this respect is slightly less, but assuming that the rate and type of energy consumption can remain constant, numerous studies claim that the petroleum will be exhausted in the next four decades and coal in about two centuries [1].

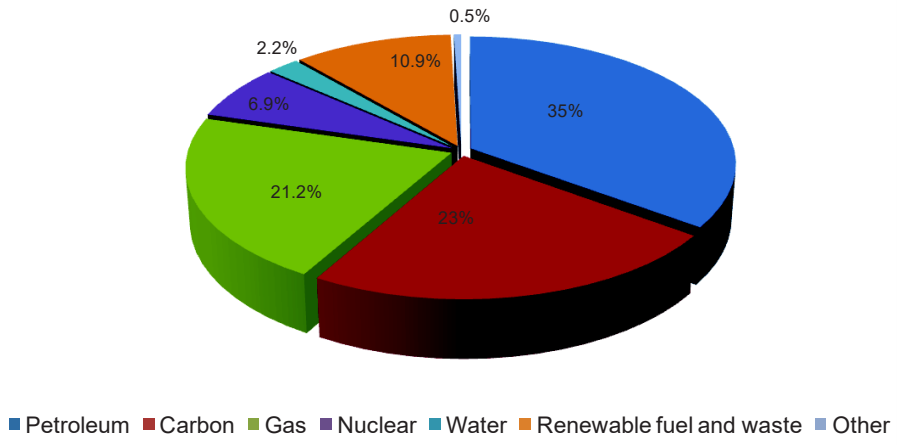


**Figure 1.1.** Energy Supply in the world [2]

Natural gas is the third important source of fossil energy, extracted from underground reservoirs. Depending on the location of its extraction, it can be composed of methane and variable amounts of nitrogen or carbon dioxide, as well as hydrogen sulphide, higher hydrocarbons and minor other contaminants. Methane has probably the lowest impact in terms of environmental

problems, because of the relatively easy separation of the main contaminants via conventional separation techniques, to yield relatively pure methane. An unexpected side effect of methane extraction, which is currently compromising its extraction in for instance the North of The Netherlands, is the occurrence of earthquakes due to the reduction of the pressure in the gas bubble, with significant effect on the surface above.
It is generally recognized that upon the combustion of fossil fuels the emission of toxic chemical substances, greenhouse gases like $CO_2$, and other air pollutants causes climate change and environmental pollution of air, land and water. This has a negative impact on the health and the living quality of humans, animals, plants and other living species on earth. From here derives the need for look to the development and expansion of new energy sources that are green and renewable.

## 1.2 Biogas as a renewable source of energy

Biogas is a renewable energy source, generally referred to as the gas produced from organic matter by anaerobic digestion. Biogas is indicated by the U.E as an energy source that can provide a gradual reduction of the current state of pollution and it is a viable answer to the growing global energy demand [3].

### 1.2.1 Environmental benefits

The use of biogas as source of energy decreases the dependency on the traditional fossil fuels carbon, petroleum and natural gas, and can offer a large range of environmental benefits. The main dangerous greenhouse gases are $CO_2$ and methane and in natural degradation of biomass, these are produced in an uncontrolled way. In the biogas generation process, the $CO_2$ production is natural and the methane production is controlled. In fact, the emission of $CO_2$ during the process of anaerobic digestion is lower than the amount of $CO_2$ absorbed by plants during photosynthesis because part of the biomass is converted into methane. On the contrary, the $CO_2$ emitted by the combustion of fossil fuels is ex-novo. Different studies [4–7], demonstrated that the biogas technology can be reduce the amount of greenhouse gas emission about 2.4 billion tons for year. Furthermore, the regulated anaerobic digestion, during the biogas production, can prevent the uncontrolled emissions of the methane released naturally during the decomposition of carcasses or organic material. In fact, methane is one of the most potent greenhouse gases and

it is therefore desirable to control its formation in an anaerobic digester rather than in open field composting, and to assure its subsequent conversion into $CO_2$ and water by controlled combustion with energy recovery.

**Figure 1.2.** Schematic representation of the sustainable cycle of anaerobic co-digestion of animal manure and organic wastes [8].

Another important aspect is that the use of organic materials as substrate for biogas production can be a promising solution to the organic garbage disposal. Moreover the organic solid materials digested during the biogas production, generally have a high content of nitrates which can be added to the soil as fertilizer. This allows the increase of the soil productivity, reducing the necessity to expand the croplands and helping the soil conservation. In addition, biogas production via anaerobic digestion can be carried out via relatively small-scale processes outside industrialized areas. Especially in such areas the use of biogas as a source of energy decreases the dependency on the traditional fuels like wood, avoiding the problem of deforestation and related problems. The preservation of the forest, promoting the natural $CO_2$ adsorption by the plants, decreases the concentration of this greenhouse gas into the atmosphere, thus mitigating the process of global warming.

### 1.2.2 Health and social benefits

The use of biogas technology presents numerous health and social benefits. The uncontrolled decomposition of the animal dung, livestock waste and urban waste, is the main cause of the

spread of contagious diseases, especially in developing countries. The diffusion of the bio-digesters and of a biogas policy reduces this risk directly and can furthermore prevent the pollution of the air and as a consequence improve the quality of the life. Moreover the construction of biogas installations, starting from their first design, construction and the exploitation and use of the entire production system promotes employment and job opportunities [9].

## 1.3 Biogas status in the European context

Recently, the world Energy council and the United Nations (UN) commission on sustainable development have reiterated the need for cheap, clean and renewable energy to intensify sustainable development [8]. Furthermore, the UN declared 2012 as the "international year of sustainable energy" with the purpose to provide universal access to modern energy by 2030. The indicative target of the UN, to achieve the climate and energy goals are: 20% reduction of greenhouse gas emission, 20% increase of energy efficiency, and 22.1% of the energy had to come from renewable sources. In this directive, the biogas produced from biomass offers new perspectives to realize these objectives. In Europe, the diffusion of anaerobic digestion started in the purification of sludge, and to day it is estimated that 1.600 digesters are operative [10]. The amount of biogas produced, the starting matter which is obtained and the end-use, vary significantly in the different EU countries (Figure 1.3).

Germany is the leader in the biogas sector with more than half of the European energy output. The position of Germany is followed by the United Kingdom, Italy, France, Austria, and Sweden. In the United Kingdom, the biogas production from municipal waste of landfills represents the most important source of energy from biomass, with 450 operating plants. Organic waste produced annually in the European Union amounted to approximately 1.2 billion tons, of which about 90% are animal manure and the rest from urban and industrial organic waste [11]. The energy potentially recoverable annually from organic waste to anaerobic digestion in the 15 EU countries is higher and around 209 million MWh. With the pass of time, the biogas sector is changing its primary objective from waste treatment to energy production and currently the proposal is the conversion into methane. For example, Sweden has established a market for biomethane as fuel for car transport, whereas Germany and Austria predominantly use their biogas for electricity production.

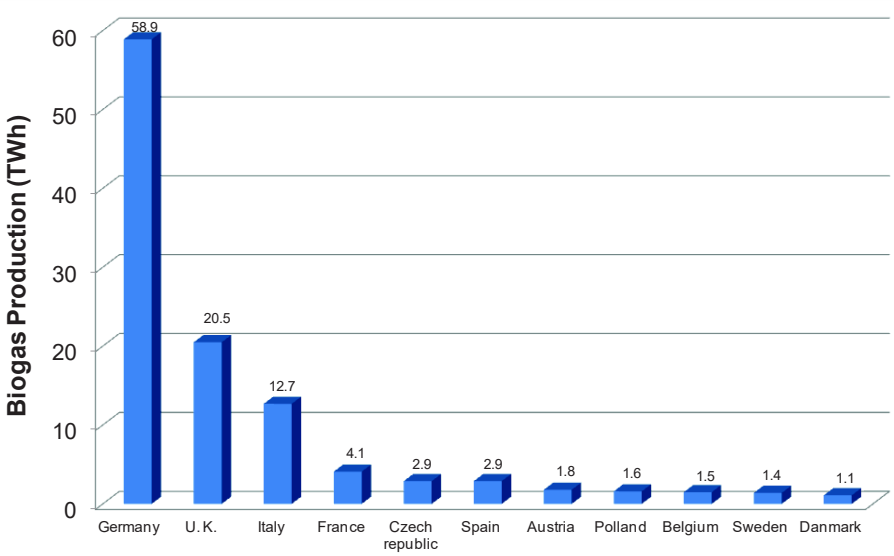


**Figure 1.3.** Biogas production in the EU countries [12] [13] [14]

## 1.4 Biogas applications

Biogas is a vehicle of renewable energy with a potential for different end-use application as heating, electricity, combined heat and power generation, transportation fuel. The main important parameters that influence the choice to convert biogas into heating, in motion or in electricity are the biogas properties and in particular its purity [12].

### 1.4.1 Heating

The conversion of biogas into thermal energy (heat) can be achieved in the most common way, using a boiler system, which does not need a high-quality biogas for combustion. The conversion efficiencies for heat production are typically 75-85%. The thermal energy obtained from the biogas is used for different applications, such as home or industrial heating, heating stables, heating greenhouse, stoves and refrigeration systems. The biogas with 65% of methane has a calorific value of about 22.35 KJ/m$^3$. The use of such biogas as source of heat present some limits: the flammability, flame temperature and it is considered important to assess the flame speed. The flammability indicates the maximum and minimum limits of fuel mixture that is required for the combustion. The limits of flammability of methane are between 5% and 15% by volume in the mixture with air. Instead, the flame temperature of methane is a function of the water vapour content. The use of biogas as thermal energy is primarily exploited for cooking and for heating. Because of the lower purity than pipeline quality natural gas, the conventional stoves

need some adjustments to the combustion system and to the other components of the stove, in order to produce a flame regularly and continuously. There are several kinds of biogas stoves in use in the world: Peking stove (China), Jackwal stove (Brazil), Patel (Kenya). The efficiency of using biogas is 55% in stoves and this is higher than the efficiency of using biogas for other applications, like engines ( (24%) or lamps (3%). These applications bring comfort and reduce the costs increasing the income of the families.

### 1.4.2 Electricity

Biogas can also be converted into electricity using a fuel cell, a gas turbine, a Stirling engine, or it in a system for CHP (cogeneration of heat and power). The performance and characteristics of these technologies depend in different ways on the biogas purity and the biomethane concentration. In general, electrical conversion efficiency decreases with an increase of the $CO_2$ concentration in the biogas. For this reason, the previous purification step is important. However, the electrical efficiency is still low and only the 2.4 kWh of electric power can be produced from $1m^3$ of biogas. The electrical power of biogas is mainly used in the form of light, especially in areas without the electrical network. Alternatively, biogas is implemented for lighting by using special gas mantle lamps with a consume about 0.07-0.14 $m^3$ of biogas per hour, during which it produces heat as well.

### 1.4.3 Power co-generation

The process based on the simultaneous production of the thermal and electrical energy is called co-generation and takes place in units indicated as “Heat and Power generation engines” (CHP). In the co-generation system an internal combustion engine is connected to an electricity generator. The spark-ignition engine generates heat during the electrical production. This heat, which is normally released in the environment, is completely recovered and converted into the thermal energy by means of heat exchangers. This leads to a threefold saving: energy savings, economic savings and environmental savings. Most of the biogas co-generation plants in Europe can be operated without biogas purification if the level of sulphur compounds is low (100ppmv). On the other hand, some gas motors require biogas purification steps. However, the co-generation system presents a lower consumption of fuel (30-40%) compared to the separate production of electricity in thermo-electric power stations and heat in a boiler.

### 1.4.4 Fuel for transportation

One of the most important potential applications of biogas is its use as fuel for transport, after being upgraded to biomethane. In fact, with respect to natural gas, biogas presents the advantage that it can be produced in all places where there is biomass. On the other hand, biogas has about half the calorific value of purified natural gas. For this reason the world Energy council decided that biogas can be used as an automotive fuel when it has a "Wobbe number" ranging between 43.9 and 47.3 $Mj/m^3$, which that corresponds to a percentage of methane of 97±2%. Many countries are investing on the production of biogas as a fuel for cars, in particular Brazil and Sweden. The most important limitation is that the stored energy for a given volume of biogas is lower than for the same volume of liquid diesel fuel. For this reason the overall performance of the vehicle tends to be lower for biogas. A solution can be the use of liquefied biogas for the heavier vehicles that require a large amount of fuel. The liquefaction process can be achieved via further compression and refrigeration, after which storage in specific tanks is needed.

## 1.5 Biogas production via anaerobic digestion

Biogas is obtained from biomass by anaerobic digestion. The anaerobic digestion is a complex bioprocess consisting of successive, often interactive steps carried out by groups of microorganisms with different growth rates and sensitivity to environmental conditions (pH, temperature, partial pressure of hydrogen, etc.). The process can be outlined as consisting of the following steps (Figure 1.4).

Disintegration: The complex particulate waste disintegrates to organic polymers such as carbohydrates, proteins and lipids. Disintegration lumps a number of steps such as lysis, non-enzymatic decay, phase separation and physical breakdown.

Hydrolysis: The organic polymers (carbohydrates, proteins and fats) are hydrolysed (depolymerised) by extracellular enzymes to their respective monomers (sugars, amino acids, lipids), which can be taken up by the microorganisms for further degradation. In the case of particulate complex organic matter consisting of lignocellulosic material (mainly of plant origin), pretreatment steps are necessary to enhance hydrolysis by rendering the substrate matrix more amenable to enzyme attack.

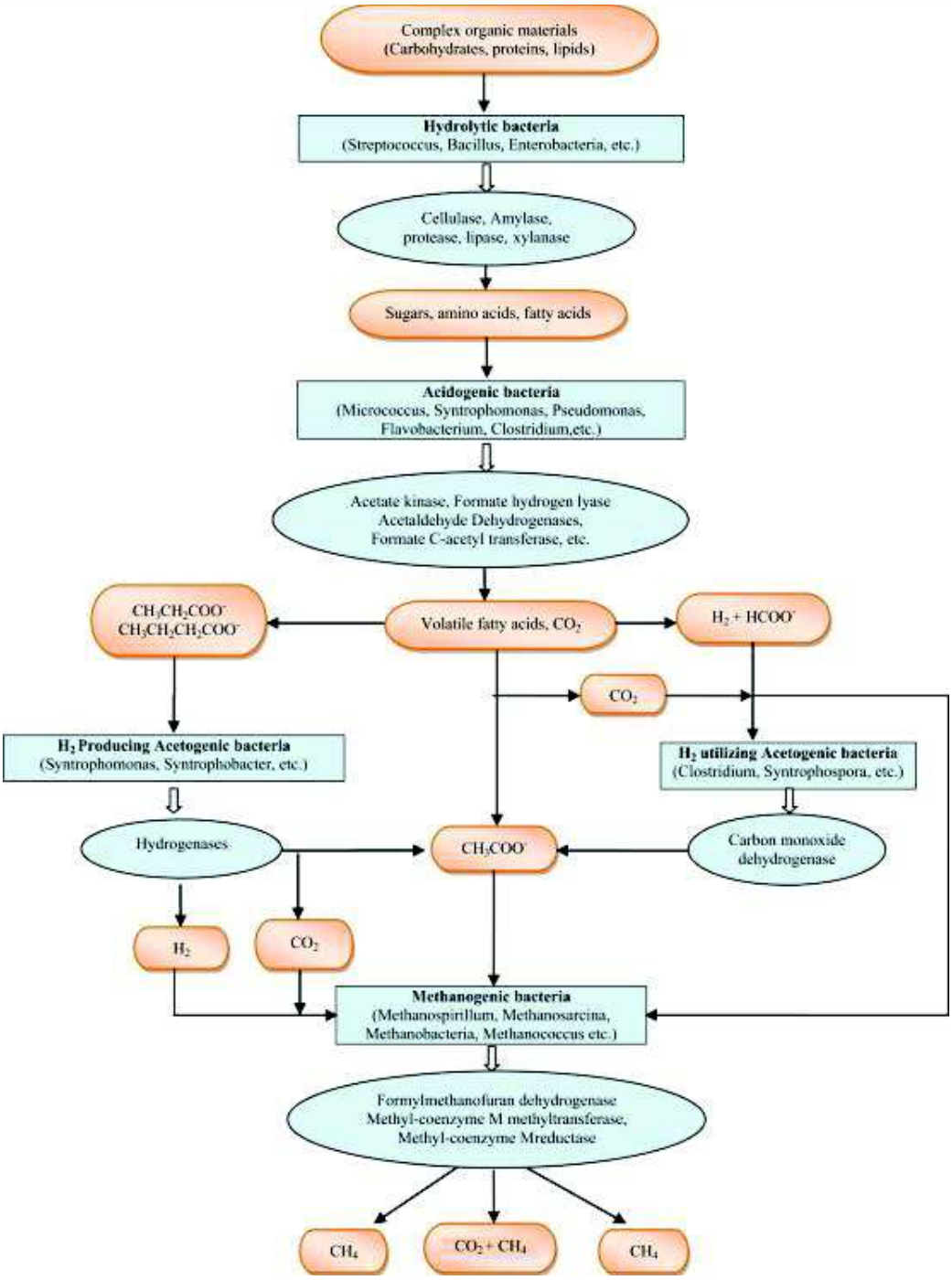


**Figure 1.4.** Steps of anaerobic digestion and microbial enzymes catalyzed carbon flow during anaerobic digestion [16].

Acidogenesis: A versatile group of microorganisms is able to convert the simple monomers to a mixture of volatile fatty acids, alcohols and other simpler organic compounds. This step is also often called fermentation. During acidogenesis, large amounts of carbon dioxide are produced as well as hydrogen. Especially in the case of sugars fermentation, the amount of hydrogen produced can be high and may be harvested for energy recovery. The growth rate of acidogens is

quite high with a doubling time of the order of one hour or even less. They are resistant to relatively low pH (5–6), giving them the advantage of prevailing in the anaerobic environment under adverse conditions.

Acetogenesis: The higher volatile fatty acids (propionate, butyrate, valerate, etc.) as well as the other organic molecules produced in the acidogenesis step are transformed to acetic acid, carbon dioxide and hydrogen by the acetogenic bacteria. This step is thermodynamically inhibited by hydrogen, meaning that there is an accumulation of mainly propionic and butyric acid, unless hydrogen is depleted by the hydrogen-consuming bacteria in other steps. The acetogenic bacteria are slow growing microorganisms with a doubling time of the order of days.

Methanogenesis: There are two distinct groups of microorganisms that produce methane and carbon dioxide: (1) the acetoclastic methanogens that grow on acetic acid and produce approximately 70% of methane in the biogas, and (2) the hydrogen utilizing methanogens that consume hydrogen and carbon dioxide [15].

The biogas production can be influenced by process characteristics as: pH, temperature and pressure, and by the type of wastewater and the type of biomass. Feedstocks with high biomethane potential can be classified as follows:

- Agricultural (livestock manure, agricultural residues, animals mortalities, energy crops)
- Industrial (wastewater, sludges, by-products, slaughterhouse waste, biosolids)
- Municipal (sewage sludge, organic fraction of municipal solid waste)

The choice of the kind of biomass can be made in view of its potential productivity or its environmental impact, and depends of course on its local availability. The choice of substrate based on its nature is a strategy to obtain the maximum possible energy content into biogas. Table 1.1 reports the electrical and heating power, based on the feedstock composition. The lignocellulosic wastes mainly include dedicated crops and specific crop residues. There are dedicated crops as corn, *Sorghum vulgare*, *Triticale*, that ensure profitable production of biogas. Studies indicated that young plant materials possess a relatively soluble nature, hence it can generate comparatively higher amounts of biogas and less solid residues than woody plant materials that possess more non-water soluble components such as lignin, cellulose, hemicelluloses and polyamides [4]. However, lignocellulosic wastes have a high C/N ratio (the ratio between carbon and nitrogen atoms present into the substrate) that leads to a decrease in biogas production. For this reason the co-digestion with the organic matter is preferred, allowing higher production of biogas.

Table 1.1. Quantification of the yield of biogas as function of $m^3$ of biomass [6]

| Feedstock | ADT[a] [°C] | DT[b] [day] | Biogas production [mL/g VS] | Methane production [mL/g VS] |
|---|---|---|---|---|
| Lignocellulose waste: | | | | |
| Rice straw | 37 | 40 | 325.3 | 178.3 |
| Corn straw | 37±1 | 35 | - | 216.7 |
| Wheat straw | 35±0.5 | 31 | 449 | 296 |
| Municipal waste | 35 | 200 | - | 340 |
| Waste sludge | 37 | 10 | Increase 50% | Increase 43.5% |

a) Anerobic digestion temperature
b) Digestion time

The biogas production from municipal solid waste is a matter of great interest, opening up new opportunities in relation to the complex requirements for the disposal of waste and production of energy from renewable sources. The main advantage of this substrate is that its anaerobic digestion does not necessitate a higher reactor volume, while a lower amount of water and energy can be used in the process. The controlled anaerobic digestion of biomass for biogas production takes place in suitable structures designed to maximize the production of methane from the substrate, facilitating the fermentation of components under anaerobic conditions. The biogas composition and the methane concentration depend on the operation conditions and on the origin of the substrate (Table 1.2).

Table 1.2. Composition of the biogas by landfill and of the biogas by digestor compared with the composition of natural gas extracted from North Sea and from the Slochteren gas field in The Netherlands [17].

| | *Biogas landfill* | *Biogas digester* | *North sea* | *Netherlands* |
|---|---|---|---|---|
| *Calorific power ($MJ/Nm^3$)* | *16* | *23* | *40* | *31.6* |
| *Methane (%vol)* | *30-65* | *53-70* | *70* | *-* |
| *$CO_2$ (%vol)* | *15-50* | *30-50* | *1.2* | *1* |

The methane concentration of the biogas produced by landfill or in a digester is lower than that of most sources of natural gas. For this reason, biogas can fed into the home network or it can be used as a fuel only after various steps of treatment that allow adequate purification of methane from the other components such as $CO_2$. Another important parameter for the estimation of biogas that can be produced by different types of biomass, is the percentage of the so-called volatile solids. The volatile solid compounds are the amount of degradable matter respect to the

quantity of raw material introduced into the digester. The volatile solids are on average 70-80% of the total solids, and knowing their content allows the estimation of amount of biogas that can be extracted from each tonne of biomass (Table 1.3).

Table 1.3. Amount of biogas produced per $m^3$ of biomass.

| Matter | Biogas yield ($m^3$/ ton SV) |
|---|---|
| *Livestock* | 200 - 500 |
| *Crop waste* | 350 - 400 |
| *Agro-industrial organic waste* | 450 - 800 |
| *Organic waste from slaughter* | 550 - 1.000 |
| *Sewage sludge* | 250 - 350 |
| *Organic fraction of urban waste* | 400 - 600 |
| *Crops energy* | 550 - 750 |

With increasing volatile solids content the biogas yield increases to a certain extent, but the equilibrium and productivity of the digestion process can also be greatly affected by other factors. The addition of large amounts of new material in the digester may cause a temporary inhibition of bacterial activity and thus a decrease in the yield of the process. For this reason it is important to control other process parameters such as temperature, pH and retention time. Moreover, many actions can increase gas production during biogas digestion, including introduction of accelerants, biological or chemical additives. The biogas produced through anaerobic digestion is collected, dried, compressed and stored to be directed to the processes of purification.

## 1.6 Purification process: transforming Biogas into biomethane

The biogas from anaerobic digestion and landfills consists primarily of methane, $CO_2$ and water vapour. Trace components that are present in raw biogas are hydrogen sulfide, siloxanes, hydrocarbons, ammonia, oxygen, carbon monoxide and nitrogen (Table 1.4). A purification treatment is needed in order to reach a comparable heat power between biogas and methane extracted from natural resources. In order to convert biogas into bio-methane two steps are

necessary: a *cleaning process* to remove the harmful components and an *upgrading process* to increase the heating value by removal of inert and mostly harmless species [18].

Table 1.4. The raw biogas composition [8]

| *Main compounds* | *Amount (%)* | *Trace compound* | *Amount (%)* |
|---|---|---|---|
| $CH_4$ | 40-75 | $H_2S$ | 0.005-2 |
| $CO_2$ | 15-60 | Siloxanes | 0-0.02 |
| $H_2O$ | 5-10 | VOC [a)] | <0.6 |
| | | $NH_3$ | <1 |
| | | $O_2$ | 0-1 |
| | | CO | <0.6 |
| | | $N_2$ | 0-2 |

[a)] Volatile Organic Compounds, mostly Halogenated hydrocarbons

### 1.6.1 Cleaning

The purification from components, present in low concentration, is called ***cleaning.*** In this step the trace components that are harmful for the bio-methane pipeline and appliances are removed.

The ***dehydration*** of the biogas is carried out by condensation, compression, adsorption (on silicon oxide or activated carbon) or absorption (salts or solutions based on glycols). The pipeline quality standards require a maximum water content of 100 $mg/m^3$ and the water removal is important to avoid the reaction with $H_2S$, $NH_3$, and $CO_2$, and as a consequence the formation of corrosive acids or basic compounds. It is also needed to prevent possible condensation of water in pipelines under cold conditions.

***Hydrogen sulfide*** removal can be do with chemical-physical precipitation in the liquid phase of the digester (adding ferrous/ferric chloride to fix the sulfur) or acting on the biogas with adsorption, absorption and biological treatment to achieve its oxidation.

***Oxygen*** can be separated from the biogas with classical separation processes (e.g. adsorption on activated carbon or molecular sieves, or in some cases by selective membranes). The oxygen and nitrogen removal is expensive. Preventing the introduction of air in the biogas is far cheaper than gas treatment. Removal of ***nitrogen*** is more difficult than that of oxygen because of its inert nature and more similar properties to those of methane.

The ***ammonia*** is contained in higher amounts in biogas produced from food waste. Typically, the systems are designed to minimize the production of ammonia. However, to respect the quality

standards of biomethane, almost always a further reduction of ammonia is required. Removal systems dedicated to other pollutants, such as $CO_2$ removing units, often have good separation ability for $NH_3$ as well.

The ***Halogenated hydrocarbons*** are potentially highly corrosive agents and they are strongly polluting. Generally they are captured by activated carbon products, specifically designed for this scope.

The ***siloxanes*** form a group of component that contain Si-O bonds in the backbone**.** Linear and cyclic siloxanes are present in significant concentrations (1-400 $mg/m^3$). When using raw biogas, this in raw biogas these can cause severe damage to engines of the biogas network system. Because silicones tend to form inorganic glassy material upon combustion of biogas, their removal is necessary. The siloxanes can for instance be removed by adsorption (e.g. Active carbon), absorption (e.g. in mixtures of organic solvents of low volatility), cryogenic condensation, chemical killing (hydrolysis of the silicon-oxygen bond) or bacterial degradation.

### 1.6.2 Upgrading: Removal of CO2

The calorific value of biogas is proportional to the methane concentration. The upgrading is the process in which the $CO_2$ is removed to adjust the relative density and to increase the concentration of methane to about 97-99% (typical concentration in purified natural gas) [19]. The process of biogas upgrading generates new possibilities for biogas use since it can then replace natural gas in applications where this is currently used. The main techniques for the removal of $CO_2$ are:

- Pressure swing adsorption (PSA)
- Water scrubbing (SW)
- Physical and chemical $CO_2$-absorption
- Membrane processes

The process of ***pressure swing adsorption*** exploits the potential of some materials to adsorb carbon dioxide in a selective way at high pressures, in particular on activated carbon and on zeolites. In fact, at high pressures the $CO_2$ is adsorbed by the material that is then regenerated by reducing the pressure. The disadvantages of this technique are related to the materials used, which can lose efficiency as a consequence of irreversible adsorption of $H_2S$, water and other contaminants. Furthermore, the cyclic compression-decompression can be quite energy intensive.

The ***scrubbing processes*** are based on the greater solubility of carbon dioxide than methane, or on the reactivity of $CO_2$ with a specific component in the scrubbing solution. In this process the biogas flows upstream in a flow column. The scrubbing solution is enriched in carbon dioxide, whereas biogas, is enriched in methane, exits the column at the top. This process also requires a relatively energy-intensive regeneration of the scrubbing solution.

The ***water scrubbing*** under pressure is the most common technique and exploits the lower solubility of methane in water compared to carbon dioxide. In the case of the physical **scrubbing with organic solvents**, modified ethylene glycol (Selexol®) is often used. The advantage is that carbon dioxide is more soluble in this solvent than in water.

In the case of ***chemical scrubbing***, amine solutions are used as absorbents. In particular, monoetanolammina (MEA) or dimethylethanolamine (DMEA) are highly reactive with $CO_2$, but also with the $H_2S$, while they have a low compatibility with the $CH_4$. In spite of the high efficiency of this process, a major problem is that significant amounts of the amines evapourate during this process and get lost in the environment. Secondly, the regeneration of the solvents is relatively energy intensive.

***Membrane processes***

Membrane separation processes are based on the selective permeability property of a membrane. The separation can take place in one step or in multiple stages. With the current state-of-the art membranes the raw gas can be purified to maximum 92% of methane in a single step. Two or more steps allow to purify raw biogas to a level of 96% or more methane. Two basic systems of membrane separation exist for possible biogas upgrading. Firstly gas-gas separation with a gas phase at both sides of the membrane and secondly, gas-liquid absorption separation with the gas phase at one side of the membrane and the liquid absorbing the diffused molecules at the other side of the membrane. To extend the life of the membranes and obtain optimum separation, the raw gas must be carefully dried and desulphurized before putting it in contact with the membrane. The membrane processes present various advantages with respect to the conventional techniques, such as: operation simplicity, easy maintenance, safety and low operation cost. Table 1.5 shows a comparison between the different techniques upgrading, highlighting the advantages and disadvantages for the respective techniques.

Table 1.5 Comparison of the requirements and performance of different upgrading techniques

| Technique / Characteristics | Pressure swing adsorption | Water scrubbing | Chemical scrubbing | Physical scrubbing | Membrane processes |
|---|---|---|---|---|---|
| *Preventive purification* | Yes | No | Yes | No | No |
| *Operating pressure* | 4-7 | 4-7 | 0 | 4-7 | Variable |
| *Methane concentration (%)* | 98 | 97 | 92-98 | 96 | 89.5 |
| *Efficiency (%)* | 93 | 91 | 90 | - | 80-96 |
| Energy consumption (KWh/$Nm^3$) | 0.25 | 0.3-0.6 | 0.15 | 0.24-0.33 | 0.14 |
| Heat demand | no | no | 160°C | 55-80°C | no |

# Chapter 2. Membranes for $CO_2$ removal

## 2.1 Introduction

Carbon dioxide separation from natural gas streams is an important industrial process where membrane systems are expected to play a more significant role in the coming years. In this work the attention will be concentrated on the current state-of-the-art membranes for $CO_2/CH_4$ separation. After a general introduction, different membrane types will be described: dense polymeric membranes, facilitated transport membranes and mixed matrix membranes. The purpose is to highlight the structural properties, membrane morphologies, gas transport mechanism and performance of the different kinds of membrane for $CO_2/CH_4$ separation.

## 2.2 Membrane definition and classification on the basis or morphology

A membrane can be defined as an interface between two phases that regulates in a selective way the flux of chemical species (gas, liquids, positive or negative ions). The membrane controls the exchange of mass between the two phases, favoring the passage of a substance relative to another, according to mechanisms that control selectively the transport (Figure 2.1) [20].

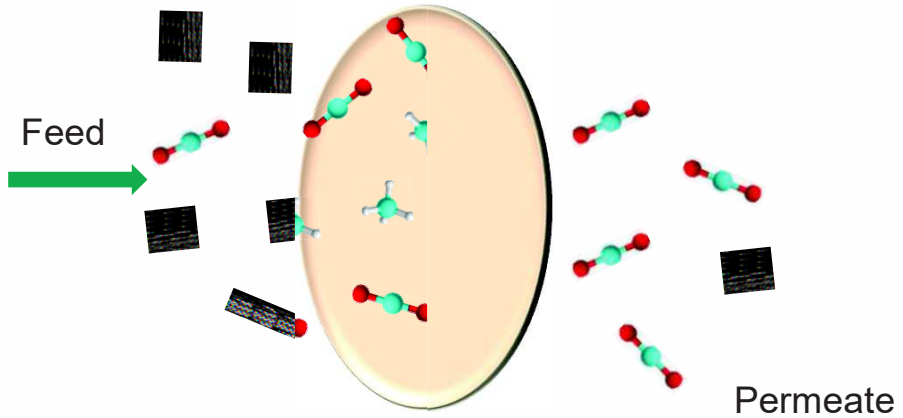


**Figure 2.1.** Membrane for $CO_2/CH_4$ gas separation

The selective action of the membrane, allows to obtain a phase called “permeate”, enriched of the more permeable species. Instead, the phase called retentate is enriched in the less permeable species.

### 2.2.1 Membrane morphology

Membranes can be classified from the morphological standpoint as:

- Porous membranes: They have pores with a more or less ordered distribution, depending on the preparation techniques. The separation is based on different mechanisms that depend on the size and the structure of the pores, and on the nature of the species to be separated [21]. Porous polymer membranes are generally not sufficiently selective for gas separation and in this field they are normally used as a porous support for thin film composite membranes or for supported liquid membranes. Therefore they will not be described in detail in the present thesis. membranes
- Dense membranes: they are dense and homogeneous films, in which the transport of the species generally occurs thanks to a concentration gradient of the permeant across the membrane as the driving force, and a diffusive transport mechanism. Besides a pressure or a concentration gradient, the trans-membrane driving force can also be a temperature gradient or an electric potential. The transport properties are mainly dictated by the intrinsic characteristics of the material. This kind of membranes is typically used for pervapouration or for gas separation processes.

### 2.2.2 Transport properties in relation to the membrane morphology

Regarding the gas separation process, the gases permeate through the membranes with different mechanisms that depend on the size of the pores and of the free spaces of a membrane. They are divided into (Figure 2.2):

- Convective flow, pore d = 0.1-10 μm
- The Knudsen diffusion, pore d <0.1 μm
- Molecular sieving, d = 0.5-2 nm pore.
- Solution- diffusion, dense membranes.

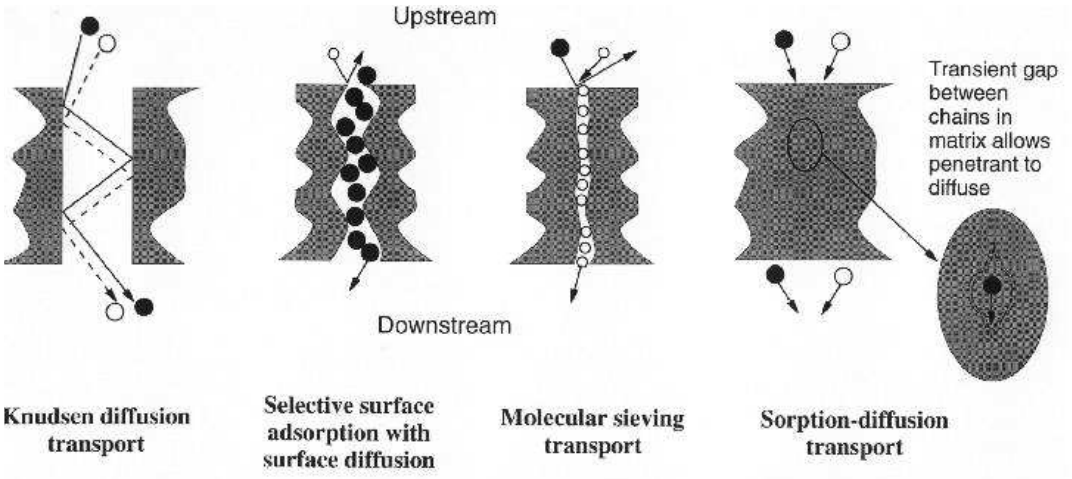


**Figure 2.2.** Gas permeation mechanisms through membranes

In the case of very large pores **convective flow** occurs and the pressure difference leads the gas mixture through the pores without any selectivity. For this reason, membranes with a large size of the pores are not usable for the separation of gas mixtures.

**Knudsen flux** occurs when the size of the pores is smaller than the mean free path of the molecules, λ, (cm):

$$\lambda = \frac{RT}{\pi \cdot d^2 \cdot P\sqrt{2}} > r_p \qquad \text{Eq. 2.1}$$

Where *T* is the temperature, *P* the pressure, *R* is the constant of the gas, d is the diameter of the molecule and $r_p$ is the pore radius. In this case, the number of collisions of the gas molecules with each other is negligible compared to the number of collisions between the gas and the pore wall. The selectivity depends exclusively on the ratio between the square roots of the molar masses of the diffusing permeants. This means that the gas with smaller molecular weight diffuses faster than the gas with the higher molecular weight.

**The flow by surface diffusion** is the permeation mechanism in which a component of the gas mixture presents high affinity with the material of the membrane. The chemical species interacting strongly with the surface is thus adsorbed on the material and the diffusion through the pores takes place predominantly through the transport of the species along the surface of the membrane pores.

The **solution-diffusion** mechanism is the most common mechanism occurring in dense polymeric membranes. The molecules are absorbed onto the surface of the membrane, subsequently diffuse through the bulk of the polymer to the downstream side of the membrane,

and finally they are desorbed from the permeate side of the membrane. The solution-diffusion model will be discussed in more detail in Section (2.4.1).

## 2.3 Dense polymeric membranes: structure and preparation

### 2.3.1 Membrane structure

Dense membranes can be further classified according to their structure in three main categories, displayed in Figure 2.3:

- ❖ Symmetric
- ❖ Asymmetric
- ❖ Composite

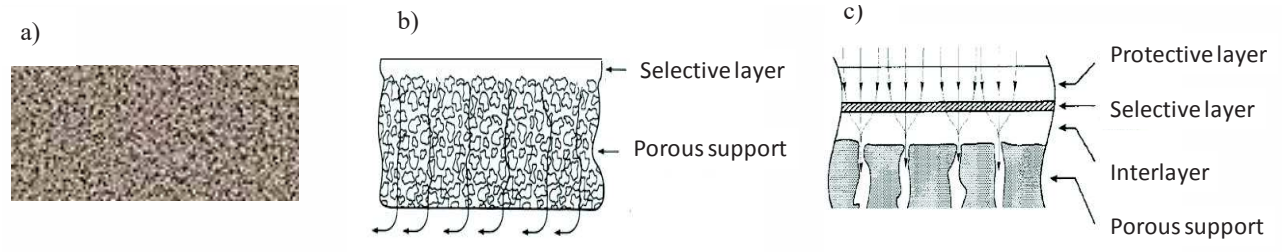


**Figure 2.3.** a) Dense membrane; b) asymmetric integrally skinned membrane; c) thin film composite membrane.

#### 2.3.1.1 Symmetric dense membranes

The symmetric dense membranes are homogeneous, they do not present pores but they have voids between the molecular chains with a size the order of 5-10 Å, which constitute the so-called "free volume" (Figure 2.3a).

The symmetric dense membranes can be prepared by different techniques:

- Solution casting: this is a technique that allows to obtain a dense flat membrane by means of the spreading of a polymeric solution with a defined concentration on an appropriate surface, followed by evapouration of the solvent. The polymeric solution is spread by knife having a precise gap, which defines the thickness of the membrane. Alternatively, the polymer solution can be cast in a petri dish or similar. A thin dense uniform polymer film is finally obtained by the controlled solvent evapouration.

- Melt pressing: the polymer is compressed between two heated plates. Typically, a pressure of 2000–5000 psi is applied for 1–5 min, at a plate temperature just below the melting point of the polymer.
- Melt extrusion: the molten polymer is extruded through a thin slit or through an annular opening into the form of a sheet or a hollow tube, respectively. The sheet can be mono- or bidirectionally stretched to increase the area and to reduce the thicknesss. The tube can be blown to reduce the final film thickness to several tens of microns.
- Polymerization : in this case the membrane is obtained by means of the direct polymerization, for instance of a two-component silicone resin.

The resistance to mass transport is proportional to the thickness of the membrane. The techniques of preparation try to find a compromise between productivity and selectivity. A reduction in the thickness involves an increase in productivity due to the decrease of the resistance to transport. However, a thinner membrane is more likely to have defects and thus a lower selectivity. For this reason, the choice often falls on membranes with an "integral skin" or on composite "multilayer" membranes.

#### 2.3.1.2 Asymmetric dense membranes

Asymmetric membranes have a very thin dense skin, responsible of the membrane selectivity and a thicker macroporous support, responsible for the mechanical reisstance (Figure 2.3b). The low thickness of the skin allows to obtain a better efficiency, while the porous support facilitates the handling and improves the mechanical strength. Dense asymmetric membranes can be obtained by:

- D*ry-wet phase separation* (or nonsolvent induced phase separation, NIPS) the precipitation of the polymer solution takes place upon contact of the stable polymer solution with a non-solvent.
- *Thermally induced phase separation* (TIPS) the phase inversion takes place by cooling the stable hot polymer solution, sometimes accompanied by partial evapouration of the solvent.
- *Dry phase inversion* method (Dry NIPS), the stable polymer contains besides the volatile solvent also a small amount of nonvolatile nonsolvent and evapouration of the solvent leads to the phase separation by the action of the increasing nonsolvent concentration [22].
- *Solvent evapouration* method the complete evapouration of the solvent leads to the formation of a completely dense, homogeneous film.

In all cases, except for the latter where a single dense phase is formed, phase inversion leads to the formation of two phases: a solid phase, rich in polymer, which will form the matrix of the membrane, and a liquid phase with a low polymer concentration, constituting the pores

#### 2.3.1.3 Thin film composite membranes

**Thin film composite membranes** are dense and structurally similar to the dense asymmetric membranes, but they are built by an assembly of different materials (multi-layer): the porous support, the intermediate layer, the selective film and, in some cases, protective layer (Figure 2.3c).

- The porous support: has the function of ensuring mechanical strength without inducing significant resistance to the transport through the membrane.
- The intermediate layer: vents the gas from the selective layer towards the pores of the porous support, ensuring the adhesion between the two surfaces even when made of materials which are not similar; at the same time it prevents the infiltration of the polymer of the selective film into the porous support, in fact, this phenomenon could cause clogging of the pores and thus have a negative effect on the performance of the selective membrane. This layer may not be necessary in the case of highly permeable polymers, which can be deposited directly onto the porous support.
- Protective layer: the selective layer generally must be as thin as possible to guarantee a high flux and is therefore very delicate. It must be protected with a highly permeable protective coating. This layer does not affect the transport significantly but it protects the membrane during handling.
- The selective layer: this is the intermediate layer, responsible of the separation of different molecular species, and represents the actual membrane and defines its efficiency.

### 2.3.2 Dense polymer membrane materials

On the basis of their base constituents, dense polymeric membranes can generally be classified in three different categories:

- Glassy polymeric membranes
- Rubbery polymeric membranes
- Membranes of semi-crystalline polymers

This classification is made on the basis of the thermal properties of the polymer used to fabricate the membrane.

*Rubbery polymers* are materials operating above their glass transition temperature, $T_g$. Above their transition temperature they appear in their rubbery state due to a large free-volume present between the polymer chains, combined with a relatively flexible polymer backbone, which guarantees a high mobility.

*Glassy polymers*, instead, operate below their glass transition temperature where the motion of the polymer chains is frozen in a highly rigid state. With the exception of a few special classes, they are characterized by a low fraction of free-volume with few points of voids interconnection. The chains are generally much stiffer than those of the rubbery polymers. Exceptions are the glassy Perfluoropolymers (PFPs), which have a stiff polymer backbone but nevertheless present a high fractional free volume due to their low cohesive forces, and the so called polymers of intrinsic microporosity (PIMs). The latter have extraordinary stiff chains, often with a ladder structure, in combination with a highly contorted polymer backbone. The latter will be discussed in more detail in Chapter 5.

*Semi-crystalline polymers* have a sufficiently regular chain structure to allow the polymers to rearrange themselves spatially into an ordered system and to crystallize. Depending on the chain stiffness, the non-crystallized amorphous phase may be either in the glassy or in the rubbery state. Since the crystalline phase is typically impermeable to mass transport, these polymers are rarely used for gas separation membranes, unless the degree of crystallinity is very low. This is for instance the case for the thermoplastic poly(ether-amide) elastomer, Pebax®, described in Chapter 3, in which the microcristallinigy serves as physical crosslinks of the rubbery phase.

These structural differences influence the gas transport properties dramatically. The glassy polymers generally have high selectivity and lower flux. Instead, the rubbery polymers present high flows and low discriminating capacity as shown in the Robeson plot (Figure 2.4).

The Robeson plot underlines the permeability-selectivity tradeoff in polymeric membranes and given example illustrates the $CO_2/CH_4$ separation performance of the rubbery and glassy membranes from the original 1991 Robeson curve and how it shifted during the following decades up to 2008. The choice of the right polymeric membrane material for a given gas separation generally depends on different parameters as the cost, the chemical and thermal stability, permeability and selectivity.

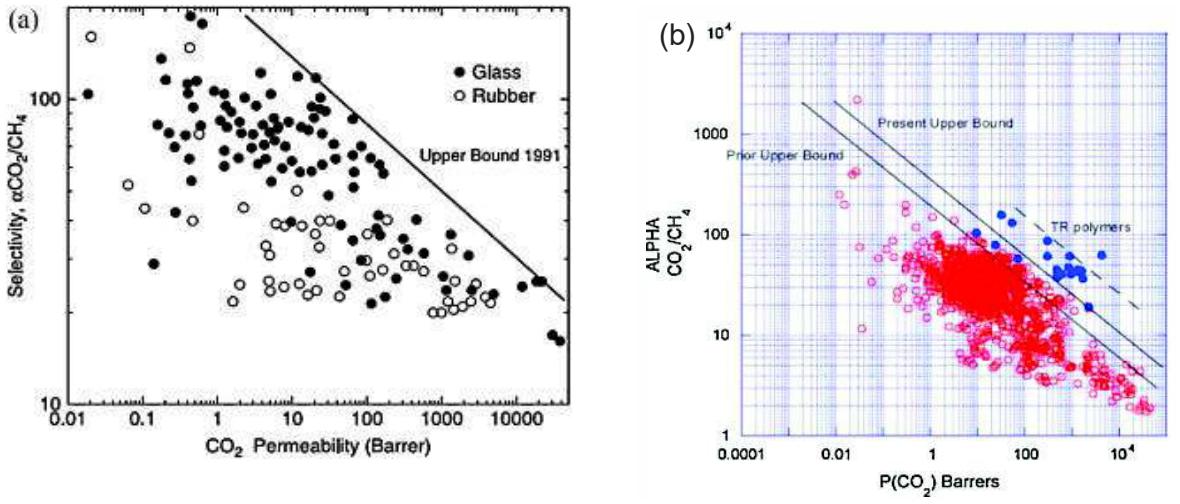


**Figure 2.4.** Robeson plot showing the rubbery and glassy membrane performances for $CO_2/CH_4$ separation (a) 1991 and (b) 2008 .

Many different polymers are investigated as materials for gas separation: *Polyimides* (PI), *Polyammidi*, *Polyalkynes, Perfluorinated polymers*, *Polyphenyleneoxide* (PPO), *Polysulfone* (PSf), *Polydimethylsiloxane* (PDMS). The performances of these polymers, in terms of $CO_2/CH_4$ separation, are reported in Table 2.1.

Table 2.1. Permeability and selectivity of polymeric membranes

| Type | Material | Pe $CO_2$ [Barrer] | $CO_2/CH_4$ Selectivity | Ref. |
|---|---|---|---|---|
| **Rubbery** | **Poly(organosiloxanes):** | | | |
| | *-PDMS (polydimethylsiloxane)* | 2700 | 3.38 | [23] |
| | **Poly(ether-*block*-amides):** | | | |
| | *- Pebax® 1657* | 76.2 | 18.6 | [18] |
| | *- Pebax® 2533* | 257 | 8.3 | [24] |
| **Glassy** | **Polyimides (PI):** | | | |
| | - Matrimid | 10 | 35.71 | [24] |
| | - Kapton | | | |
| | **Polyalkynes:** | | | |
| | *- PTMSP (poly(1-trimethylsilyl propyne)* | 84.6 | 5.75 | [25] |
| | *- PMP Poly(4-methyl-2-pentyne)* | 6700 | 3.75 | [18] |
| | **Perfluorinated polymers:** | | | [2,8,25,26] |
| | *- Hyflon AD60x-AD80x* | 260-280 | 9-11 | |
| | *- Teflon AF 2400* | 3600 | 5.7 | |
| | ***PSf** (polysulfone)* | 5.6 | 22.4 | [28] |
| **Semi-crystalline** | ***PPO** poly(phenyleneoxide)* | 60.93 | 22.40 | [18] |

Among these different classes of polymers listed here, PDMS presents a very high $CO_2$ permeability with a relatively lowest $CO_2/CH_4$ selectivity. Instead, Polysulfone (PSf) has the lowest $CO_2$ permeability. PI-based membranes present a higher $CO_2/CH_4$ selectivity than PPO (35.7 and 22, respectively). An important fact is that PPO membrane showed a stable permeation rate with the time, while the permeability of PI decreased notably over 3 months of operation [29]. Regarding the Perfluorinated polymers, Teflon AF 1600 presents a higher $CO_2$ and $CH_4$ permeability than Hyflon AD60 [30][26]. For both Perfluorinated polymers the loss of permeability, which generally occurs in the presence of water, was minor relative to other polymeric membranes. This behavior reflects the low solubility of water in these systems. These features mean that both perfluorinated polymeric membranes can be utilized in applications where gas pretreatment to remove water is difficult, like in biogas upgrading. The polymers PTMSP and PMP are characterized by a high free-volume and present a higher $CO_2$ permeability but very low efficiency to discern between $CH_4$ and $CO_2$ (low selectivity) [31]. For this reason it is important to reach a compromise between the permeability and the selectivity finding a material with high efficiency (high $CO_2/CH_4$ selectivity) and elevated productivity (excellent $CO_2$ permeability). The rubbery Pebax® is a good candidate for the separation of this pair of gases. It presents a good compromise between $CO_2$ permeability and $CO_2/CH_4$ selectivity.

## 2.4 Gas transport in dense membranes

### 2.4.1 The solution-diffusion mechanism in homogeneous membranes

As anticipated above, the molecules of gases move in the polymeric membrane with different transport mechanisms, depending on the nature of the membrane. Generally, in the dense glassy or rubbery membranes the gases are transported on the basis of the well-known solution-diffusion mechanism. In the solution-diffusion model the gas permeation in the membrane is constituted by three stages:

- **Absorption** of the molecules from the gas or vapour phase at the side of the membrane in contact with the feed and **dissolution** into the polymer bulk. The degree of solubility of a component in the first step of the process is related to the energy required for the species to dissolve in the polymer.

- **Diffusion** is the step during which the species diffuse through the membrane matrix. The diffusion depends on the concentration of the feed, by the kind of polymer that makes up the membrane, the dimensions of the permeating species, and by the operating conditions.
- **Desorption** is the last step of the process in which the permeating species desorb from the polymer at the permeate side of the membrane. The diffusion of the gases trough the membrane in the stationary state can be described by Fick's law (Figure 2.5).

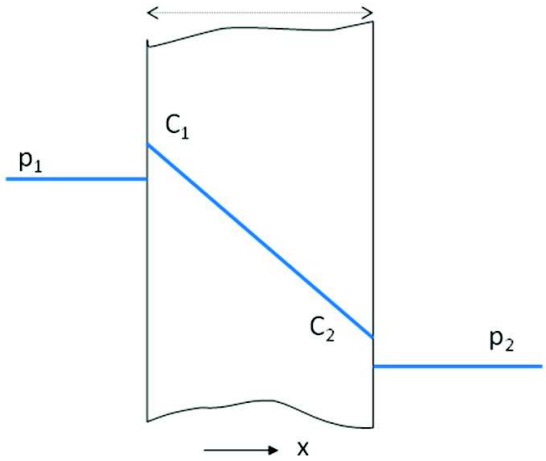


**Figure 2.5.** Representation of the concentration profile of a gas across a dense polymer membrane governed by Fick's law.

The flux of permeate trough a membrane can be described by the following equation:

$$J = -D\frac{\delta_C}{\delta_x} = D\frac{(C_1 - C_2)}{\ell} \qquad \text{Eq. 2.2}$$

Where $J$ is the permeate flux, $C_1$ and $C_2$ the concentration of species at the two sides of the membrane, and $D$ isthe diffusion coefficient. When there is a linear relationship between the gas pressure $P$ and the concentration $C$ at the interface of the membrane, the concentration at the interface is given by Henry's law:

$$C = S \cdot p \qquad \text{Eq. 2.3}$$

where $S$ is the solubility coefficient of the gas that assumes a constant value. When $D$ is a constant, replacing Eqs. (2.2) in (2.3) and integrating gives:

$$J = DS\frac{(p_h - p_l)}{\ell} = \left(\frac{P}{\ell}\right)\Delta p. \qquad \text{Eq. 2.4}$$

Where $P$ is the gas permeability at steady state across the membrane having a thickness $\ell$, when applied pressures $P_h$ and $P_l$ at the high pressure (feed/retentate) side and the low pressure (permeate) side, respectively.

The solubility and diffusion contribute differently to the determination of the permeation. In fact, the permeability can also be expressed as the product of the two:

$$P = D \cdot S \qquad \text{Eq. 2.5}$$

where $S$ is the solubility coefficient, and $D$ the diffusion coefficient.

The selectivity of component i with respect to the component j is given by their permeability ratio, which in turn can be expressed as the product of the diffusivity selectivity, $D_i/D_j$, and the and the solubility selectivity, $S_i/S_j$:

$$\alpha_{i/j} = \frac{P_i}{P_j} = \left(\frac{D_i}{D_j}\right) \cdot \left(\frac{S_i}{S_j}\right) \qquad \text{Eq. 2.6}$$

The Diffusion is a kinetic phenomenon and is strongly linked to the free volume of dense materials and to the molecular size of the penetrating species. In the membrane, the extension of free volume elements or 'voids' like a 'network of channels' can be advantageous for the transport. This is the principle to which the so-called Polymers of Intrinsic Microporosity (PIMs) owe their high perm3ability, as will be discussed in Chapter 5.

How much the diffusion depends on the molecular size of the permeating species is clearly shown in Figure 2.6 for the Van der Waals volume of a large number of molecules.

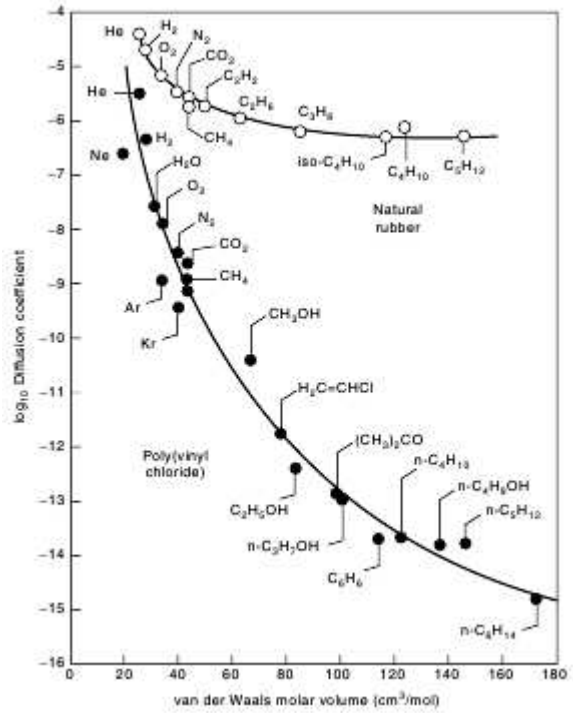


**Figure 2.6.** Diffusion coefficient as a function of molecules dimension [21].

The permeability tends to increase with the decreases of kinetic diameter (Table 2.2). This is generally valid for all different species, but several factors may determine deviations of this trend:

- ✓ Chemical nature of the permeating species, the occupation of the orbitals and the distance between the atoms vary from substance to substance and make the molecules more or less compact. For instance, fluorinated species may behave different from the equivalent hydrocarbons.
- ✓ Form of molecules, the distribution of atoms makes the molecules more elongated (eg. planar form of the $CO_2$) or more compact (tetrahedral, e.g. $CH_4$).

Table 2.2. Kinetic diameter and molecular weight of various gases [33]

| Gas | Kinetic Diameter (Å) | Molecular weight (g/mol) |
|---|---|---|
| He | 2.6 | 4 |
| $H_2$ | 2.89 | 2 |
| NO | 3.17 | 30 |
| **$CO_2$** | **3.3** | 44 |
| Ar | 3.4 | 40 |
| $O_2$ | 3.46 | 32 |
| $N_2$ | 3.64 | 28 |
| CO | 3.76 | 28 |
| **$CH_4$** | **3.8** | 16 |

On the contrary, the solubility is a thermodynamic parameter. It depends on the interactions between the gas and the polymeric matrix of the membranes. The solubility increases with the size of the permeating species [32], which in turn is correlated with for instance its critical volume or its Van der Waals volume (Figure 2.7).

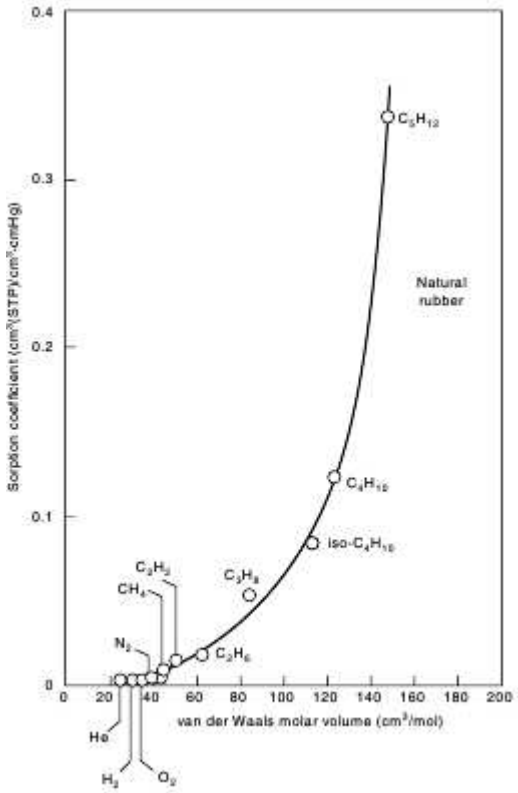


**Figure 2.7.** Solubility coefficient as a function of the molecular dimension, expressed as the Van der Waals volume [21].

Moreover, the main factor that determines the solubility in a polymer matrix is the ability of the penetrant gases to condense. For example, the $CO_2$ is more permeable than $CH_4$ due to the larger condensability, as indicated by the critical temperature, Tc ($CO_2$, Tc = 304K; $CH_4$,Tc = 191 K).

### 2.4.2 Dual mode sorption

For glassy polymers, the solubility of penentrant molecules in the matrix is usually described by the dual-mode sorption model, which consists of two types of sorption: Langmuir sorption mechanism and a Henry's law dissolution mechanism (Figure 2.8).

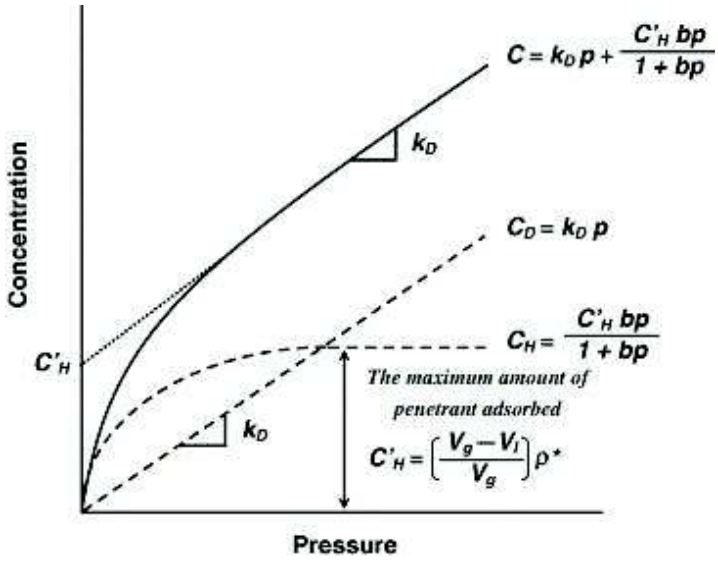


**Figure 2.8.** Schematic representation of a dual-mode sorption [21].

Henry's law can be expressed as:

$$C_D = K_D \cdot f \qquad \text{Eq. 2.7}$$

Where $C_D$ is the gas concentration in the polymer due to its dissolution in the matrix membrane, $K_D$ is Henry's law solubility coefficient and $f$ is the gas fugacity. In ideal cases, the gas pressure rather than its fugacity can be used in this equation.

The Langmuir equation is the following:

$$C_H = \frac{C'_H bf}{1 + bf} \qquad \text{Eq. 2.8}$$

$C_H$ is the gas concentration in the microvoids "frozen" in the polymeric matrix, $C'_H$ the gas concentration in the saturated hole and $b$ is the Langmuir affinity constant, which represents the ratio of the rate constant of gas adsorption and desorption in the microvoids or defects. The basic idea of the Langmuir sorption mode is that in a glassy matrix part of the sorption takes place in pre-existing voids, similar to sorption in porous materials such as zeolites. Its capacity is limited and the occupation of the voids at any pressure depends on the pressure itself, the total capacity and on the gas affinity. The Henry type sorption is proportional to the feed pressure and is the only mechanism present in rubbery polymers. Within certain limits, it linearly increases with the pressure as a result of the gradual swelling of the polymer matrix.

The total concentration of gas in the membrane will be given by the sum of the two contributions:

$$C = C_D + C_H = K_D f + \frac{C_H' bf}{1 + bf} \qquad \text{Eq. 2.9}$$

This equation, defined as the dual mode sorption model, thus consists of the combination of the Langmuir isotherm and Henry's law. It is schematically illustrated in Figure 2.8.

### 2.4.3 Facilitated transport membrane

In the last years the membranes with the facilitated transport have found an increasing interest in the $CO_2$-$CH_4$ separation process. The separation process of these membranes is based on the use of a specific carrier for the gas. The difference with the standard solution-diffusion mechanism is that the carrier is actively involved in the transport, usually via chemical reaction or via a specific interaction. In the case of facilitated $CO_2$ transport, the carrier is most of the time a basic compound, specific for the interaction with $CO_2$. The reactive carrier interacting with the $CO_2$ achieves high selectivity without sacrificing the permeability or vice versa. The carrier reacts with the $CO_2$ dissolving on the feed side and forms a carrier-$CO_2$ complex. The carrier-$CO_2$ complex itself moves across to the membrane and releases the $CO_2$ on the low pressure side along the direction of concentration driving force. Alternatively, the carrier helps $CO_2$ to achieve a much higher concentration and the facilitated transport consists in an accelerated 'hopping' of a $CO_2$ molecule from one carrier molecule to the next one.

The $CO_2$ reacting with the basic compound passes through the membrane with a facilitated diffusion mechanism in addition to the regular solution-diffusion transport. The gas that does not show any affinity for the carrier will permeate only according to the normal solution-diffusion mechanism. As a result, higher $CO_2$ selectivity can be achieved while the permeability is also maintained or even increased. The basic compound can be a fixed carrier on the surface of the membrane (Figure 2.9) or a mobile carrier dissolved in a liquid (Figure 2.9)b. The last situation is the case in for instance supported liquid membranes (SLMs).

In the case of basic carriers, the most efficient facilitated $CO_2$ transport is based on the mechanism in which the $CO_2$ is transformed into $HCO_3^-$ due to the interaction between $CO_2$ and a water molecule. The $CO_2$ transfer will be facilitated in the form of the small mobile ion.

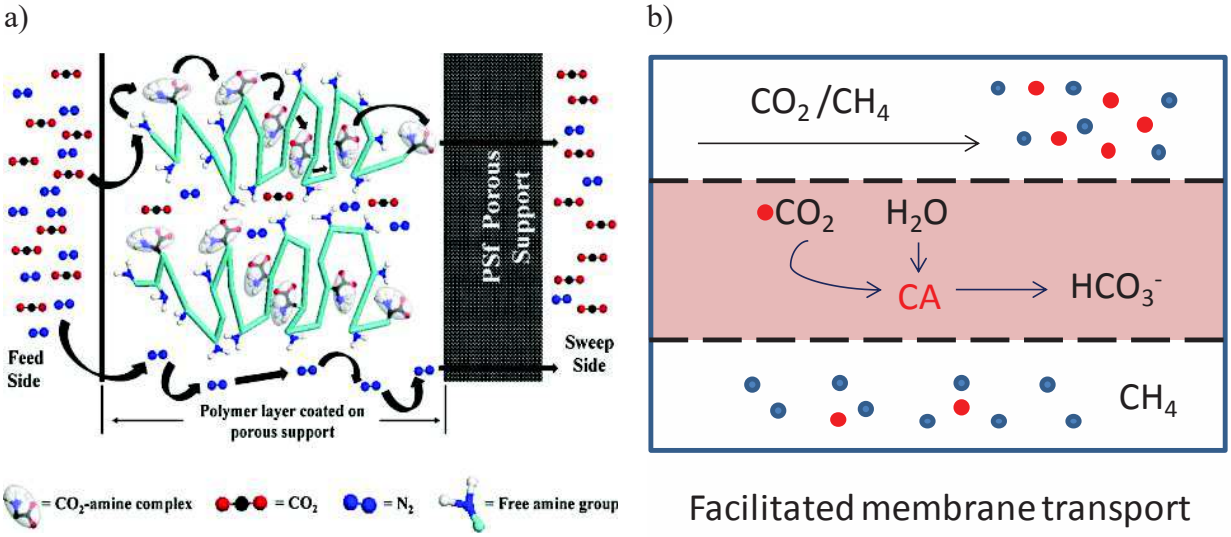


**Figure 2.9.** a) Schematic representation of a facilitated transport with a fixed carrier. b) Schematic representation of a facilitated transport with a mobile carrier.

#### 2.4.3.1 Fixed carrier membranes (FCMs)

In the case of fixed carrier membrane, the $CO_2$-carrier is usually in the form of small molecules containing amine groups, incorporated by blending the membrane material with the $CO_2$-transporter [33–35] The amino groups can be part of a mono, di or tri-substituted amine (R-$NH_2$, $R_2$-NH, $R_3$-N). It depends on the bond between the carrier and the surface membrane but also by the reaction between the amino groups and the $CO_2$. In the last case, the tri-substituted or tertiary amine is used, there is no hydrogen atom available to be displaced by $CO_2$ to form $HCO_3^-$. This phenomenon is called deactivation of the carrier and it is the more important limitation for this membrane. It can be happen when the carrier is tri-bound on the membrane surface or when the mono or di-substituted amines react for prolonged time. For this reason, the mobile carriers are preferred respectively to the fixed carrier membrane. The deactivation of the carrier can be avoided when the $CO_2$ facilitated transport is carried out in the water swollen membrane. Many studies have demonstrated that the water swollen membranes have a higher permeability and selectivity than the corresponding dry membranes. In fact, the presence of water guarantees a high hydrogen availability. In this way, the amino group is not consumed and it can act only as base catalyst to improve the hydration of the $CO_2$ and the transport in the form of $HCO^{3-}$.

### 2.4.3.2 Mobile carrier membrane (MCMs)

On the other hand, in membranes with a mobile carrier, the transport of $CO_2$ is facilitated in the form of different small mobile molecule as ion $HCO_3^-$, which gives similar transport mobility as in a mobile carrier membrane. The enzyme most widely known for catalysis of specific reactions with carbon dioxide is carbonic anhydrase (Figure 2.10). This is a zinc metal-protein that catalyzes the reversible hydration of carbon dioxide:

$$CO_2 + H_2O \leftrightarrow HCO_3^- + H^+.$$

Many studies on gas separation are focusing on the use of this enzyme for the $CO_2$-facilitated transport [36,37]. For mobile carrier membranes, one of the main disadvantages is the loss of carriers by evapouration. For this reason, new solvents are continuously investigated in order to find new classes with a higher solubility for $CO_2$, lower vapour pressure, low viscosity and moderate hydrophilicity.

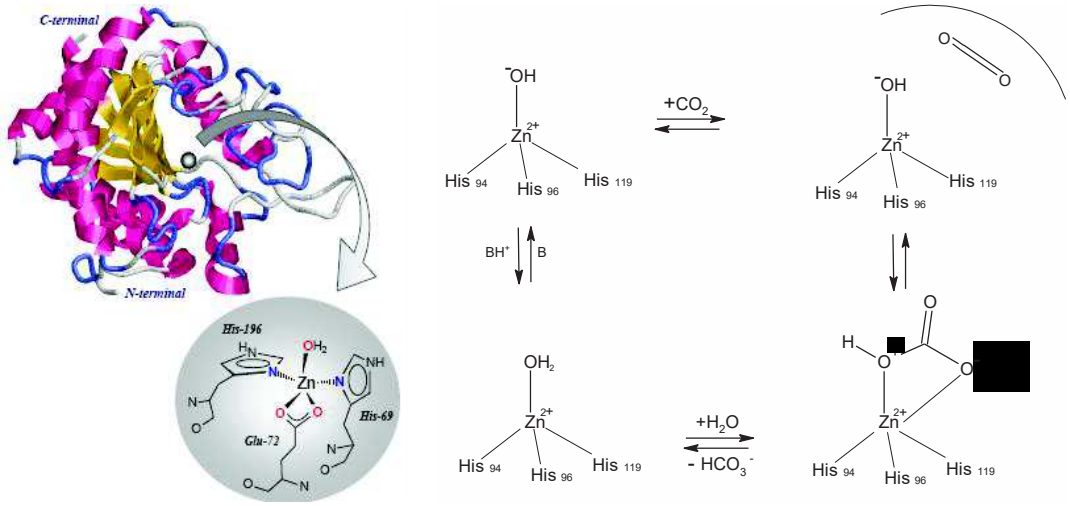


**Figure 2.10.** Carbonic Anhydrase Enzyme structure and schematic representation of the catalytic reaction

## 2.4.4 Mixed matrix membranes

The mixed matrix membranes (MMMs) represent a different type of membranes relying on the solution-diffusion mechanism. They are prepared via dispersion of organic, inorganic or metalorganic particles in a dense polymeric matrix. The filler particles can be linked to the polymeric matrix by covalent bonds, by van der Waals forces or via hydrogen bonds. The scope

is to combine the characteristics of two different materials and to improve the membrane performance in terms of permeability and selectivity. The particles can affect the membrane transport in two different ways. In the first case they can act as molecular sieves and, as a consequence, they form a barrier for large molecules and reduce their permeability, with a positive consequence on the selectivity. In the second case they improve the permeability by increasing the free volume of the MMM with respect to the neat polymeric matrix. The first studies of hybrid membranes for gas separation date back to the 70s' with the discovery of the effect of the addition of zeolites into the polymer matrix (PDMS) [40]. Since then, the effects of adding heterogeneous fillers as additives to polymer membranes on their properties have been the subject of many studies.

#### 2.4.4.1 Filler materials

Typical fillers are: functionalized zeolite nanoparticles, carbon molecular sieves (CMS), carbon nanotubes (CNTs), metal–organic frameworks (MOFs) and covalent organic frameworks (COFs), graphite and non-porous silica that offer attractive gas transport properties (Figure 2.11).

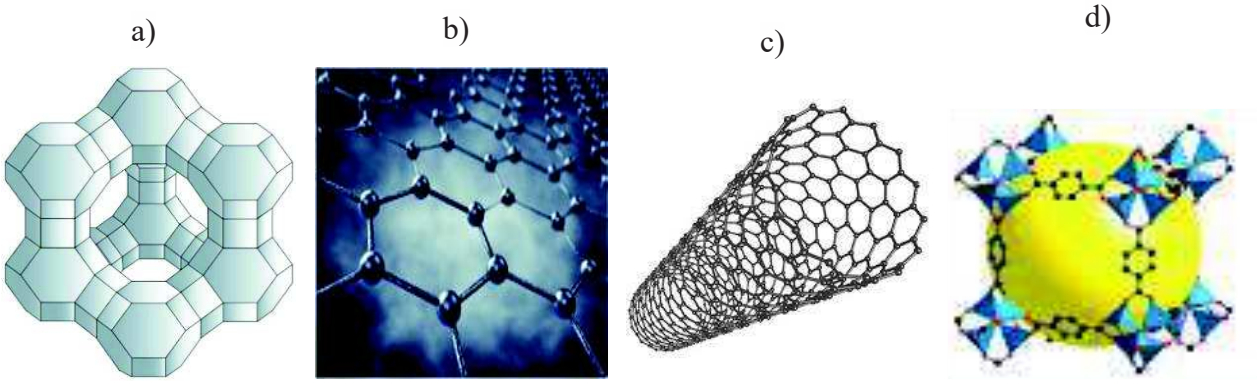


**Figure 2.11.** Several examples of the molecular sieving materials: a) zeolite; b) carbon molecular sieves (CMS); c) carbon nanotubes (CNTs); d) metal–organic frameworks (MOFs).

**Zeolites** are crystalline aluminosilicates consisting of $AlO_4$ and $SiO_4$ tetrahedra that are connected to form a network of channels and cavities with size that vary in the range of molecular dimensions between 0.3 and 1.0 nm (Figure 2.11a). Substitution of Si atoms by Al atoms in the crystal structure results in excess negative charge compensated by monovalent or divalent cations ($K^+$, $Na^+$, $Ca^{2+}$), rendering the structure more polar. As a result, the polar species (e.g. water, ammonia, carbon dioxide, nitrogen and aromatic hydrocarbons) are strongly

adsorbed by these zeolites [41]. This is not necessarily an advantage because in the case of humid gases, such as raw biogas, this might eventually lead to the undesired pore blocking by the condensed water.

**Carbon molecular Sieves (CMSs)** are prepared from carbon containing chemical compounds and polymers (Figure 2.11b). These materials have high surface area to volume ratios, a relatively uniform pore size and small pores. Swaidan et al. have demonstrated that a CMS membrane derived from a conventional polyimide precursor (P84) exhibited a good $CO_2$ permeability (499 Barrer) but a somewhat unusual, because higher, selectivity for the mixture ($CO_2/CH_4$ = 97) compared to the pure-gas selectivities ($CO_2/CH_4$ = 87) [42].

**Carbon Nanotubes (CNTs)** are long cylinders of covalently bonded carbon atoms and the $CO_2$ adsorption takes place on both the external and the internal surfaces of the nanotubes (Figure 2.11c). Deng et al. reported that the $CO_2$ permeance of the CNTs reinforced nanocomposite membranes improved significantly compared to the membrane without CNTs, while the $CO_2/CH_4$ selectivity remained similar [43]. On the other hand, Sedláková et al. showed that CNTs in a rubbery poly(ethylene-co-octene) matrix behave as an impermeable barrier, rather than promoting the transport [44].

**Metal organic frameworks (MOFs)** are a relatively new family of nanoporous crystalline compounds formed by self-assembly of transition metal ions or clusters that are linked by bridging organic ligands through strong bonds (Figure 2.11d). They present a new class of compounds with a many attractive characteristics, such as adjustable chemical functionality, pore shape and connectivity, high thermal stability, low density, ordered structure, high porosity, and tunable pore structure. Moreover, the $CO_2$ storage capacity in some MOFs is remarkably higher compared to zeolites and other carbonaceous materials. They are studied in more detail in this thesis work for the preparation of mixed matrix membranes based on the archetypal polymer of intrinsic microporosity, PIM-1.. Their effect on the $CO_2/CH_4$ transport properties and on the transport of other gases will be studied in Chapter 5.

#### 2.4.4.2 Gas Transport in mixed matrix membranes.

In the ideal case, the gas transport through MMMs depends above all on the properties of the polymer matrix and on those of the filler particle itself. In less ideal cases, the polymer-particle interface can play a major role, making even membranes based on non-porous filler particles more permeable and/or more selective than the neat polymer [45]. It can be mathematically described by different theoretical models of which most are adapted from thermal/electrical

conductivity models [46]. In fact, the constitutive equations governing electrical potential and the flux through membranes are analogues. A particularly useful model was developed by Maxwell in 1873 to predict the permittivity of a dielectric and this model can be use to predict the transport in mixed matrix membranes.

Maxwell model provides a simple and quantitative framework to calculate gas permeability in mixed matrix materials with aspect ratio near unity (e.g. spherical particles) for the dispersed phase and a relatively low particle loading. For such situations, the effective gas permeability in the mixed matrix membrane can be described according to two-phase equation:

$$P_{eff} = P_c \left| \frac{P_D + 2P_C - 2\Phi_D \left(P_C - P_D\right)}{P_D + 2P_C + \Phi_D \left(P_C - P_D\right)} \right| \qquad \text{Eq. 2.10}$$

where $P_{eff}$ is the effective permeability in the mixed matrix material, $\Phi$ is the volume fraction and the subscripts $D$ and $C$ refer to the dispersed and continuous phase, respectively. Other relations have also been proposed to describe the gas transport properties in MMMs, including three-phase Maxwell model, Higuchi model, effective media theory and Bruggeman model [45,46]. Several studies have compared the predictions of these various models and the results have been quite similar [49]. These models, however, are complicated in nature and the results do not always provide significant improvement over the two-phase Maxwell equation. Therefore, the two-phase Maxwell equation has been widely used as the key theoretical framework to correlate the transport properties in a polymer matrix embedded with spherical inorganic particles. MMMs with non-spherical particles, especially with high aspect ratio, require also different approaches, for instance the model proposed by Cussler for flake-like particles [50].

# Chapter 3. Pebax®/PAN hollow fibre membranes for $CO_2/CH_4$ separation [#]


## Abstract

Poly(ether-b-amide) (Pebax®1657)/ polyacrylonitrile (PAN) composite hollow fibre membranes for a potential use in $CO_2/CH_4$ separation were prepared by a new continuous coating method, referred to as cross-flow filtration. This technique allows to obtain the simultaneous coating of a large number of fibres, facilitating the scale-up. The dense layer was deposited in the lumen of the fibres allowing the coating of all the fibres in a single step. The coating on the inner surface of the fibres avoids the negative effects such as sticking or accidental mechanical damages occurring in the case of external coating. The membrane preparation was optimized by modulating different parameters. The optimal range of viscosity and concentration of the polymer solution to obtain a selective homogeneous Pebax® layer was identified. The presence of the Pebax®1657 dense layer was confirmed by IR spectroscopy and the morphology of the composite membranes was observed by SEM analysis. The gas separation performance of the membrane modules was determined by single gas permeation measurements. A preliminary optimization yielded membranes with $P_{CO2}$= 5*10$^{-3}$ [m$^3$ m$^{-2}$ h$^{-1}$ bar$^{-1}$], $\alpha_{CO2/CH4}$ = 18 equal to that of the neat dense polymer. The PEBAX®/PAN hollow fibres modules are potentially useful for application in the purification of biogas.


## 3.1 Introduction

Nowadays, the development of green alternative sources of energy is an active research area owing to an increase of the global energy demand. The use of sustainable and renewable energy sources is necessary because of environmental pollution and global warming due to the emission of greenhouse gases. In this context, biomass is one of the most promising alternative energy sources. The biomass is converted into biogas via anaerobic digestion by microorganisms. The

[#] Chapter based on the manuscript : E. Esposito, G. Clarizia, P. Bernardo, J.C. Jansen, Z. Sedláková, P. Izák, S. Curcio, B. De Cindio, F. Tasselli, Pebax®/PAN hollow fiber membranes for $CO_2/CH_4$ separation, *Chem. Eng. Process. Process Intensif.* 94 (2015) 53-61. DOI: 10.1016/j.cep.2015.03.016.

resulting is saturated water vapour saturated and contains 50-65% of methane, 30-40% of $CO_2$, traces of hydrogen sulphide, oxygen, nitrogen, ammonia, siloxanes and volatile organic compounds [51]. Since the heating value of biogas is proportional to the methane concentration, the removal of $CO_2$ and other impurities is required. Furthermore, these components can cause corrosion and freezing problems in pipes and connections. Cleaning and upgrading of biogas can be carried out either by conventional techniques (pressure swing adsorption, water scrubbing, absorption with organic solvents) or by innovative techniques such as the separation and purification of biomethane by membrane processes.

Among the possible biogas purification techniques, membrane processes present the advantage of operation simplicity, easy maintenance, safety and low operation cost [52] [53]. The choice of a membrane material for gas separation applications is a key factor based on specific physical and chemical properties, since these materials should be tailored to separate specific gas mixtures. Among the materials with high $CO_2$ affinity, Pebax® is a thermoplastic elastomer suitable for the $CO_2/CH_4$ separation. It is a multiblock copolymer containing linear chains of rigid polyamide segments interspaced with flexible polyether segments [54]. The balance of the hard and soft blocks provides a good $CO_2$ separation performance without loss of its permeability [55]. The hard polyamide blocks supply mechanical strength and the presence of the polar ethylene oxide (EO) group, increases the affinity for $CO_2$, allowing a good $CO_2$/non polar ($H_2$, $N_2$, and $CH_4$) species separation and permselectivity [56]. For these reasons, the polyether/amide block copolymers are interesting membrane materials for the particular gas polar-non polar mixture of $CO_2/CH_4$ from a natural stream as raw biogas.

Another very important aspect in the membrane preparation for gas separation is the polymer processability into hollow fibre membranes. Tasselli *et al*. [57]reported that the preparation of Pebax®-based composite hollow fibre membranes by direct spinning is not a viable route to fabricate stable, defect-free hollow fibres. However, Pebax® can be successfully used as a coating material for composite membranes, especially asymmetric hollow fibers for gas separation, adopting other preparation techniques. Composite Pebax®3533/PEI membranes were reported by Kim et al. [58]as suitable materials for the separation of sour gases ($SO_2$ and $CO_2$) from non-polar $N_2$. Ren et al. [59] used Pebax®1657 as selective material for $CO_2$ with multilayer PEI/PDMS/Pebax®1657/PDMS composite membrane according to dip-coating method. Liu et al. [60] investigated the effects of several parameters involved in the procedure of polysulfone hollow fiber spinning and Pebax®2533 coating on the permselectivity of the resulting composite membrane. For the Pebax®/polysulfone composite membranes a

permselectivity very close to the intrinsic permselectivity of a Pebax® dense membrane was found. Hollow fibre membranes for gas separation are usually made of a selective layer on the outer side according to the dip-coating method. However, in the case of the hollow fiber modules, it is difficult to obtain an inner separation layer using this method [61].

In this work, the possibility to obtain a poly(ether-b-amide) (Pebax®1657)/ polyacrylonitrile copolymer (PAN) composite hollow fibre membranes by a dynamic coating in the inner side of hollow fibres was studied. This method is promising for a future preparation of hollow fibres on an industrial scale because it allows the simultaneous and continuous preparation of many fibres. In addition, the deposition of the dense selective layer on the inner side is an advantageous configuration as it ensures the protection of the dense selective layer. The gas transport into the hollow fibre composite membranes was studied and the possibility to apply hollow fibre modules in the process of biogas purification was evaluated.

## 3.2 Experimental

### 3.2.1 Materials

Polyacrylonitrile containing 8 wt.% of vinyl acetate comonomer (PAN), MW 40,000 Da was supplied by Montefibre SpA (Italy). Pebax®1657**,** composed of 60% polythyleneoxide (PEO) and 40% of nylon 6, was supplied by Arkema (Italy) as pellets. Polyvinylpyrrolidone (PVP) and dimethylformamide (DMF) were purchased from BASF (Germany) and Sigma–Aldrich (Italy), respectively. Ethanol (99.5%) (EtOH) was purchased from Carlo Erba Reagenti (Italy) and used without further purification. All polymers were used as received. A two components epoxy resin (Stycast 1266, Emerson&Cuming, Belgium) was used in membrane module assembling. The gases for the permeation tests (nitrogen, methane, helium and carbon dioxide, all with purity of 99.99+ %) were purchased from Pirossigeno (Italy).

## 3.3 Membrane preparation

### 3.3.1 Hollow fibre preparation

Polymer solutions were prepared by adding the polymer powders (first PAN and then PVP) to DMF in a glass flask at 70 °C, under mechanical stirring until complete polymer dissolution. The

dope solution was then transferred into a tank, kept at a constant temperature (70 °C) and degassed under vacuum.

Asymmetric porous PAN hollow fibre supports were prepared by the dry–wet spinning technique according to the phase inversion process. The spinning set-up was already described previously[62]. Tap water was used as the external coagulant, while a mixture of distilled water and DMF was used as the bore fluid. The spinning conditions are reported in Table 3.1. The spun fibres were cut in pieces of 30 cm and immersed for 24 hours in pure water by refreshing water at least three times to remove residual solvent and soluble additive (PVP). The fibres were then kept in a 20 wt.% aqueous glycerol solution for further 24 hours to prevent the pore collapse upon drying at room temperature.

Membrane modules were prepared by potting four hollow fibres with epoxy resin inside 20 cm long glass tubes. The effective length of fibres was 18 cm and the membrane surface area was about 25 $cm^2$.

Table 3.1. Summary of spinning conditions for the preparation of PAN hollow fibres.

| | |
|---|---|
| Dope composition ( wt.%) | PAN: 15 |
| | PVP: 15 |
| | DMF: 70 |
| Dope flow rate (g $min^{-1}$) | 12 |
| Bore fluid flow rate ($cm^3$ $min^{-1}$) | 15 |
| Bore fluid composition: DMF/Water (wt./wt.) | 60/40 |
| External coagulant temperature (°C) | 25±2 |
| Air gap (cm) | 60 |
| Spinneret dimensions (ID/OD)(mm) | 1.0/2.0 |
| Room temperature (°C) | 20±2 |
| Relative Humidity (%) | 60 |

### 3.3.2 Composite Pebax ® /PAN membrane preparation by dynamic coating method

Composite membranes were produced by inner coating of the porous PAN hollow fibres with Pebax®1657. Pebax® solutions were prepared by swelling polymer pellets in a mixture of distilled water and ethanol (ratio 30:70 wt./wt.) at room temperature. Subsequently, a homogeneous dope solution was obtained by heating up to 80 °C under magnetic stirring.

The experimental setup used for the cross-flow filtration is illustrated in Figure 3.1. The Pebax® solution was fed into the lumen side of the PAN hollow fibres by means of a circulation pump and forced to filtrate through the hollow fibre bundle under a fixed trans-membrane pressure. Thereafter, the module was dried by flushing air in the shell side.

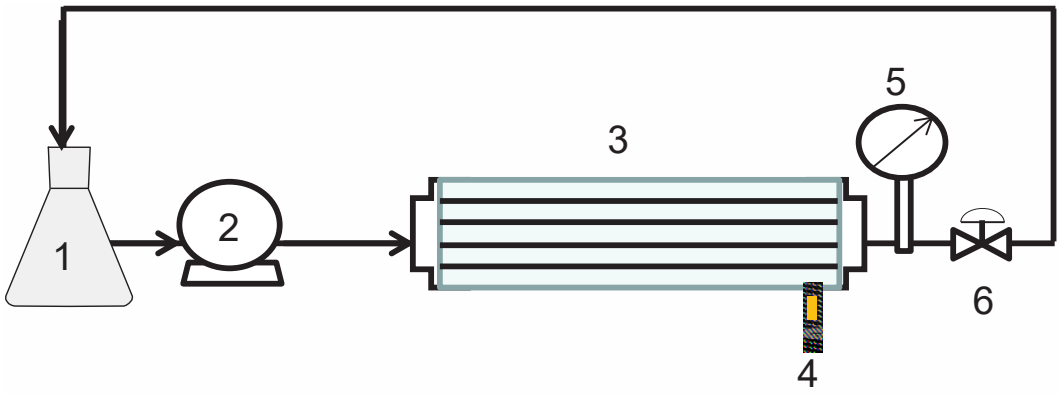


**Figure 3.1.** Scheme of the cross-flow filtration coating setup: 1) Pebax® solution tank; 2) circulation pump; 3) PAN hollow fibre module; 4) permeate; 5) manometer 6) pressure control valve.

## 3.4 Characterization techniques

### 3.4.1 Chemical and morphological analysis

The morphology of the hollow fibres was investigated by scanning electron microscopy (SEM) using a FEI QUANTA 200 instrument. Infrared spectroscopy (FTIR) analyses were performed by using a Spectrum Spotlight Chemical Imaging Instrument (Perkin Elmer). Membrane samples were immersed in liquid nitrogen to avoid deformation and to ensure a quick and uniform break, the cross section were observed. The presence and the thickness of the Pebax® coating layer on the inner surface of the hollow fibres were also determined via SEM observation.

### 3.4.2 Rheological characterization of the Pebax ®1657 solution

The viscosity of Pebax®1657 solutions at different concentrations was determined using a DV-III ultra rheometer (Brookfield), with concentric cylinders having a diameter of 82 mm. Rheological measurements were carried out on an ARES-RFS rheometer (TA Instruments, USA), equipped with a parallel plate geometry ($\Phi$ = 50 mm with a gap of 1.5±0.1 mm). A strain sweep test was

carried out in the deformation range from 1 to 100% (10 steps per decade) at a frequency of 1 Hz to determine the linear response region that was found between 6 and 20%. A value of 10% was assumed for all measurements that were carried out at 25°C. Silicon oil was used to prevent solvent evapouration.

The rheological properties of one representative Pebax® solution of 8 wt.% were determined by small amplitude oscillation tests, measuring the dynamic moduli, $G'$ (storage modulus) and $G''$ (the loss modulus), and the 'loss angle' tan(δ), the latter defined as [63]:

$$\tan(\delta) = \frac{G''}{G'} \qquad \text{Eq. 3.1}$$

This in turn is a measure of the relative weight of the liquid like behavior respect to the solid like one: less tan(δ) more solid like behavior and *vice versa*.

A time sweep test 1 Hz in the linear region lasting about 6000s was performed to investigate the occurrence of a change from liquid to gel structure.

## 3.5 Transport properties

### 3.5.1 Water permeability

The water permeance of the PAN hollow fibres was measured using distilled water fed into the bore side of the fibres. The water flux ($J_w$) is determined from the volume of permeate ($V_P$) collected per unit of time ($t$) through a membrane surface area ($A$) at fixed trans-membrane pressure ($\Delta P$) values:

$$J_w = \frac{V_P}{t \cdot A} \qquad \text{Eq. 3.2}$$

The measurements of the permeation rate were performed at steady-state condition under different $\Delta p$. The water permeance is defined as:

$$P_w = \frac{J_w}{\Delta P} \qquad \text{Eq. 3.3}$$

and can be calculated from the slope of the plot of $J_w$ versus $\Delta P$.

### 3.5.2 Gas permeability

The gas transport properties of both the porous PAN support and the Pebax®/PAN composite membranes were determined by pure gas permeation measurements in the set-up indicated in Figure 3.2. The effective thickness of the coating was determined from a plot of the measured permeance as a function of the known permeability coefficient for different gases. The measurements were carried out at different feed pressures ($\Delta p$ = 1-4 bar) and at room temperature (25 °C), in a dead-end mode, flushing the permeate side of the module with the same gas before each measurement to ensure that polarization of back-diffusion phenomena can be excluded.

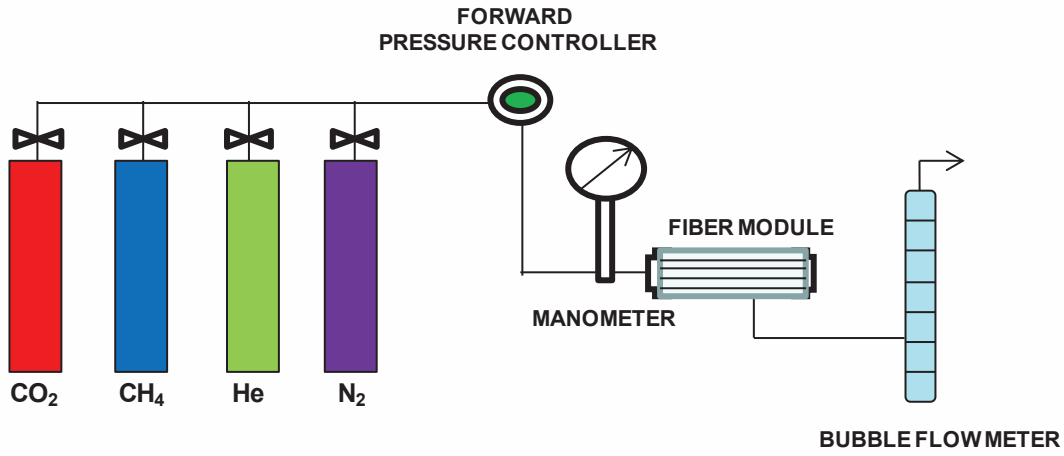


**Figure 3.2.** Scheme of the single gas permeation setup.

The gas permeance was calculated by the following equation:

$$P = \frac{Q_p}{A \cdot \Delta p} \qquad \text{Eq. 3.4}$$

where $Q_P$ is the permeate flow rate through a membrane with an effective area $A$ under a trans-membrane pressure difference, $\Delta p$ [64]. The flow rate $Q_P$ is measured volumetrically with a

manual soap bubble flow meter (Supelco, 0-1cc for composite membrane, 100-1000cc for the uncoated support).

The ideal permselectivity was calculated as:

$$\alpha_{A/B} = \frac{P_A}{P_B} \qquad \text{Eq. 3.5}$$

where $P_A$ and $P_B$ are the permeances of the pure gas *A* and *B*, respectively.

## 3.6 Results and discussion

### 3.6.1 Porous hollow fibre supports

The characteristics of the membranes prepared and used as support are given in Table 3.1 Since PAN solutions tend to undergo instantaneous demixing, resulting in the formation of a dense skin, PVP was added as a pore former [21]. A proper matching of the dope and bore fluid composition is fundamental for obtaining an open porous structure with sufficient mechanical resistance, without adding significant resistance to the gas transport in the final composite membrane.

The morphology of the support and of the composite hollow fibre membranes was investigated by SEM (Figure 3.5). The hollow fibre support shows an asymmetric morphology, characterized by a three-layer structure: a sponge-like structure in the fibre core, and two regions with finger-like macrovoids of different size close to the inner and outer surface (Figure 3.5a). The latter is due to the different compositions of the bore fluid and coagulation bath, as reported in Table 3.2. DMF was added to the bore fluid in order to delay the demixing rate and to reduce the polymer concentration in the interface, thus avoiding the formation of a dense skin layer on the inner surface of the fibre which would cause an additional resistance to the mass transport. The amount of DMF in the bore fluid also allows to tailor the pore size, a fundamental property for successful coating of the support [65]. Measurements of the pore size distribution of the prepared hollow fibres, carried out with $N_2$ at pressure up to 15 bar, showed that 90% of the pores lies in the 10-100 nm range.

The transport properties of the porous support were evaluated measuring the water and single gas permeability at room temperature. The water flux, $J_w$, increased in ca. 10 minutes to a plateau

value due to the removal of viscous glycerol during this operation. It is a function of the applied $\Delta p$ and it is linear up to 1.5 bar; the water permeability coefficient was determined as the slope of the corresponding straight line (Figure 3.3a). The value of 184 L $h^{-1}$ $m^{-2}$ $bar^{-1}$ lies in the typical range of porous ultrafiltration membranes. Permeation rate measurements with pure He, $CH_4$, $N_2$, and $CO_2$ confirm the expected Knudsen transport mechanism, where the permeance is inversely proportional to the square root of the molar mass of the gases (Figure 3.3b). This mechanism makes the porous support slightly selective for methane, with a $CO_2/CH_4$ permselectivity of 0.6. Minor deviations from the linear trend may indicate a not completely negligible resistance of the more open support structure in the core of the hollow fibre membrane, where viscous transport may also occur.

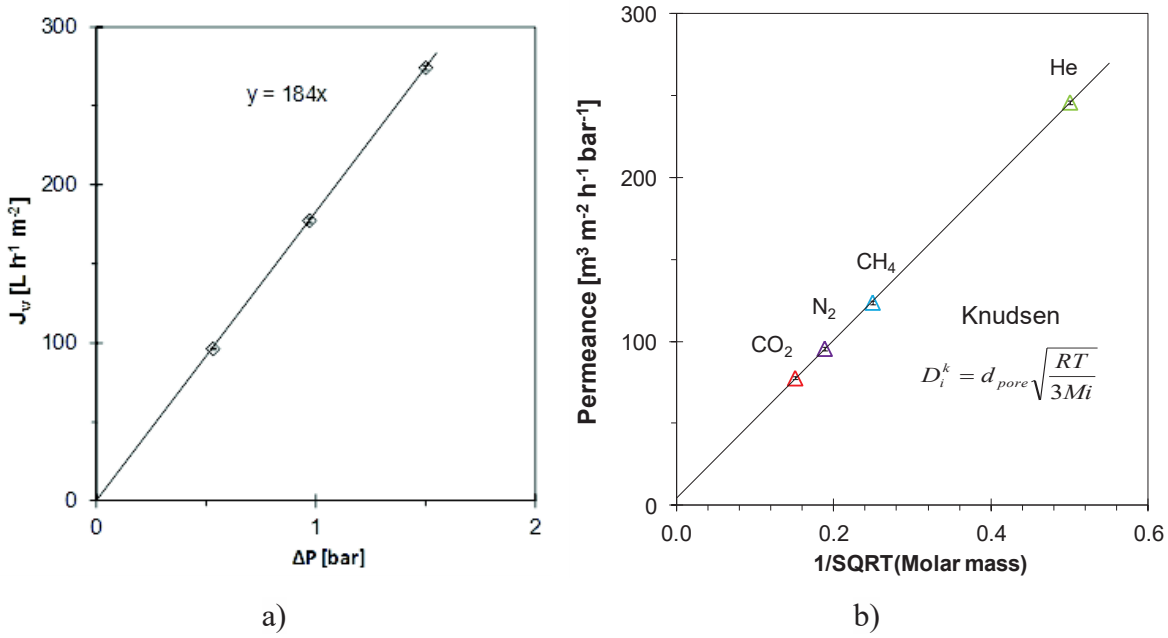


a) b)

**Figure 3.3.** Transport properties of the hollow fibre porous support. a) Water permeability. b) Gas permeance of He, $CH_4$, $N_2$, $CO_2$ at room temperature and $\Delta P$ = 0.5 bar.

## 3.7 Thin film composite hollow fibre membranes

### 3.7.1 Membrane preparation

During the preparation of the composite membrane by cross-flow filtration of the Pebax® solution (Figure 3.1), the porous structure of the PAN fibres allows the permeation of the solvent, while a sufficiently small pore size guarantees that a Pebax® layer can be deposited on

the fibre internal surface. Thus, the formation of the coating on the inner surface of the hollow fibre support occurs similarly to that of the cake layer during membrane fouling. To enhance the coating efficiency, the coating treatments were carried out in laminar flow conditions (Reynolds number lower than 10). Finally, the evapouration of the solvent consolidates the thin selective Pebax® layer.

The effect of different parameters such as concentration and viscosity of Pebax® solutions, coating time, operation pressure was investigated in order to identify the best conditions to obtain thin defect-free Pebax® layers. All the coating experiments were carried out at $\Delta P = 2$ bar with a temperature solution of 25 °C.

For a better understanding of the mechanism of the coating layer formation, different amount of Pebax® was dissolved in the mixture of EtOH/water (70/30 wt./wt.). The permeation of liquid mixture of EtOH/water (70/30 wt./wt.) was also compared with that of these polymeric solutions.

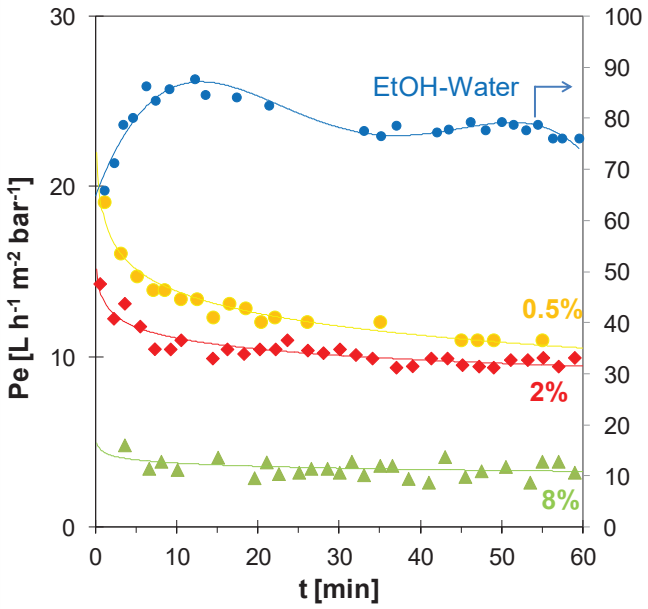


**Figure 3.4.** Permeation rate of Pebax® solution at different concentration (left side) and of the EtOH/water mixture (right side) through a PAN porous support during coating process.

As shown in Figure 3.4, the permeance of the EtOH/water mixture is higher than that of Pebax® solutions, and as expected, the permeance further decreases as the Pebax® concentration increases. The permeance of the polymer solution becomes virtually constant after few minutes of filtration at high Pebax® concentration (8 wt.%), while at low concentration (≤ 2 wt.%) it takes more than 30 minutes. This means that the dense layer formation takes place at different time,

depending on the Pebax® concentration. Interestingly, compared to the uncoated film, the liquid permeability of the membranes is ten times lower. This is in stark contrast with the gas permeability of the dried membranes, which decreases by more than 4 orders of magnitude as discussed below. This shows that the deposited polymer film during the cross-flow filtration process remains in a highly swollen state, resulting in a relatively low resistance to transport.

### 3.7.2 Membrane morphology and structure

The presence of the Pebax® coating layer on the inner surface of the hollow fibre is shown in Figure 3.5a The zoom in Figure 3.5b shows the good adhesion of the homogeneous, dense Pebax® coating layer on the support. Depending on the operating conditions, thicknesses ranging from ca. 1 to 15 microns were obtained. The thickness of the Pebax® layer for the most selective samples was about 5 microns.

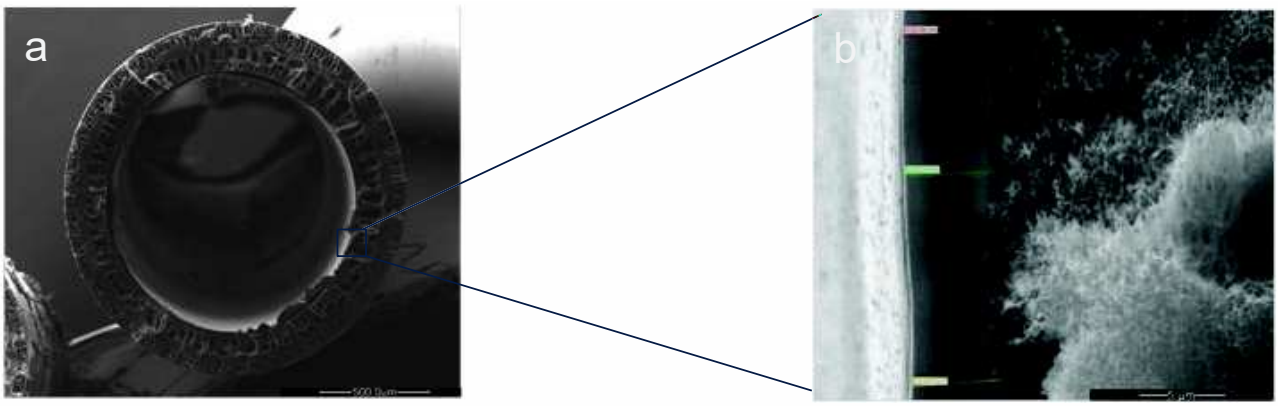


**Figure 3.5.** SEM images of the cross section of: a) C3 composite hollow fibre membrane; b) detail of the Pebax® coating layer on the inner surface.

The FTIR analysis of Pebax®/PAN composite membrane (Figure 3.6b) confirms the presence of the Pebax® coating layer on the support. The characteristic peak at 2243 $cm^{-1}$ due to nitrile stretching of acrylonitrile [66] is absent after the cross-flow treatment, while two distinct peaks, characteristic for the different Pebax® blocks, appear. The ether stretching of the PEO block is present at 1106 $cm^{-1}$ while nylon-6 gives a peak at 3300 $cm^{-1}$ due to N-H stretching [67] and a peak at 1640 $cm^{-1}$ related to the amide -C=O stretching [57]. Other peaks in the spectrum of composite membrane at 2920 $cm^{-1}$ and 2852 $cm^{-1}$ can be attributed to the asymmetric and symmetric stretching of C-H bond .

PAN

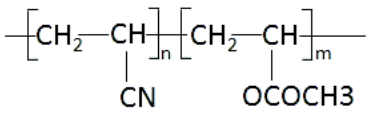


Pebax® 1657

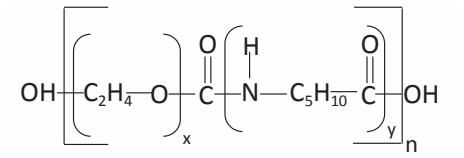


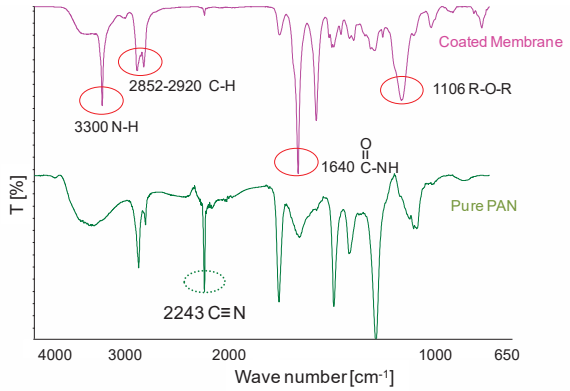


**Figure 3.6.** a) Structure of the polymers; b) FTIR spectra of PAN porous support and of a Pebax® composite membrane.

### 3.7.3 Transport properties of Pebax® /PAN composite hollow fibre membranes

An overview of the most significant samples and their transport property are given in Table 3.2.

Table 3.2. Transport properties of composite hollow fibre membranes coated at different conditions.

| Composite membrane | Pebax® wt.% | Coating layers | Treatment time [min] | Permeance [$m^3\ m^{-2}\ h^{-1}\ bar^{-1}$] | | $\alpha CO_2/CH_4$ |
|---|---|---|---|---|---|---|
| | | | | $CO_2$ | $CH_4$ | |
| A1 | 2 | 1 | 60 | 0.18 | 0.095 | 1.9 |
| B1 | 4 | 1 | 30 | 0.045 | 0.017 | 2.6 |
| C1 | 4 | 1 | 60 | 0.13 | 0.020 | 6.5 |
| C2 | 4 | 2 | 60 | 0.071 | 0.0096 | 7.4 |
| C3 | 4 | 3 | 60 | 0.041 | 0.0022 | 18.6 |
| D1 | 8 | 1 | 6 | 0.074 | 0.0097 | 7.6 |
| D2 | 8 | 2 | 6 | 0.047 | 0.0026 | 18.1 |
| E1 | 10 | 1 | 3 | 0.052 | 0.0029 | 18.0 |
| F1 | 10 | 1 | 6 | 0.0194 | 0.0011 | 18.0 |

The coating treatment significantly reduces the gas permeance of the original porous fibres by 3-4 orders of magnitude for all membranes and increases the permselectivity, as shown in Table 3.2, relating to the $CO_2/CH_4$ pair. The permselectivity for $CO_2$ means that the gas transport in composite membranes obeys to a solution-diffusion mechanism, typical for non porous

membranes. The Pebax® layer controls the gas transport, while the presence of pinholes/defects in some samples causes a difference between the actual $CO_2/CH_4$ permselectivity and the ideal value of ca 18.5 [55], reported as reference line in Figure 3.7a.

### 3.7.4 Effect of the Pebax® concentration

A Pebax®concentration below 4 wt.% always produces poorly selective samples, also after a prolonged treatment time. At a concentration of 4 wt.%, the $CO_2/CH_4$ permselectivity increases from 3 to 6 when increasing the coating time from 30 to 60 minutes (samples B1,C1 in Table 3.2). However, a single treatment is never effective for reaching the ideal of the neat polymer, even if the time of the treatment is further increased. Only after three successive coatings with intermediate drying, the composite membrane becomes completely selective (Figure 3.7a), while $CO_2$ becomes three times less permeable with respect to the first treatment (samples C3 and C1) . The single gas permeation measurements, carried out in the pressure range 1-3 bar on membrane $C_3$, allow to determine the effective thickness of the coating layer. The permeance for all gases results quite constant in the investigated pressure range (Figure 3.7b) and the gas permeance order is the following: $P_{CO2} > P_{He} > P_{CH4} > P_{N2}$, in line with the values for neat Pebax® and with the hypothesis of a solution-diffusion mechanism.

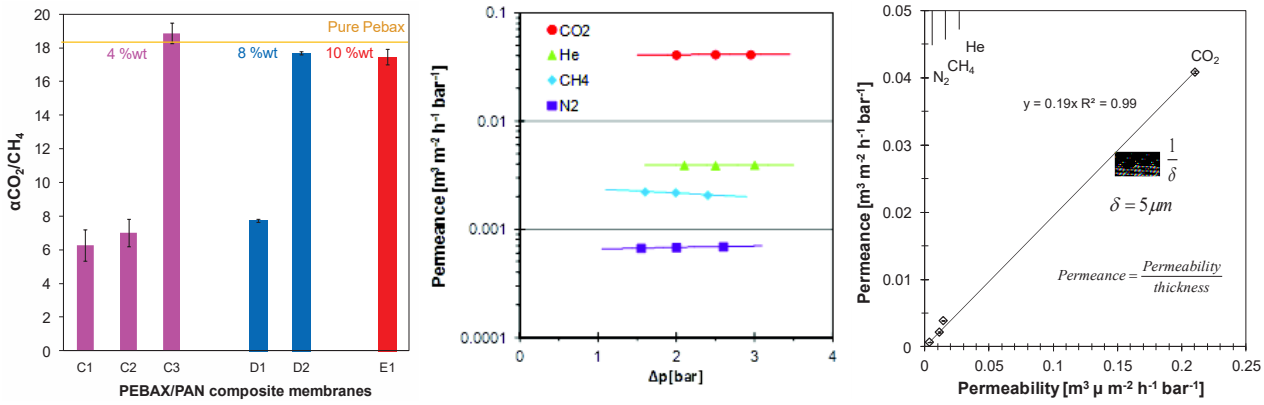


a) b) c)

**Figure 3.7.** a) $CO_2/CH_4$ permselectivity vs. concentration and number of coating for Pebax®/PAN composite membranes; b) Influence of feed pressure on gas permeability of $CO_2$, He, $CH_4$, and N2 at room temperature for membrane C3; c) Permeance through C3 membrane vs. the permeability of different gases through a neat Pebax® dense membrane [24].

The gas permeance of all composite membranes, is plotted *vs*. the permeability of the same gases in the neat Pebax®, expressed in $m^3$(STP) μm $m^{-2}$ $h^{-1}$ $bar^{-1}$. Thus, the effective thickness of the coating layer for permeation can be calculated from the slope of the linear regression in this plot [24]. In the case of membrane C3, the effective Pebax® layer was found to be 5 μm thick (see Figure 3.7c); this estimation is in a good agreement with the thickness observed in SEM micrograph (Figure 3.5b). The good correlation between the permeance of the composite membrane and the neat Pebax®, confirms that the transport is not affected by the porous support.
Starting from a 8 wt.% Pebax® solution, a final composite membrane with the permselectivity close to that of the neat polymer is already obtained after 2 coatings of 6 minutes each (Sample D2). After a single coating, the membrane still has some pinhole defects, decreasing the permselectivity to 8.
A further increase of the Pebax® concentration to 10%, yields composite membranes with the appropriate permselectivity with a single coating. The time of the treatment does not affect but the effective thickness reduces from ca. 11 to 5 microns when reducing the treatment time from 6 to 3 minutes (samples E1 and E2).

### 3.7.5 Effect of Pebax® solution viscosity

The solution viscosity depends on the polymer concentration [68], and in order to explain in-depth the effect of the Pebax® concentration during the coating treatment, the viscosity of the solutions was measured as a function of time and concentration. The viscosity of 4 wt.%, 8 wt.% and 10 wt.% Pebax® solutions at 25 °C is plotted as a function of time in Figure 3.8. The initial viscosity of the solutions increases from 13 cP to 100 cP as the Pebax® concentration increases from 4 to 10 wt.%. The viscosity of 4 wt.% solutions at 25 °C is approximately constant in the time. On the contrary, for the 8 wt.% solution, the viscosity increases from 30 cP to 40 cP and for the10 wt.% Pebax® solution it increases dramatically up to 800 cP after 30 minutes. This means that, at low Pebax® concentrations, the viscosity of the solution remains roughly constant during the coating treatment, whereas at high Pebax® concentrations (e.g. 10 wt.%) only short coating treatments can be carried out with a stable solution. On the other hand, only when operating with the concentrated solutions with a viscosity of about 100 cP, defect-free composite Pebax®/PAN membranes were obtained after a single coating. Less concentrated solutions require multiple or long time treatment to reach a homogeneous defect-free Pebax® layer with the ideal Pebax® permselectivity. The less concentrated solutions are not viscous enough to

prevent the massive infiltration into the porous support and are unable to produce a continuous layer that covers all pores on the inner surface of the hollow fibres. Subsequent treatments allow to repair the residual small pinholes still present in the selective layer.

Interestingly, in spite of an increase in viscosity of the 8 wt.% solution as a function of time, a prolonged coating treatment does not lead to a better membrane. While the permeance decreases as could be expected for an increased layer thickness, the permselectivity decreased as well (Figure 3.8b).

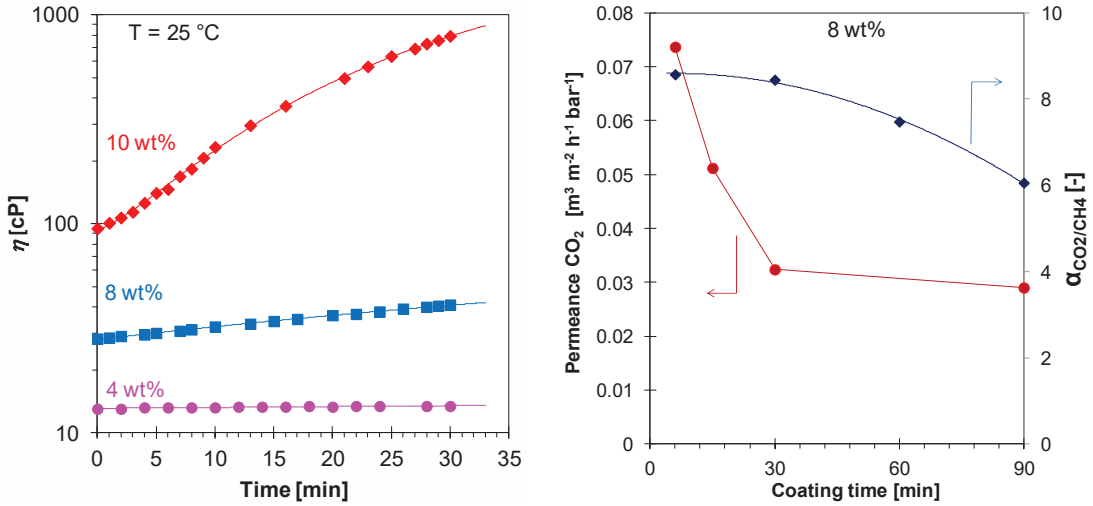


a) b)

**Figure 3.8.** a) Viscosity (T = 25°C) as a function of time for Pebax®1657 solutions with different concentrations. b) Resulting permeability and permselectivity of membranes coated with the 8 wt.% solution for different coating times .

The origin of the viscosity increase as a function of time was studied in more detail by rheological analysis under small-amplitude oscillatory shear during a time sweep test. Figure 3.9 shows that at beginning the solution behavior is liquid like because the value of the liquid component prevailed (G"＞G'), thereafter a very strong increase of both the moduli G' and G" is exhibited in two hours, but, while G' increases over more than 5 orders of magnitude, G" still increases significantly but much less. Then, a cross-over of G' respect to G" at 30 minutes occurs and according to Winter gel theory [69], this corresponds to the onset of a gel structure to which corresponds either a high value of viscosity and elasticity, with a marked solid like behavior corresponding to a value of tagδ≅ 0,3. This result apparently appears in contrast with the data found for the 8% solution in the shear viscosity test that does not give this great change in the rheological behavior. It is well known that the shear viscosity experiment, even at low

shear rates, tends to continuously destroy the onset of the forming gel structure. On the contrary, oscillatory measurement are at equilibrium, thus allowing the gel structure formation. In Figure 3.8b it was seen that the $CO_2$ permeance decreased up to approximately the same coating time while longer coating times give comparable $CO_2$ permeances. This effect can be ascribed to an increased thickness of the deposited polymer layer up to ca. 30 minutes, whereas the microgel particles formed in the solution at longer times are subject to too high shear forces to be effectively deposited onto the membrane surface. The microgel particles also compromise the formation of a defect-free film and may even damage the existing film, resulting in a slightly lower permselectivity. Apparently, an increasing viscosity of the coating solution is only beneficial if this viscosity derives from the increasing polymer concentration and not from time related gelation. Although after gelation of the more dilute solutions, the latter are still capable of coating the membrane, the integrity of the resulting membrane is insufficient, leaving pinhole defects and reducing the permselectivity.

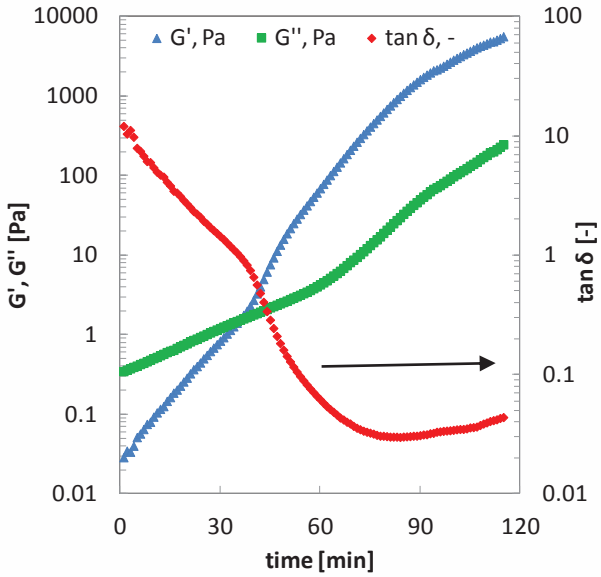


**Figure 3.9.** Influence of time on the rheological properties of a 8wt.% Pebax® solution at 25°C.

### 3.7.6 Effect of Pebax® solution temperature

Gelation in semi-crystalline polymers is normally due to the formation of microcrystalline domains, in this case of the polyamide block in Pebax®. The solution stability is thermodynamically controlled and depends on the temperature, while the crystallization rate is

kinetically controlled and depends on the degree of supercooling and on the polymer concentration. As a further validation of the combined role of concentration and viscosity of the coating solutions, the effect of the temperature on the dense layer formation was investigated. Thus, a set of composite membranes was prepared using a 10 wt.% solution and a coating time of three minutes, at three different temperatures. The viscosity analysis of the starting polymeric solutions and the performance of the prepared composite membranes are reported in Figure 3.10.

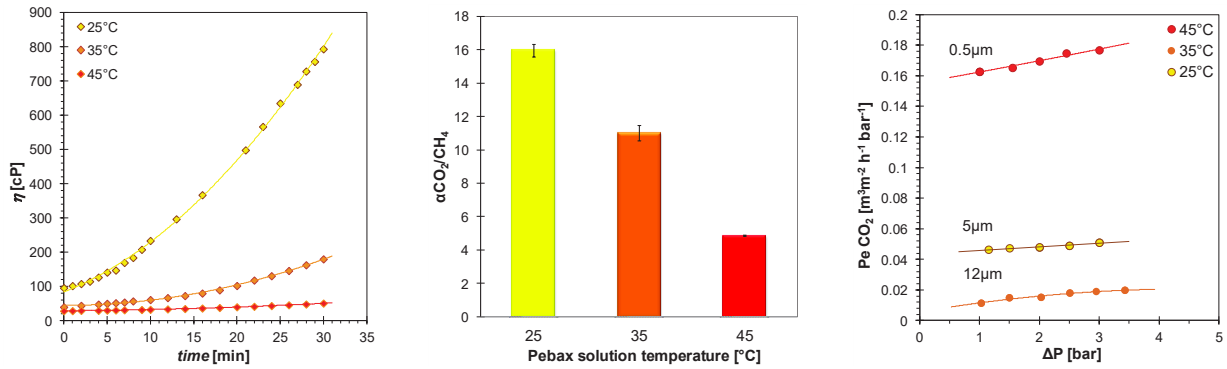


a) b) c)

**Figure 3.10.** Effect of temperature on: a) Viscosity of 10 wt.% Pebax®1657 solutions. b) $CO_2/CH_4$ permselectivity and c) $CO_2$ permeance of composite membranes coated with a 10 %wt solution at three different temperatures ( 25 °C; 35 °C; 45 °C).

The viscosity of a 10 wt.% Pebax® solution at 25 °C, 35 °C, and 45 °C was monitored for 30 minutes (Figure 3.10a). The initial value decreased from 100 cP to 30 cP as the temperature increased from 25 °C to 45 °C. The solution at 45 °C keeps an almost constant viscosity during the experiment, whereas the solutions at 35 °C and especially at 25 °C show an exponential increase of their viscosity. The composite Pebax® /PAN membranes, prepared by a single coating for 3 minutes with these three different solutions, were tested for the gas separation: $CO_2/CH_4$ permselectivity and $CO_2$ permeance are reported in Figure 3.10b and 10c. $CO_2/CH_4$ permselectivity decreases as the temperature of the coating solution increases. This trend can be explained in terms of low viscosity causing a significant permeation of the coating solution through the porous support. This makes more difficult the formation of a homogeneous dense layer on the inner surface and consequently, the membrane permselectivity decreases. It occurs in analogy with the results obtained in a single coating when diluted Pebax® solutions were used (A1, B1 and C1 samples in Table 3.2). As shown in Figure 3.10c, the highest $CO_2$ permeance was observed on the sample treated with the solution at 45 °C. In this case, a defective layer of less

than 1 μm was formed. The Pebax® solution at 35 °C with an initial viscosity of 45 cP shows the lowest $CO_2$ permeance probably due to the filling of the support pores by the Pebax® . Only at 25 °C the polymer solution has the appropriate viscosity that guarantees a layer of 5 μm, well adhered to the porous support, and having the same $CO_2/CH_4$ permselectivity of thicker neat Pebax® films. This confirms again that a solution with a viscosity around 100 cP is required for obtaining defect-free Pebax® /PAN composite membranes.

## 3.8 Modelling of the transport properties

For a better understanding of the parameters playing a role in the membrane preparation process, a model was developed in collaboration with D. I. M. E. S. This model correlates the preparation conditions to the two most important parameters describing the membrane performance: the $CO_2$ permeability, which can also be expressed as an effective membrane thickness, and the $CO_2/CH_4$ selectivity, which is a measure of the membrane integrity for a given material.

### 3.8.1 Setup of an Artificial Neural Network

The ANN is composed of a number of neurons operating in parallel. It is possible to distinguish two kinds of neurons: input neurons and output neurons. The simplest kind of neuron is characterized by a scalar input, predicting the performance of Pebax®/PAN membranes as a function of some key coating process variables, such as the number of coatings, the polymer concentration, the duration of the treatment and the trans-membrane pressure (Inputs). These input variables exhibit a major influence on both $CH_4$ and $CO_2$ permeance (Outputs). Among the possible neural models, one of the most common ones is the perceptron, which represents a single layer network, whose weights and biases are continuously adjusted to obtain a correct target vector when presented with the corresponding input vector. A multilayer perceptron (MLP) network is a supervised network consisting of, at least, three layers: an input layer, one or more hidden layers and an output layer Figure 3.11.

The developed ANN consists of an input layer with 4 neurons (corresponding to the system inputs); a hidden layer with 20 neurons, and an output layer comprising 2 neurons, which correspond to system outputs. The proposed model has to be considered as general and versatile, since it allows predicting both system outputs, the two gas permeances. The latter produces the

final network output, which is compared to a target vector, generally represented by a set of available experimental data. The proposed neural model was implemented to predict the dependence of system outputs upon the considered inputs. An iterative algorithm was exploited to eventually achieve the final neural model structure:

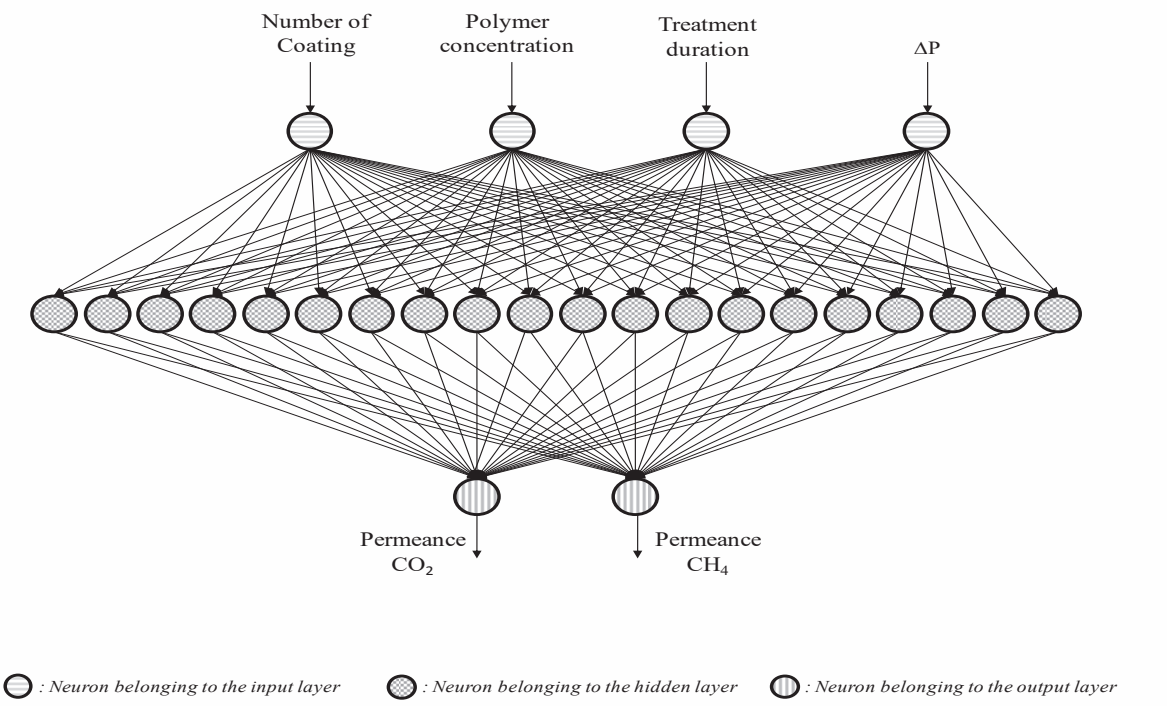


**Figure 3.11.** Structure of the implemented ANN model

The original experimental data, corresponding to 40 unique measurements, was randomly subdivided into three different datasets, reserving 70% of the points to achieve neural network training and 15% of the points to validate the neural model predictions during ANN development. The remaining 15% of the experimental measurements were finally used to perform the so-called post-simulation analysis, aimed at testing the neural model reliability in a set of conditions never exploited before. A set of proper convergence criteria, based on the calculation of the maximum errors between the experimental data (target) and the neural model predictions, was used to verify that the ANN was actually capable of predicting the influence of the operating conditions used in membrane preparation on its macroscopic performance, expressed in terms of $CH_4$ and $CO_2$ permeance.

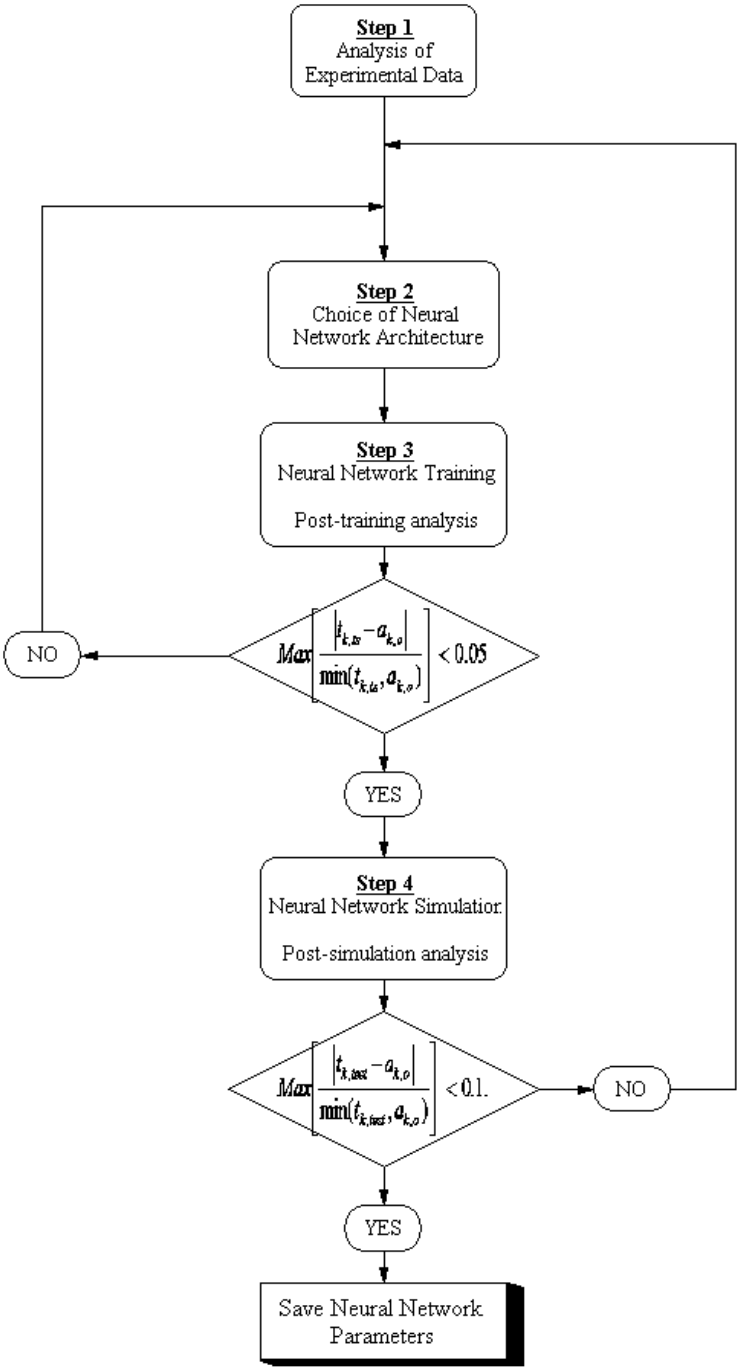


**Figure 3.12.** The flow diagram of the ANN algorithm.

The following two figures prove that the developed neural model can be actually considered as highly reliable. A comparison between the original experimental values (target) and the neural model outputs shows a very good agreement either with a dataset used during ANN development (training) or with a set of data never exploited during the so-called learning phase.

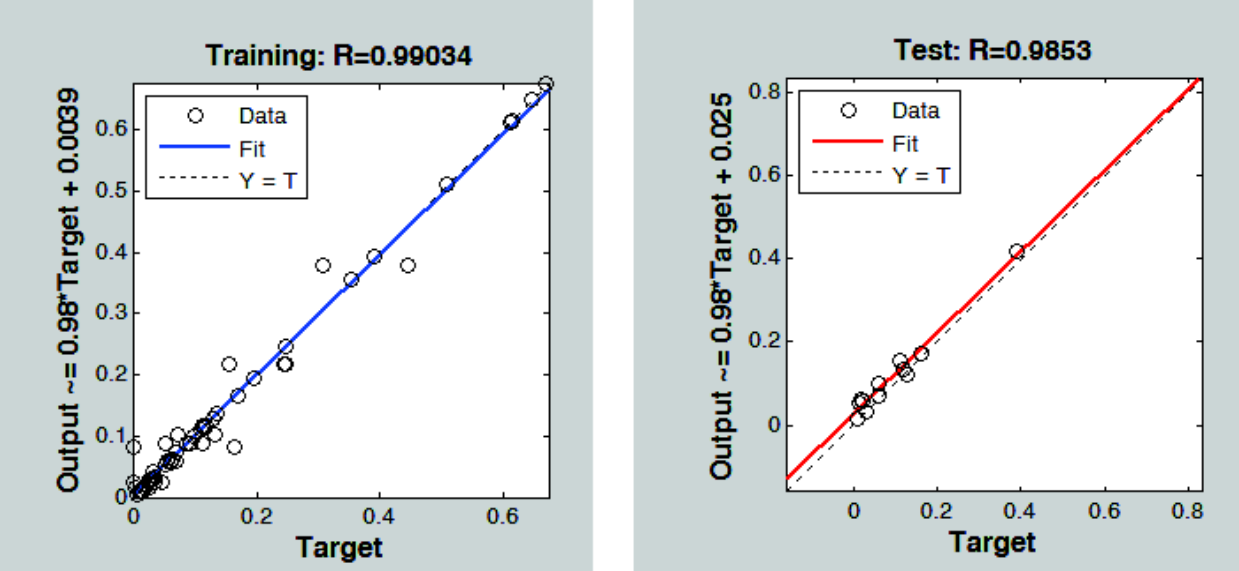


**Figure 3.13.** Neural model performance referred to training and structure of the test data.

Based on the previous results, the present ANN represents a power fool to obtain indications about the actual system behaviour in a set of conditions never tested during the already-performed experimental analysis. This is particularly useful because it enables the prediction of the membrane performance under given permeation conditions, even if these conditions have never been tried before. Obviously, the next step would be to find a model which is able to predict the optimum conditions for designing the membrane with the best possible performance. Figure 3.14a and Figure 3.14b show the effect of the polymer concentration on the $CH_4$ and $CO_2$ permeance.

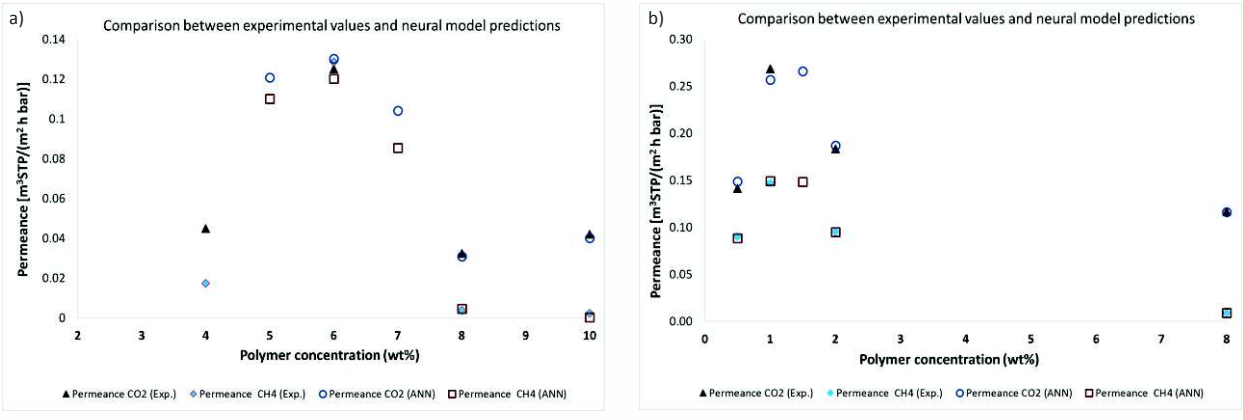


*Number of coating:1; Treatment duration: 30 min; TMP = 2 bar*

*Number of coating:1; Treatment duration: 60 min; TMP = 1 bar*

**Figure 3.14.** Comparison between experimental values and neural model predictions using as input variables: a) a single coating, 30 min coating time and trans-membrane pressure bar. b) a single coating, 60 min coating time and trans-membrane pressure bar.

The ANN was exploited both in a set of conditions already tested in the lab-scale plant (a very good agreement can be noticed) and in a completely new set of experimental conditions. This is important and means that since the proposed model allows achieving a detailed knowledge of the system at hand, without performing costly and labor intensive experiments. In addition, by the proposed neural model, it will be possible to identify which set of operating conditions has to be chosen in order to achieve specific objectives, regarding for instance, the maximization of $CO_2$-$CH_4$ selectivity, which is extremely important in biogas upgrading.

### 3.8.2 Construction of a hybrid model for model validation and determination of the effective thickness of the dense layer in the case of pinhole defects

#### 3.8.2.1 Introduction on the transport in thin film composite membranes

The gas or vapour permeance, $\pi$, of polymeric membranes is generally defined as the volumetric flow rate per unit area and driving force and is generally expressed in $m^3_{STP}/(m^2\ h\ bar)$:

$$\pi = \frac{Volume}{Area \cdot Time \cdot Pressure} \qquad \text{Eq. 3.6}$$

In porous membranes various mechanisms may occur, with or without interaction with the membrane material. For light gases with little or no interaction with the membrane material, the main transport mechanisms are viscous flow and Knudsen diffusion. Viscous flow dominates for large pores and at high pressures, whereas Knudsen flux is the main mechanism at low pressure and in the case of very small pores. Their ratio can be used to calculate the average pore size [70]. The permeance depends on the nature of the pores, rather than on the membrane material.
In dense membranes, the permeance $\pi$, relates to the materials properties and it is inversely proportional to the dense film thickness. Multiplication of the permeance and the film thickness, $L$, therefore yields the permeability coefficient, $P$, which is only a property of the material:

$$P = \pi \cdot L \qquad \text{Eq. 3.7}$$

The transport in dense membranes is governed by the well-known solution-diffusion mechanism [59] and the permeability coefficient is a product of the gas diffusion coefficient, $D$, and its solubility, $S$:

$$P = D \cdot S \qquad \text{Eq. 3.8}$$

In ideal cases $P$, $D$ and $S$ are constants and knowing two of them is sufficient to calculate the third.

In thin film composite membranes without a gutter layer only the film above the open pores of the porous support membrane is active for transport. Hence, the permeance is a function of the dense film thickness and of the surface porosity. In this case, one can define an effective thickness of the dense skin, $L_{eff}$, as the ratio of the known permeability coefficient of the dense polymer and the measured permeance of the composite membrane. The value of $L_{eff}$ can be calculated from the measured permeance via the equation:

$$L_{eff} = \frac{P}{\pi} \qquad \text{Eq. 3.9}$$

This is an important performance indicator for the membranes, because a lower thickness corresponds to higher fluxes.

The second performance indicator of a membrane is its selectivity. The ideal selectivity, $\alpha_{A/B}$, is defined as the ratio of the permeability coefficient of two different gases A and B:

$$\alpha_{A/B} = \frac{P_A}{P_B} \qquad \text{Eq. 3.10}$$

#### 3.8.2.2 Quantification of the transport properties of thin film composite membranes

In real membranes, the selectivity is often lower than the ideal selectivity due to the presence of pinhole defects in the thin selective layer. Indeed, in the present work, due to incomplete coating of the porous support fibres the selectivity of various membranes is lower than that of a defect-free neat Pebax film. Gas transport in the small pinholes takes place via Knudsen diffusion, which is inversely proportional to the square root of the molar mass. Thus the permeance of gas

species *i* for a membrane with pinhole defects can be expressed by the sum of a solution-diffusion term through the dense film, and a Knudsen diffusion term through the pinhole defects:

$$\pi_i = \frac{P_i}{L_{eff}} + \frac{C_{Kn}}{\sqrt{M_i}} \qquad \text{Eq. 3.11}$$

Where $C_{Kn}$ is a constant related to Knudsen diffusion, depending on the surface porosity, tortuosity, pore size and temperature. These parameters do not depend on the gas type and therefore $C_{Kn}$ is the same for all gases. For two different gases, Eq. 3.11 can be solved numerically, yielding the value of the effective thickness and the Knudsen constant. Thus, this equation allows the correct calculation of the effective thickness of the skin, even in a membrane with pinhole defects if the number of pinholes is not so large that they dominate the transport. When the permeation data are known for more than two gases, the same equation can be used but it must be solved by a least squares optimization method, as described previously [13],[60]. Alternatively, $C_{Kn}$ and $L_{eff}$ can be calculated numerically using only two gases, and the additional gases can be used for the validation of the model.

An example of the calculation of the effective membrane thickness, $L_{eff}$, via Eq. 3.11 is given in Figure 3.15 for two different representative membranes. For a selective membrane, a plot of the permeance as a function of the permeability coefficient of He, $N_2$, $CO_2$ and $CH_4$ yields a virtually perfect correlation (Figure 3.15A) and the effective membrane thickness is given by the reciprocal slope of the curve and equals 5 μm. At the same time there is no correlation between the permeance and the square root of the molar mass of the gases (Figure 3.15C), excluding the Knudsen diffusion mechanism. For the less selective membrane, there is a fair correlation between the permeance and the permeability coefficient, but the fit clearly does not pass through the origin (Crosses and blue line in Figure 3.15B). Similarly, there is a fair correlation with the square root of the molar mass, except for $CO_2$ (Crosses and blue line in Figure 3.15D) which has a much higher permeance than predicted by the Knudsen diffusion mechanism due to a significant contribution of the solution-diffusion mechanism. Interestingly, the total permeance can be decomposed into a contribution of solution-diffusion (green circles and line in Figure 3.15B) and a contribution of Knudsen diffusion magenta circles and line in Figure 3.15D). In spite of the clear presence of pinhole defects, giving rise to significant contribution of Knudsen diffusion for the relatively less permeable He, $N_2$ and $CH_4$, the slope of the green line in Figure 3.15B still allows an accurate estimation of the effective membrane thickness (3.3 μm)

The procedure discussed here to calculate the effective membrane thickness based on the permeation data of each membrane for all available gases thus allows the construction of a hybrid model which will be the aim of future work.

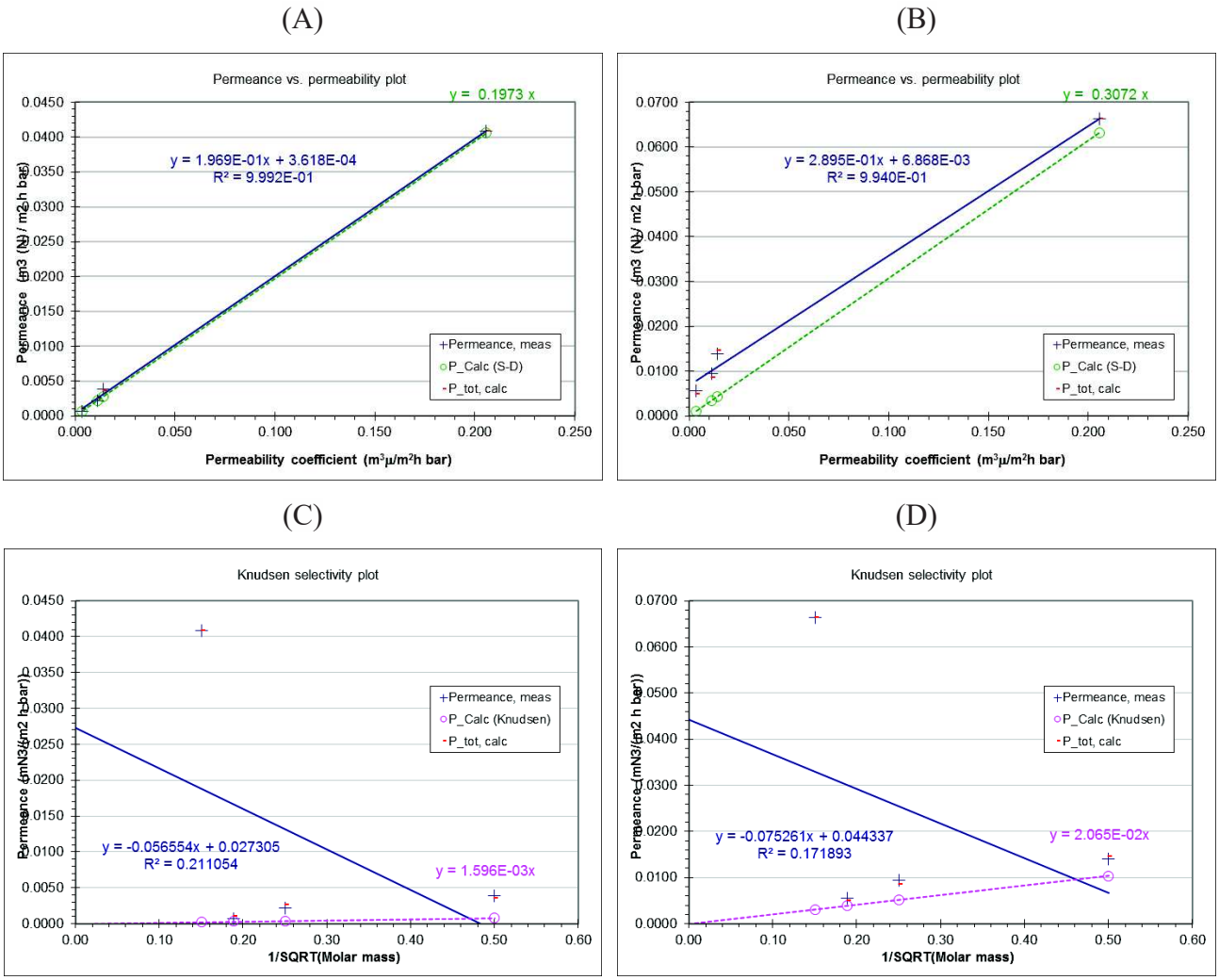


**Figure 3.15.** Graphical visualization of the determination of the effective membrane thickness for two representative thin film composite membrane according to the fitting procedure with Eq. 3.11 described in the text. Graphs (A, C) represent a selective membrane with negligible pinhole defects; graphs (B,D) represent a moderately selective membrane with pinhole defects. Neat Pebax® 1657 data are taken from Ref. [61].

## 3.9 Conclusions

Composite Pebax® /PAN hollow fibre membranes were successfully prepared by means of a dynamic cross-flow filtration coating method. This method is suitable for coating of fibres at the

inside and has the advantage that it can be applied simultaneously to a large number of fibres while they are already mounted in a membrane module. By controlling different parameters, such as the concentration and the viscosity of the polymer solution, the time and number of coating treatments, the thickness and the permeability of the membranes can be tailored. It was found that the viscosity of Pebax® solutions is the most influent parameter determining the dense layer formation during the coating process.

The viscosity depends on two parameters: the concentration and the temperature of the Pebax® solution, related to the amount of polymer and its aggregation state, respectively. Both factors have a strong effect on the dense layer formation. Increasing the concentration of the polymer solution yields dense film after a smaller number of coatings. In particular, three subsequent coatings are needed when using a 4 wt.% solution, two for an 8 wt.% solution and only one for a 10 wt.% solution. This can be explained because a high polymer concentration prevents intrusion of the polymer solution into the support pores and forms a more coherent film. On the other hand, a high coating temperature increases the solution stability but decreases the viscosity of the polymer solution, making the formation of a dense layer more difficult and causing a decrease of the $CO_2/CH_4$ permselectivity. The time of the treatment has an effect on the gas permeance but hardly on the permselectivity. The appropriate conditions to obtain in a single coating a dense and selective Pebax® layer were found: Pebax® viscosity of 100 cP and dynamic coating time of 3 minutes. The membranes prepared with these parameters demonstrate an optimum thickness of less than 5 μm and a $CO_2/CH_4$ permselectivity of ca.18, similar to that observed for the neat polymer. The FT-IR analysis confirms the presence of Pebax® dense layer, while the single gas permeation tests and the SEM analysis tests of the composites allow the calculation of the effective membrane thickness. The selective composite Pebax®/PAN hollow fibre membranes can be used to separate the $CH_4$ from $CO_2$ and could be potentially employed for biogas treatment. In the present work the coating technique was applied to obtain dense gas separation membranes and the method can in principle be extended to other membrane types.

# Chapter 4. Preliminary study on the potential use of membrane contactors for $CO_2/CH_4$ separation by facilitated $CO_2$ transport in ionic liquids

## 4.1 Abstract

The present study reports a way to increase the $CO_2$ solubility in the ionic liquid [BMIM][OTf] by the use of the enzyme Carbonic Anhydrase (CA), and the investigation of this principle as an approach to achieve $CO_2$ facilitated-transport in membrane contactors. For this purpose, a membrane contactor with polyacrylonitrile (PAN) hollow fibres, filled with the ionic liquid, is tested for gas sorption of a mixture of $CO_2$ and $CH_4$. The objective is to verify the possibility to use this principle for the purification of methane from biogas by selective removed of $CO_2$. The most abundant impurity in biogas is $CO_2$ and its removal is necessary in order to increase the methane concentration, and thus the energy density of the biomethane. Among the various $CO_2/CH_4$ separation techniques, a potentially suitable method is represented by the $CO_2$ capture with ionic liquids (ILs). The idea to use *Carbonic Anhydrase* is inspired by the fact that Room Temperature Ionic Liquids are often used as a reactive medium for homogeneous catalysis, suitable for various applications, while enzymes are known in some cases to preserve their activity in ILs.

## 4.2 Introduction

Among the different types of membranes used for the separation of carbon dioxide, a new class of membranes is becoming increasingly important: supported liquid membranes (SLMs) with a facilitated transport of $CO_2$ [68–71]. Supported liquid membranes generally consist of a selective solvent that is impregnated into the pores of a membrane support. The liquid of the selective layer can give a superior performance in terms of permeability and selectivity with respect to dense polymeric membranes. However, SLMs in industry suffer from the loss of volatile organic solvents. To address this problem, Ionic liquids (ILs) are proposed as alternatives to organic

solvents to act as separation media in SLMs. They represent a new generation of membranes: supported ionic liquid membranes (SILMs) [71–74]. The ionic liquids are molten salts at room temperature, with a negligible vapour pressure, high thermal stability, high ionic conductivity and finally they are able to solvate various compounds with their widely varying polarity [75]. They are called "designer-solvents" because ILs have malleable physical-chemical properties, given by the possibility to choose a cation and an anion among thousands of different combinations. Furthermore, their interest is rising as environmental friendly solvents for many synthetic and catalytic processes [67]. Additionally, ionic liquids with a particular ability to solubilize and concentrate $CO_2$ (task-specific ionic liquids), will provide the perfect environment for the reaction catalyzed by specific $CO_2$ carriers. Membranes, in which an enzyme, solubilized in a suitable IL as the solvent, is circulated through the lumen of hollow fibres, can be one of the most attractive facilitated transport membranes to be used in gas separation. Ionic liquids with high affinity for $CO_2$ assure an enhanced local concentration of $CO_2$ and the necessary level of water. The $CO_2$-facilitated transport is operated by a carrier and the main carrier with a high affinity for the $CO_2$ is the *enzyme Carbonic Anhydrase* (CA). This kind of facilitated transport is based on the same principle as the biological system of the human respiration, in which the enzyme catalyzes the reversible reaction of carbon dioxide with the water to produce the bicarbonate [8]. This chapter reports a way to increase the $CO_2$ solubility in the ionic liquids by the use of the enzyme Carbonic Anhydrase (CA). The investigation of this principle may eventually lead to an approach to achieve facilitated $CO_2$ transport in membrane contactors.

## 4.3 Experimental section

### 4.3.1 Materials

#### 4.3.1.1 Ionic liquids

All ionic liquids used in this chapter belong to the imidazolium-based family (Figure 4.1). The ionic liquids used are six: [BMIM][$NTf_2$], [BMIM][$PF_6$], [BMIM][OTf]; [EMIM][$NTf_2$], [EMIM][$BF_4$], [EMIM][dca] supplied by Merck (Table 4.1). The first three ILs contain the cation [$BMIM^+$] with the butyl group in the 1-nitrogen position. The others contain the cation [$EMIM^+$] with the ethyl substituent in the 1-nitrogen position. The anions are different for most ionic liquids.

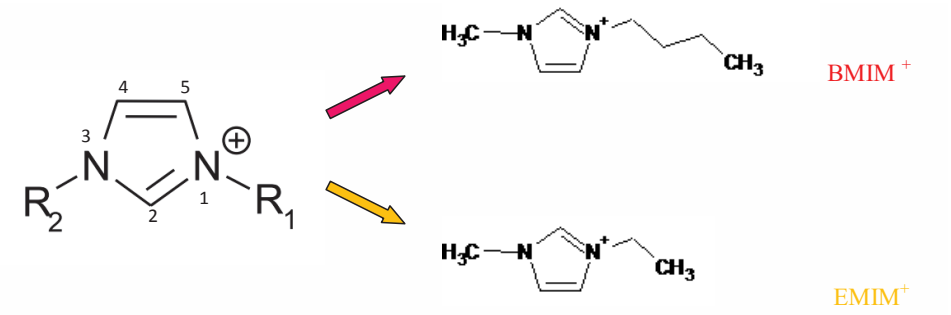


**Figure 4.1.** Imidazolium cation structure used in this work and specific structures

Table 4.1. Chemical structures and conventional codes of the ionic liquids studied

| Name | Structure | Name | Structure |
|---|---|---|---|
| [BMIM][$NTf_2$] | 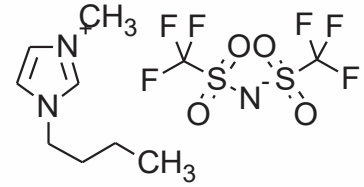 | [EMIM][$NTf_2$] | 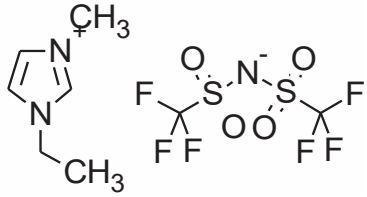 |
| [BMIM][$PF_6$] | 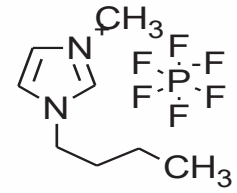 | [EMIM][$BF_4$] | 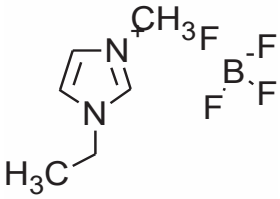 |
| [BMIM][OTf] | 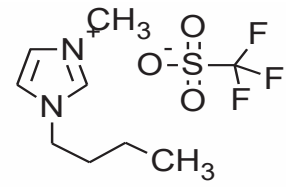 | [EMIM][dca] | 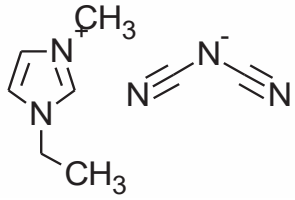 |

#### 4.3.1.2 Carbonic anhydrase enzyme

Freeze dried Carbonic anhydrase from bovine erythrocytes was obtained from Sigma–Aldrich (USA) (reference C3934) and was used in this work without any additional purification. Solutions of the carbonic anhydrase enzyme in the ionic liquid were prepared using the ionic liquid [BMIM][OTf] and adding 0.3 and 0.5% wt into 7 ml of ionic liquid.

#### 4.3.1.3 Hollow fibres

PAN hollow fibres were supplied by F. Tasselli of ITM-CNR and were prepared as described in section 3.3.1. Asymmetric porous PAN hollow fibre supports were prepared by the dry–wet

spinning technique according to the phase inversion process as described previously. The spinning set-up was described previously [61]. Contactor membrane modules were prepared by potting five PAN hollow fibres with epoxy resin inside 20 cm long glass tubes with two lateral connections for the sweep or retentate flow. PAN polymer solutions were prepared by adding the polymer powder to DMF in a glass flask at 70 °C, under mechanical stirring until complete polymer dissolution. The dope solution was then transferred into a jacketed tank, kept at a constant temperature (70 °C) and degassed under vacuum.

### 4.3.2 Pure gas sorption experiments

#### 4.3.2.1 Method

The experimental setup used to determine the gas solubility and diffusivity is show in Figure 4.2. This involved monitoring the evolution of the pressure decay with time. The pressure decay is related to the absorption of the gas by the ionic liquid. The experimental setup is composed of two parts: the feed compartment (FV) pressurized until a 1.7 bar (abs) constant pressure of the pure gas, and the absorption compartment (AC), in which a volume of 0.5ml of IL was collocated selected. The two parts were separated by a valve. At the opening the valve, the gas was expands from FV to AC. The pressure decay was followed in the system using a pressure transducer (Duck, PDCR 910 model, England).

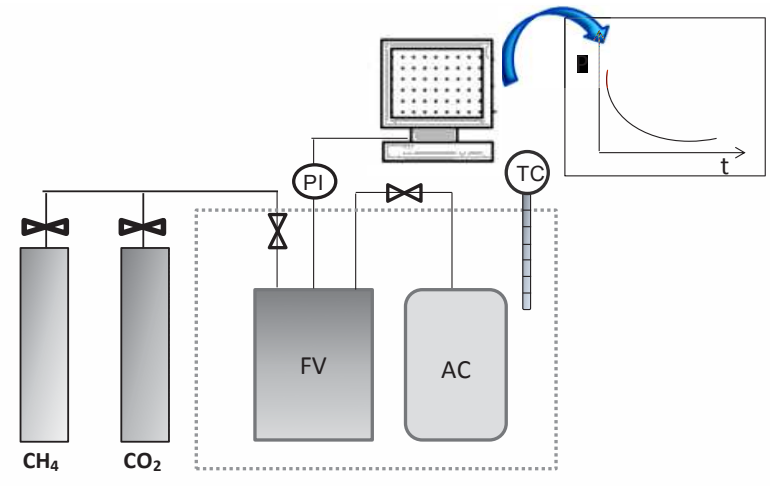


**Figure 4.2.** Pressure-decay experimental setup: FV feed volume, AC gas absorption compartment, TC temperature controller, PI pressure transducer.

The solubility and diffusivity were determined by fitting the pressure decay curve to a one-dimensional diffusion model for solute uptake into the liquid. Several assumptions were considered: (i) only diffusive transport occurs in the system; (ii), equilibrium is established at the gas/liquid interface; (iii) $CO_2$ and $CH_4$ concentration in the liquid phase boundary is described by Henry's Law and (iv) $CO_2$ and $CH_4$ diffusion coefficients are independent of their concentration for the partial pressures tested (0.7 bar). It is also considered that solvent properties such as viscosity and density are constant at a given temperature [61].

Combining Fick's first law of diffusion with a mole balance written on the liquid-phase yield:

$$\frac{\delta_{CO_2}}{\delta_t} = -D_{CO_2}\frac{\delta^2 C_{CO_2}}{\delta_z{}^2} \qquad \text{Eq. 4.1}$$

This equation may be integrated over a thin-liquid film with the following boundary conditions:

$$t = 0;\ P = P0; \qquad C_{gas} = 0 \qquad \text{Eq. 4.2}$$

$$t > 0;\ z = 0; \qquad \frac{\delta C_{gas}}{\delta_t} = 0 \qquad \text{Eq. 4.3}$$

$$t > 0;\ z = L; \qquad C_{gas} = \frac{\rho_{solvent}}{H_{gas} MW_{solvent}} \cdot P = K \cdot P \qquad \text{Eq. 4.4}$$

where $z$ is the vertical position within the solvent ($m$), $C_{gas}$ is the gas concentration (mol $dm^{-3}$), $D$ is the diffusion coefficient ($m^2 s^{-1}$), $t$ is the time (s), $L$ is the thickness of solvent film ($m$), $\rho_{solvent}$ is the solvent density (g $cm^{-3}$), $H_{gas}$ is the Henry's Law constant for the gas in the solvent (bar) and $MW_{solvent}$ (g $mol^{-1}$) is the molecular weight [77].

The method was already described previously. An analytical solution is available from Crank [78]:

$$\frac{C_{gas}}{C_{gas}/z = L} = 1 - \left(\frac{4}{\pi}\right)\sum_{n=0}^{\infty}\frac{(-1)^n}{(2n+1)}\cos\left(\frac{(2n+1)\pi Z}{2L}\right)\cdot\exp\left[\frac{(2n+1)^2\pi^2 D_{gas} t}{4L^2}\right] \qquad \text{Eq. 4.5}$$

Considering that pressure ($P$) is determined by a molar balance in the gas phase, Eq. 4.5 can be rearranged:

$$\ln\frac{P}{P_0}=\frac{k}{H_{co_2}}\sum_{n=0}^{\infty}\frac{(-1)^n}{(2n+1)}\cos\left(\frac{(2n+1)\pi Z}{2L}\right)\cdot\exp\left[\frac{(2n+1))^2\pi^2 D_{gas}t}{4L^2}\right] \qquad \text{Eq. 4.6}$$

With

$$k=\frac{8RTV_{Solvent}\rho_{solvent}}{\pi^2 VMW_{solvent}} \qquad \text{Eq. 4.7}$$

Where $V$ corresponds to the volume of gas ($cm^3$) in the gas compartment, $V_{solvent}$ is the volume of solvent ($cm^3$) in the absorption compartment (AC), respectively. Eq. 4.6 was fitted to the experimental transient pressure results, by adjusting $H_{gas}$ and $D_{gas}$ using a nonlinear regression method using the Matlab method.

Figure 4.3 shows reported the set-up for the gas mixture measurements in a membrane contactor. A mixture was prepared feeding into the gas tank $CO_2$ and $CH_4$ to a composition of 60% and 40%, respectively. The set-up is composed of two parts: the gas compartment (GC) pressurized until a 0.7 bar constant pressure of the gas mixture, and the membrane contactor (MC). The two parts were separated by a valve. At the opening of the valve, the gas mixture expanded from the GMT to the shell side of the MC. In these preliminary tests, there was no real separation.

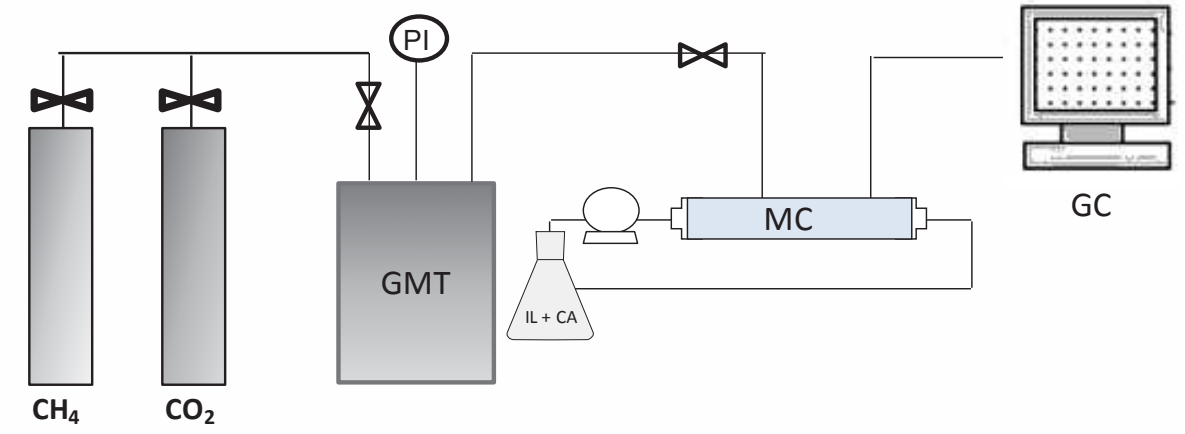


**Figure 4.3.** Gas experimental with mixture set-up: GMT Gas mixture tank, MC membrane contactor, GC Gas chromatograph with computer.

The membrane contactor served as a reservoir for the IL, allowing measurement of the pressure decay. The composition of the gas mixture was analyzed over time by gas chromatography, in order to evaluate the ability of the membrane contactor to absorb the $CO_2$.

## 4.4 Results and discussion

### 4.4.1 Comparison of the $CO_2$ solubility in different ionic liquids

#### 4.4.1.1 Effect of the cation

The $CO_2$ solubility tests were carried out with two ILs having the same anion but different cation, in order to understand the effect of cation on the $CO_2$ absorption. The $CO_2$ solubilities of [BMIM][$NTf_2$] and [EMIM][$NTf_2$] are shown in Figure 4.4.

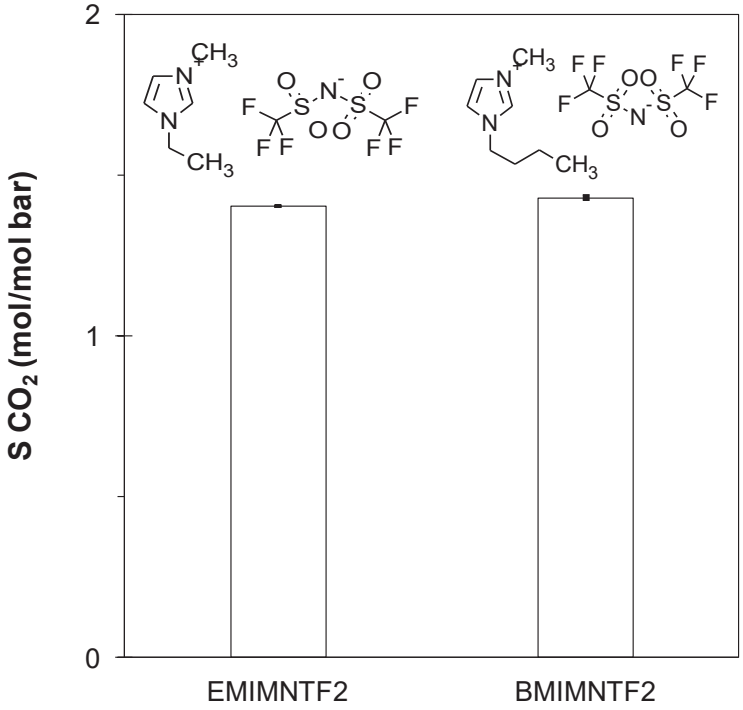


**Figure 4.4.** $CO_2$ solubility for [BMIM][$NTf_2$] and [EMIM][$NTf_2$] ILs with the same anion and different cation.

The $CO_2$ solubility increased only marginally with increasing chain length. In fact the $CO_2$ solubility of the [BMIM][$NTf_2$], with a butyl-chain on the 1-Nitrogen, is slightly higher than that of [EMIM][$NTf_2$], with an ethyl chain. However the difference of $CO_2$ solubility between

[BMIM][$NTf_2$] and [EMIM][$NTf_2$], is very little and negligible compared to the experimental errors. This suggests that the primary interaction that involves between the $CO_2$ and the ILs, occurs with the anion and not with the cation [79].

#### 4.4.1.2 Effect of different anions when the cation is the [EMIM]

In order to understand the effect of the interaction between the anion and $CO_2$, the $CO_2$ solubility for the three ionic liquids with the same cation but different anions [EMIM][$NTf_2$], [EMIM][$BF_4$] and [EMIM][dca] were investigated. All of the ILs have the same 1-ethyl-3-methylimidazolium ([EMIM]) cation, but the anions span a wide range of basicity. The anions are [$BF_4^-$], [$NTf_2^-$], [$dca^-$].

The $CO_2$ solubility for the ionic liquids [EMIM][$NTf_2$], [EMIM][$BF_4$] and [EMIM][dca] is shown in Figure 4.5. The two ionic liquids having the anion with fluorine atoms present a higher solubility than that of the ionic liquid without fluorine atoms ([EMIM][dca]). This presumes that the $CO_2$ solubility increases in the presence of fluorine because this atom makes the nitrogen more nucleophilic for the interaction with the $CO_2$ molecule. The highest $CO_2$ solubility was proven for the IL with the anion $BF_4^-$, probably because it shows a higher basicity than that of the anion $NTf_2^-$. In addition, it has a lower molecular weight and thus a higher concentration of ions. The diffusion decreases with the increase of viscosity and solubility as expected.

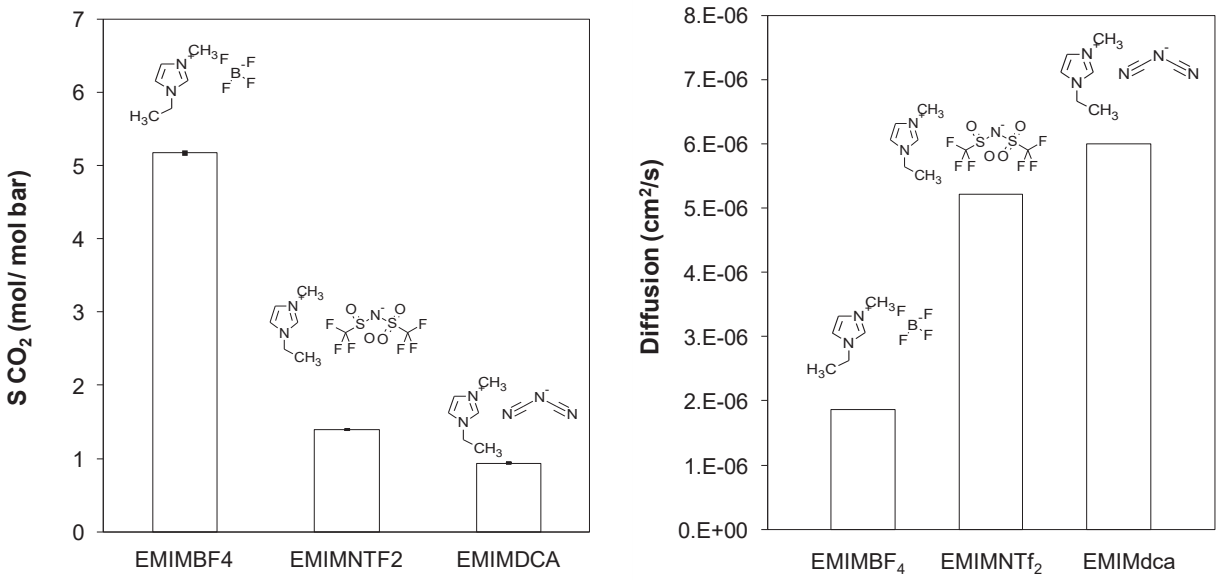


**Figure 4.5.** a) $CO_2$ solubility and b) $CO_2$ Diffusion for [BMIM][$BF_4$], [EMIM][$NTf_2$], [EMIM][dca]. ILs with different anions and same [EMIM] cation.

#### 4.4.1.3 Effect of different anion when the cation is [BMIM]

For a further validation, that the primary interaction between ionic liquids and $CO_2$ occurs with the anion, the $CO_2$ solubility in [BMIM][$NTf_2$], [BMIM][$PF_6$] and [BMIM][OTf] was investigated. All of the ILs have the same 1-buyl-3-methylimidazolium ([BMIM]) cation, but different anions: [$PF_6^-$], [$NTf_2^-$], [$OTf^-$]. Figure 4.6 shows the $CO_2$ solubility as a function of different anion present in the ionic liquids. The $CO_2$ solubility increases when increasing the presence of the fluorine containing groups in the anion ($BF_6^-$>$NTf_2$>OTf). This means that the stronger interaction of $CO_2$ with the fluorine can increase the affinity of ionic liquid for $CO_2$. The lowest $CO_2$ solubility was proved for [BMIM][OTf]. [BMIM][$PF_6$] and [BMIM][$NTf_2$] present the same number of fluorine atoms, but the $CO_2$ solubility of [BMIM][$PF_6$] is higher than that of [BMIM][$NTf_2$]. The $PF_6^-$ anion apparently has a stronger interaction with the $CO_2$ than that of the $NTf_2^-$ anion. The diffusion decreases with the increase of solubility. Probably the lower interaction of the ions with the $CO_2$ allows a faster diffusion.

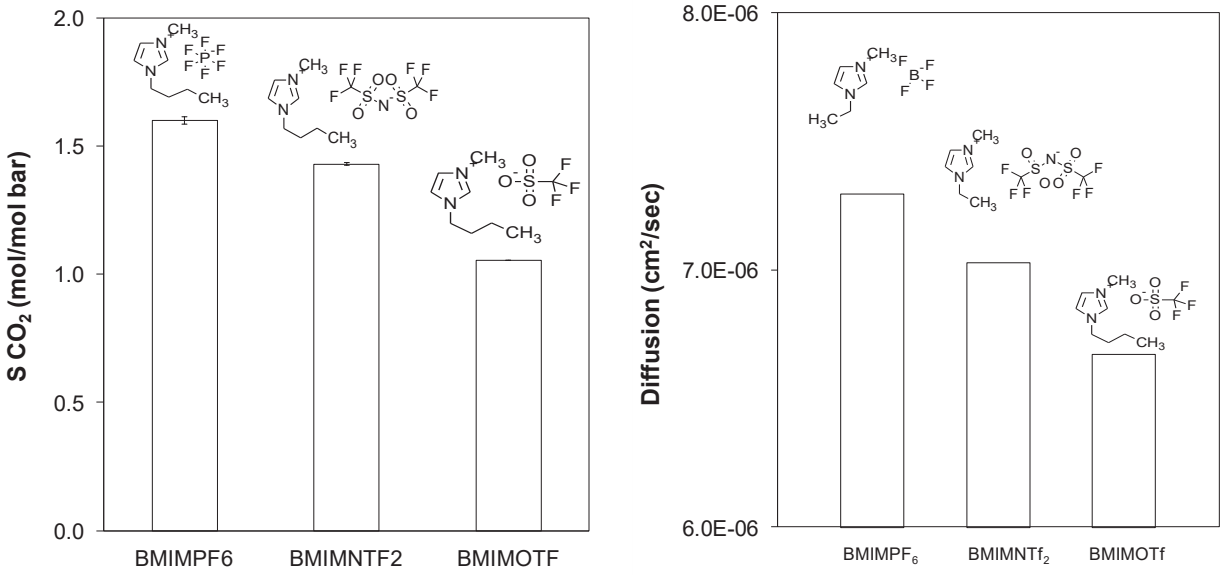


**Figure 4.6.** a) $CO_2$ solubility; b) $CO_2$ Diffusion and permeability for different ILs with same cation and different anions ([BMIM][$PF_6$], [BMIM][$NTf_2$] and [BMIM][OTf]).

### 4.4.2 Comparison of the interaction between the enzyme and hydrophilic and hydrophobic ILs

The ionic liquids show a particular ability to solubilize and concentrate $CO_2$ and provide the perfect environmental for the reaction that the thermo-resistant carbonic anhydrase enzyme

catalyzes Figure 4.7. Ionic liquids with affinity for $CO_2$ assure an enhanced local concentration of $CO_2$ and the necessary level of water [80], which guarantees the adequate enzyme activity and stability.

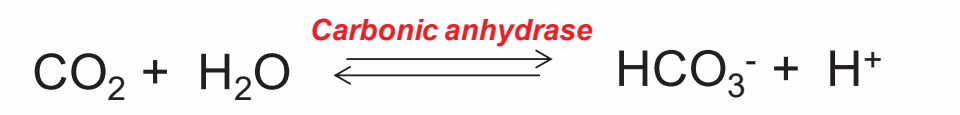


**Figure 4.7.** The equilibrium reaction of $CO_2$ to bicarbonate by carbonic anhydrase.

However, the ionic liquids that show a higher $CO_2$ affinity at the same time are the ionic liquids with high hydrophilic character and *vice versa*. For this reason, it is important to find a compromise between the hydrophilic/hydrophobic character and the affinity for $CO_2$. Among all the ionic liquids studied, those with a good affinity for $CO_2$ were chosen; at least one with a hydrophobic character [BMIM][OTf] and another one with a more hydrophilic character [EMIM][$BF_4$] were chosen.

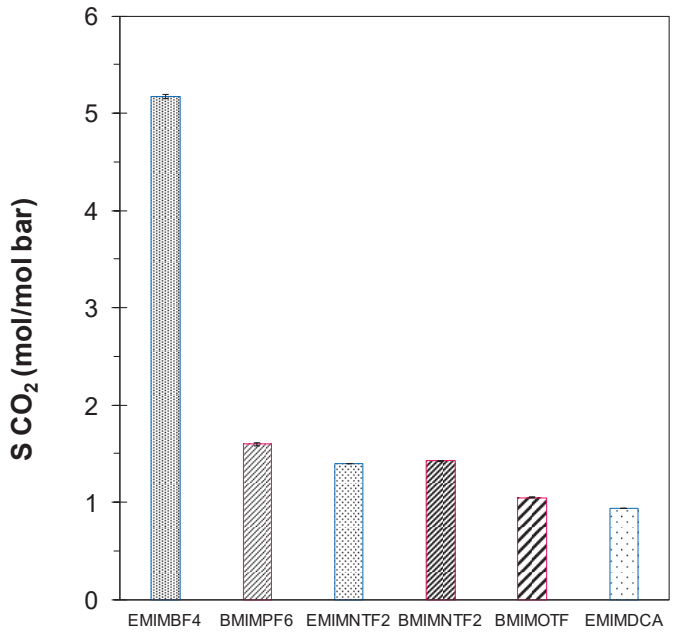


**Figure 4.8.** $CO_2$ solubility for all ionic liquids in the present studies.

As reported in Figure 4.8 and in Table 4.2, the [EMIM][$BF_4$] is the ionic liquid with the highest $CO_2$ solubility, whereas the [BMIM][OTf] showed a much lower $CO_2$ solubility. The choice of these two ionic liquids allows the study of the $CO_2$ solubility in two opposite situations. In one case the performance of a hydrophilic ionic liquid [EMIM][BF4] with high affinity for $CO_2$ was studied. In the second case an ionic liquid with lower solubility for carbon dioxide but while more hydrophobic character was used.

Table 4.2. Characteristics of ionic liquids studied

| *Ionic Liquids* | S* $CO_2$ [mol/mol bar] | Viscosity** (cP) | Density** ($g/cm^3$) | MW** (g/mol) |
|---|---|---|---|---|
| *[EMIM][$BF_4$]* | 5.14 | 37 | 1.28 | 197.97 |
| *[BMIM][$PF_6$]* | 1.60 | 182 | 1.37 | 284.14 |
| *[EMIM][$NTf_2$]* | 1.41 | 27 | 1.51 | 391.31 |
| *[BMIM][$NTf_2$]* | 1.43 | 40 | 1.43 | 419.36 |
| *[BMIM][OTf]* | 1.06 | 109 | 1.29 | 288.29 |
| *[EMIM][dca]* | 0.94 | 17 | 1.08 | 177.21 |

* Solubility of ionic liquids measured

** Viscosity, density and molecular weight (MW) reported as reference [81]

Figure 4.9 shows the $CO_2$ solubility for pure [EMIM][$BF_4$] and [BMIM][OTf] pure and with 0.5% of enzyme. The starting $CO_2$ solubility in [EMIM][$BF_4$] is higher than of [BMIM][OTf], as discussed above, probably because the anion $BF_4^-$ shows a more nucleophilic character than $OTf^-$ anion [82]. This causes a stronger interaction between [EMIM][$BF_4$] and $CO_2$, as a consequence, a higher $CO_2$ solubility was found. In the presence of the enzyme, the $CO_2$ solubility increased only for [BMIM][OTf], instead for [EMIM][$BF_4$] there is a drastic decrease. This behaviour is probably caused by the hydrophilic character of the [EMIM][$BF_4$] that subtracts the water for the reaction from the enzyme. Instead, the $CO_2$ affinity for [BMIM][OTf] increases in the presence of the enzyme.

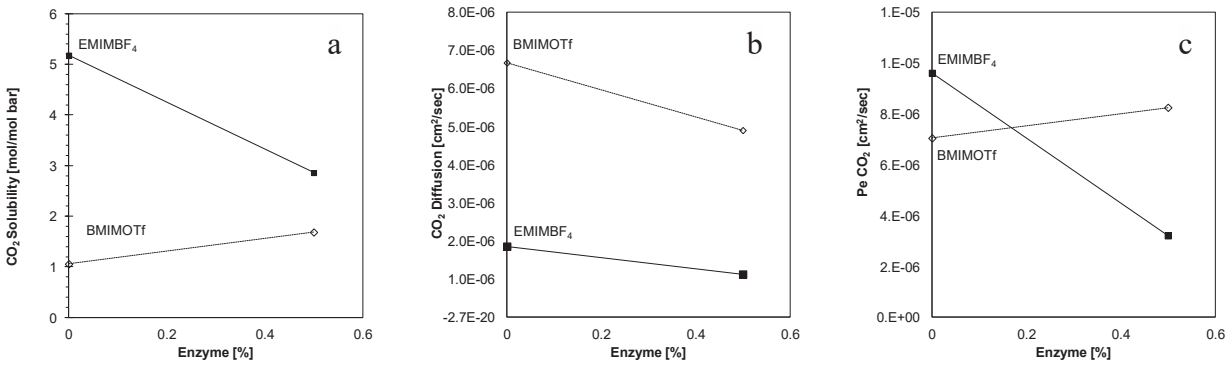


**Figure 4.9.** $CO_2$ solubility (a), $CO_2$ Diffusion (b), $CO_2$ Permeability (c) for [EMIM][$BF_4$] and [BMIM][OTf] pure and with 0.5% of enzyme.

The hydrophobic character of [BMIM][OTf] leaves the initial affinity of the ionic liquid unchanged and ensures the availability of water molecules for the enzyme catalysis. This behaviour confirms that the enzyme stability was in agreement with the hydrophobicity of ILs and that the enzyme is more stable in hydrophobic ILs [BMIM][OTf] than in the hydrophilic [EMIM][$BF_4$]. The diffusion, as expected, decreases for both ionic liquids possibly due to an increase of the viscosity after the addition of the enzyme. The $CO_2$ permeance for the [EMIM][$BF_4$] decreases dramatically in the presence of the enzyme due to the drastic reduction of the solubility. Instead for [BMIM][OTf] the $CO_2$ permeance increases as a consequence of the stronger solubility effect.

### 4.4.3 $CO_2$ sorption in IL with different water activity

The ionic liquids must have a good affinity for $CO_2$ and must contain the necessary level of water for the reaction. The biocatalytic activity is very sensitive to enzyme hydration, it is important to control water activity when determining the effect of the solvent on the enzyme activity. The water activity, *a*, is defined as a relative index to the amount of water which, in a given product is free from special links with the other components, or more simply, as the ratio of the actual pressure, *p*, and the saturated vapour pressure, $p_0$:

$$a = \frac{p}{p_0} \qquad \text{Eq. 4.8}$$

Saturated salt solutions may be used for pre-equilibrating a system to a defined water activity through the vapour phase. The salt solutions and corresponding water activity values selected for this study are shown in Figure 4.10. Saturated salt solutions were prepared by mixing inorganic salts with distilled water in order to obtain a solution with a high solid fraction. The [BMIM][OTf] pre-equilibrated in a closed vessel in the presence of the enzyme, with the vapour phase in contact with the appropriate saturated salt solution. Through the equilibrium period (one week), the temperature was controlled at 30°C. The equilibrium process was monitored by Karl-Fisher in order to determine the water content of the samples. The $CO_2$ absorption tests, with different levels of water activity were carried out Figure 4.10.

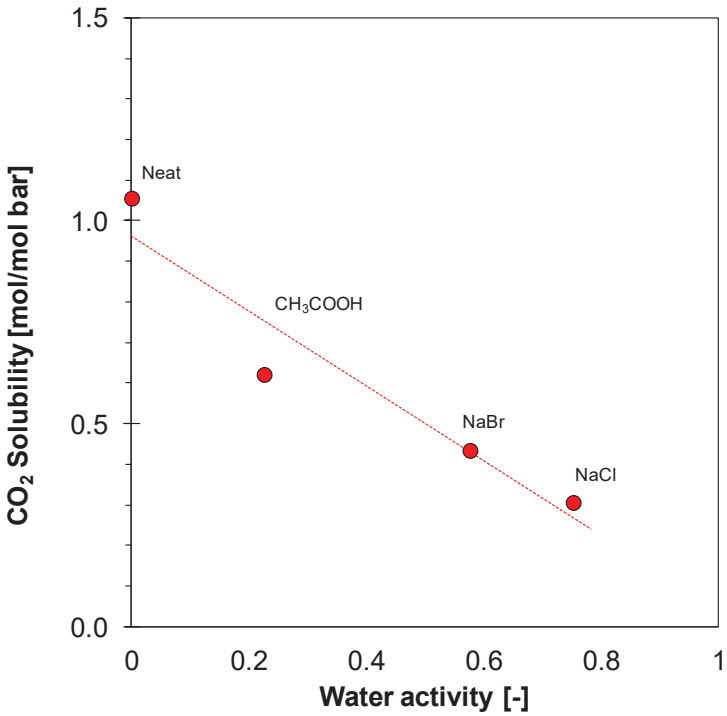


**Figure 4.10.** $CO_2$ solubility for the [BMIM][OTf] as function of different water activity. The curve is indicated as a guide to the eye.

It was found that the $CO_2$ solubility decreases with increasing water activity. This makes it necessary to choose a suitable compromise between a high enough water concentration to allow the reaction to occur, and low enough concentration not to decrease the $CO_2$ solubility significantly. In this preliminary study, the IL with a water activity of 0.2 still exhibited a good affinity for $CO_2$ (0.62 mol / mol bar).

### 4.4.4 $CO_2$ and $CH_4$ sorption results on [BMIM][OTf] IL with carbonic anhydrase

For a further validation of the positive effects of the enzyme on the $CO_2$ solubility, a set of $CO_2$ absorption experiments were carried out with different enzyme concentrations in the ionic liquid [BMIM][OTf]. As shown in Figure 4.11a, the $CO_2$ solubility increased as the enzyme concetration increased. Figure 4.11b reports the effect of the enzyme concentration on the $CO_2$ diffusion. The diffusion decreased, which might be a consequence of the increasing viscosity in the presence of the enzyme, but more likely the diffusion coefficient of the bicarbonate anion is lower than that of free $CO_2$, dissolved as a gas.

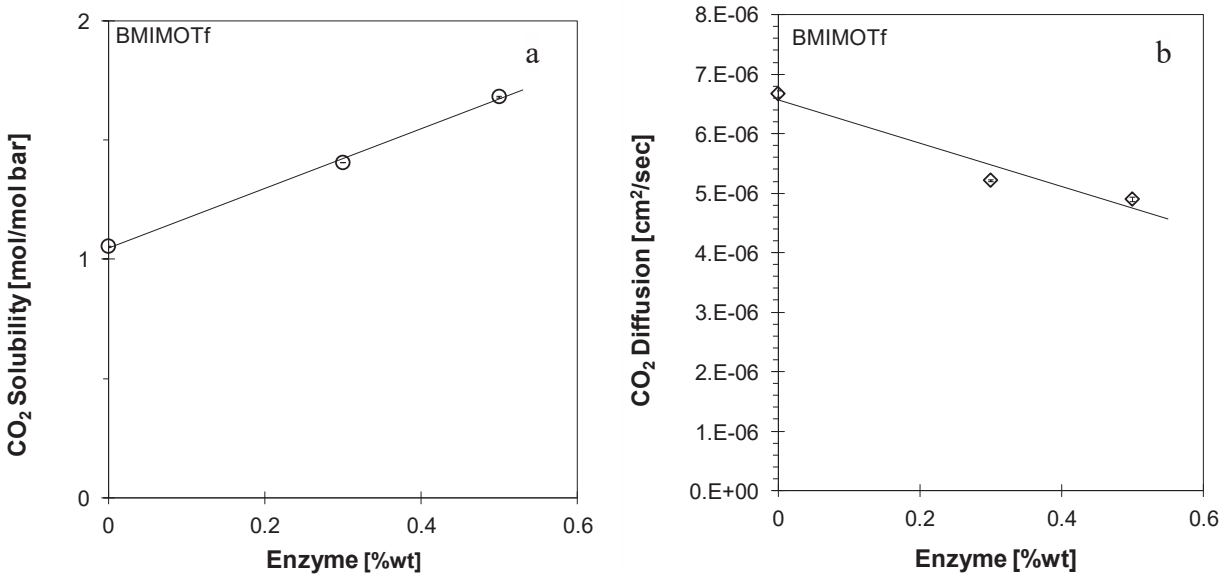


**Figure 4.11.** a) $CO_2$ solubility and b) $CO_2$ diffusion coefficient in [BMIM][OTf] as function of the enzyme concentration.

### 4.4.5 $CO_2$ and $CH_4$ adsorption in a Membrane Contactor with stagnant IL

As a preliminary test for the potential use of membrane contators for $CO_2/CH_4$ separation, some experiments were carried out to measure the sorption behaviour of the stagnant ionic liquid inside a hollow fibre membrane contactor without recirculation, in the setup shown in Figure 4.3. The bore of the PVDF hollow fibres was filled with a selected ionic liquid, [BMIM][OTf]. Gas sorption measurements were carried out with a mixture of $CO_2/CH_4$ with a composition of 60/40 vol.%/vol.%. The mixture was fed into the shell side of the module. The composition was then monitored as a function of time, assuming that the variation of the mixture composition is due to the absorption of gases by the ionic liquid.

Figure 4.12 shows the trend of the gas mixture composition in the time. The $CO_2$ decreases form 60% to 48% in two hours. Instead, the methane concentration increases from almost 40% to 51%. This behaviour can be attributed at the $CO_2$ absorption by the ionic liquid, which shows a lower affinity for methane than for $CO_2$. The addition of the enzyme in the lumen of the hollow fibres with the ionic liquid can improve in terms of velocity and efficiency in the separation process.

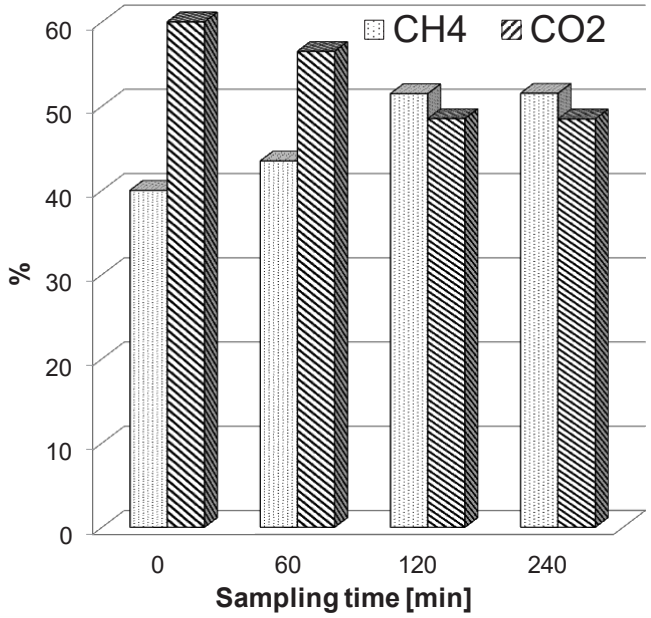


**Figure 4.12.** Gas composition in the shell side for membrane contactor with PAN hollow fibres and [BMIM][OTf].

### 4.4.6 Pure $CO_2$ sorption in membrane contactor with recirculation of the IL

The ionic liquid [BMIM][OTf], equilibrated in the presence of $CH_3COOK$ to a given water content, was fed into the lumen of the hollow fibre module under continuous recirculation, as displayed in Figure 4.3. Gas sorption measurements were carried out with a mixture of $CO_2/CH_4$ with a composition of 70/30% mol/mol. The gas mixture was fed into the shell side of the module in dead-end mode and the composition of shell side with the pressure was followed as function of time Figure 4.13.

The $CO_2$ was adsorbed in greater quantities than methane and a good sorption selectivity of 3.5 for the $CO_2/CH_4$ mixture with the membrane contactor of PAN hollow fibres was obtained.

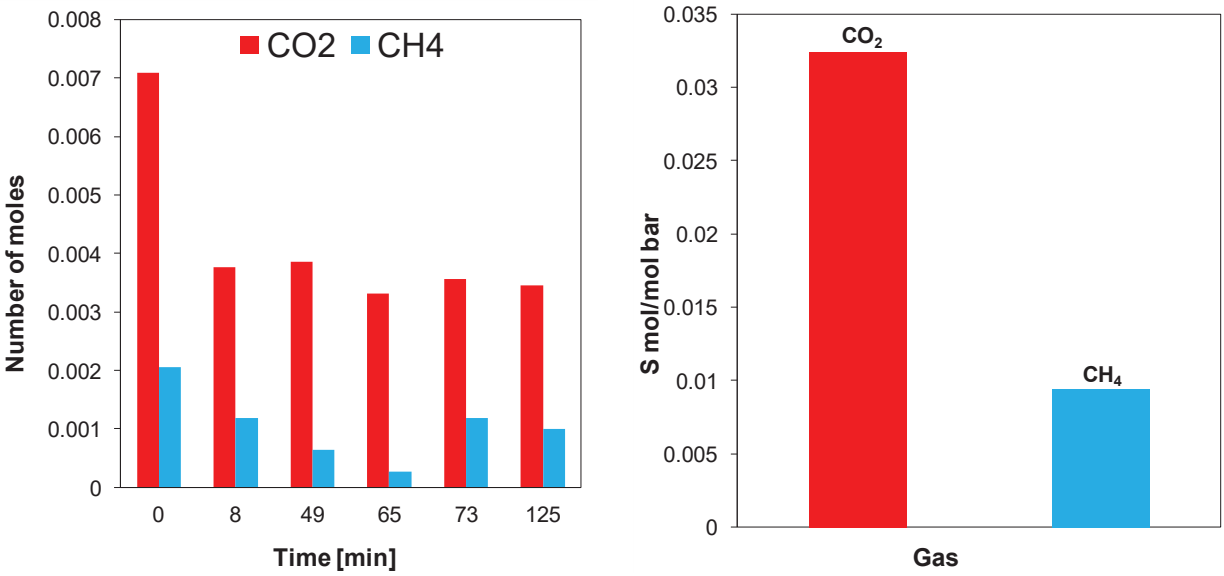


**Figure 4.13.** Trend in the gas concentration as a function of time, and calculated solubility of $CO_2$ and $CH_4$ in the IL [BMIM][OTf].

## 4.5 Conclusions

The $CO_2$ solubility was investigated for six different imidazolium-based ionic liquids to evaluate the dependence on the choice of anion and on the substituents on the cation. The interaction between the $CO_2$ and the ionic liquid occurs in primary way with the anion, the cation playing a secondary role. In fact, the ionic liquids [EMIM][$NTf_2$] and [BMIM][$NTf_2$] demonstrated the same $CO_2$ solubility. The $CO_2$ solubility increases slightly and in an almost negligible way with increasing chain length on the 1-nitrogen of the cation ring ([BMIM][$NTf_2$] ≥ EMIM$NTf_2$). The use of fluorinated groups such as $NTf_2$ or OTf might increase carbon dioxide solubility. The anion of ionic liquids with fluoro-atoms have a higher $CO_2$ solubility affinity than that of the nonfluorinated inorganic anions; In fact, the [EMIM][dca] showed the lowest $CO_2$ solubility.

In this study the effect of the enzyme carbonic anhydrase on the $CO_2$ solubility in ILs was also investigated. The $CO_2$ solubility in hydrophilic ionic liquid [EMIM][$BF_4$], decreased after the addition of the enzyme. Probably due to the hydrophilic character, the ionic liquid subtracts the water from the catalyst, and it does not allow the conversion of $CO_2$ into bicarbonate. Instead, when the hydrophobic ionic liquid [BMIM][OTf] was used, the solubility increased. Increasing the amount of the enzyme, the $CO_2$ and $CH_4$ solubility increased for both but the methane diffusion coefficient decreases more than the $CO_2$ diffusion coefficient. This means that in

presence of the enzyme a benefit in the $CO_2$ permeability can be expected and, as a consequence in the $CO_2/CH_4$ selectivity.

A good separation in the time was obtained for the $CO_2/CH_4$ mixture with the membrane contactor composed of PAN hollow fibres and [BMIM][OTf] ionic liquid. Further studies are needed for the evaluation of the contactor performance in the presence of the enzyme carbonic anhydrase for the Biogas treatment under real operation conditions.

# Chapter 5. Mixed matrix membranes with Zr/Cr-based MOFs dispersed in PIM-1 for $CO_2/CH_4$ separation


## Abstract

Gas separation using metal organic framework (MOF) based Mixed Matrix Membranes (MMMs) is becoming an active and important research field. This work presents the study of gas transport properties for the PIM-1 polymer of intrinsic microporosity loaded with two different kinds of MOF: MIL-101 and UiO-66. The effect of the ligand functionalization, as amino group ($NH_2$) and oxalic acid $(COOH)_2$, for the MOF type UiO-66(Zr) and of ethylenediamine (ED) for MOF type MIL-101 were studied. The permeability of pure He, $H_2$, $N_2$, $O_2$, $CO_2$ and $CH_4$ was studied, focusing the attention on the potential use of these membranes for $CO_2/CH_4$ separation, and on how the functionalization of these MOFs affects the gas transport through the membranes. Finally, a comparison between the two kinds of MOFs-based Mixed Matrix membranes on the gas separation performance was evaluated.


## 5.1 Introduction

Mixed Matrix Membranes (MMMs) offer the opportunity to combine the benefits of low cost and easily processable polymeric materials with the excellent transport performance of inorganic fillers. The design of these new materials for gas separation has the objective to produce innovative membranes with enhanced permeability and selectivity, exceeding the Robeson upper bound limit. Moreover, the MMMs developed for gas separation offer all the advantages of the good transport properties of polymers (high gas permeability) and the good transport properties of inorganic materials (high selectivity). The choice of the polymer and the filler particle loading are the most important parameters affecting the morphology and the performance of MMMs. In this work a polymer characterized by a high intrinsic microporosity: 5,5,6,6-tetrahydroxy-3,3,3,3-tetramethyl-1,1-spirobisindane and tetrafluoroterephtalonitrile (PIM-1) was used. The bulk structure of this polymer presents interconnected voids or free volume elements. The interconnected voids are formed as a direct consequence of the highly contorted shape and extreme rigidity of the polymer backbone [83]. The presence of high free volume, due to by the

existence of a bulky group with a contort site in the main chain combined with the highly stiffness of the main chain, makes this polymer a successful candidate for the development of highly permeable membranes [84]. There is an active research field that is developing MMMs using the PIM-1 as the polymer matrix. MMMs derived from a polymer of intrinsic microporosity and silicalite-1 were prepared by et Ahn et al. They found that the incorporation of fillers increased overall gas permeability compared to the neat polymer but the trend is not linear with the amount of the silica nanoparticles added [85]. Bushell et al. prepared MMMs based on the polymeric matrix of PIM-1 and the zeolitic imidazolate framework, ZIF-8 [87]. They reported that an increase in MOFs incorporated results in an increase in the permeability coefficient and selectivity, but there is an exception for the $CO_2/CH_4$ pair where the selectivity is more or less independent of the ZIF-8 loading in the membrane.

In the present chapter, the effect of the addition for different MOFs on the gas transport properties of the PIM-1 will be investigated. The MOFs are a new group of nanoporous materials made by linking organic units with metal inorganic complex [88]. The inorganic units form the vertices of a frame work, on the other hand the organic linkers form the porous structure with a definite dimension and size shape [87]. The MOFs present a lot of advantages respect to the inorganic fillers: as a better compatibility with the polymer due to the organic nature of MOFs, they have a large variety of structures with different pore size and shapes and finally they have higher pore volume with a lower density [88]. The pre-defined dimension of the cages and eventually the fictionalization of the ligands can make the MOFs more affine for specific gases, making the MOFs interesting for the gas separation application [89]. In this work the effect of the addition into the PIM-1 of different functionalized Zr-based MOFs and Cr-based MOFs on the gas transport properties was evaluated. Nik et al., prepared and characterized $CO_2/CH_4$ gas separation properties of mixed matrix membranes made with Zr-based MOFs (UiO-66) and 6FDA–ODA polyimide as the polymeric matrix. They compared the gas transport of non-functionalized and (-$NH_2$) functionalized UiO-66 MOFs, demonstrating that the presence of –$NH_2$ functional groups in the MOF structure decreases the $CO_2$ permeability from 50 to 13.7 Barrers, while the $CO_2/CH_4$ selectivity increases from 46 to 51 [90]. Instead, Wu et al. reported that UiO-66(Zr)–$(COOH)_2$ based membranes is highly $CO_2$-selective for $CO_2/CH_4$ separation respect to the non-functionalized UiO-66(Zr)-based membrane on the basis of a computational exploration study [91]. Instead, Jeazet et al. incorporated metal-organic framework MIL-101 into a polysulfone matrix and demonstrated an almost 7-fold increase in permeability for the fast gas $CO_2$ (from 5 to 35 Barrers) with a slight increases in ideal $CO_2/CH_4$ selectivity (from 15 to 20)

with the increasing MIL-101 content [92]. In this work the pure gas permeation properties of PIM-1/ Zr-based MOFs and Cr-based MOFs MMMs for of He, $H_2$, $O_2$, $N_2$, $CO_2$, $CH_4$ were investigated for different MOF loadings. The measured permeability coefficient and permeselectivities were compared with the state of art data using Robeson diagrams.

## 5.2 Experimental

### 5.2.1 Materials

#### 5.2.1.1 Polymers

The polymer used is the PIM-1 synthesized by the School of Chemistry, University of Manchester, (UK) (Figure 5.1) [83]. The crude polymer was dissolved in chloroform and reprecipitated from methanol. The product was refluxed for six hours in deionized water and then dried at 100 °C for two days, yield. The thus polymer was used for the membrane preparation.

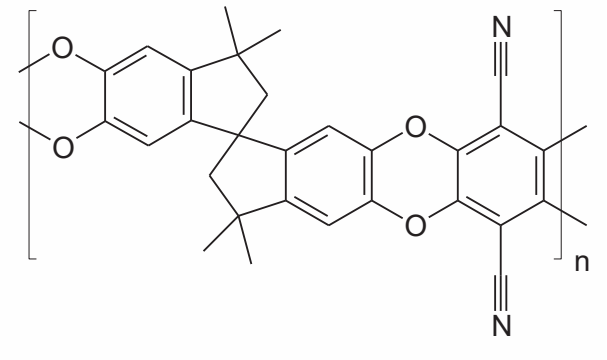


**Figure 5.1.** Chemical structure of PIM-1

#### 5.2.1.2 MOFs

The MOFs used in this work are a family of Zr-terephthalate and Cr-terephthalate based metal–organic frameworks, namely UiO-66 and MIL-101, respectively [93][97]. In the cubic Zr-terephthalate (UiO-66), each Zr6O4(OH)4 octahedron is surrounded by maximally 12 terephthalate linkers, resulting in large octahedral and small tetrahedral cages [98]. For this reason, these MOFs can have a cubic and 3D structure, characterized by octahedral and tetrahedral cavities with diameters of 11Å and 8Å, respectively (Figure 5.2a). Triangular

windows with a diameter of 6Å guarantee the selective gas passage [99]. In the literature it is possible to find that the UiO-66 materials generally were synthesized with eight benzene-1,4-dicarboxylates. Each of these UiO-66 MOFs differs from the others for the functionalization of the benzene-1,4-dicarboxylates linker that allows to obtain a family of isoreticular UiO-66. The UiO-66-isoreticular used in this work are UiO-66-$NH_2$ and the UiO-66-$(COOH)_2$ functionalized with an amino group (-$NH_2$) and with two carboxylic groups (-$COOH)_2$, respectively (Figure 5.2c).

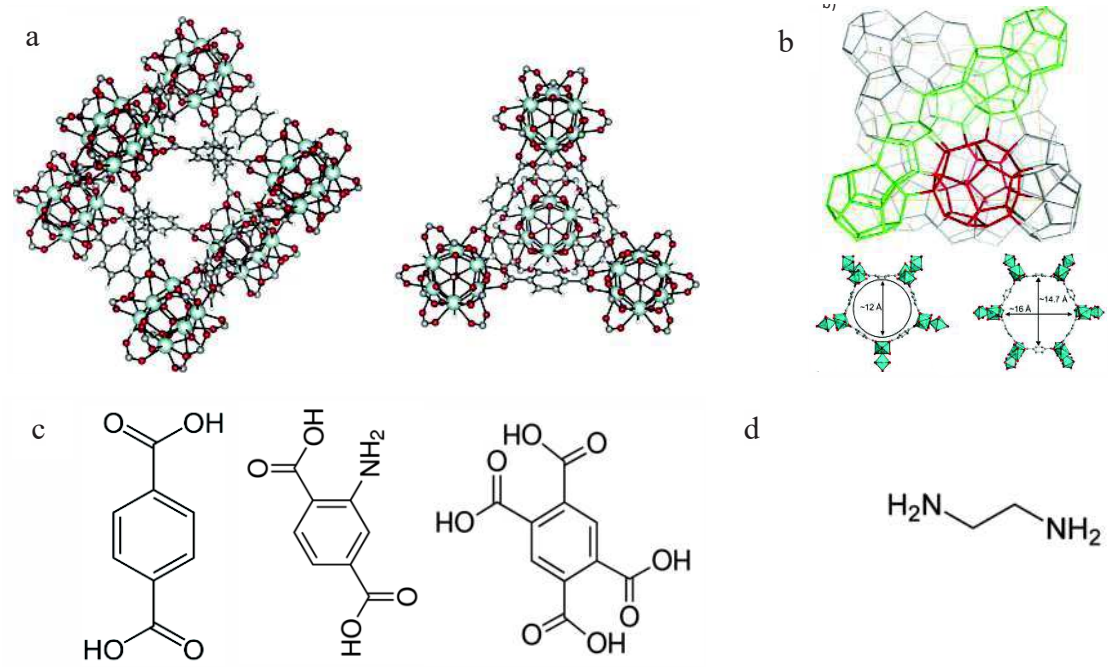


**Figure 5.2.** a) Illustration of Octahedral (left) and tetrahedral (right) cages of UiO-66 Color scheme: Zr (cyan); O (red); C (gray); H (white), adapted from [99]; b) non-functionalized benzene-1,4-dicarboxylates and functionalized with (-$NH_2$) and $(COOH)_2$ ligands . c) Zeotype architecture of MIL-101 showing mesoporous cages with diameters of 29 Å (green) and 34 Å (red). d) 12 Å pentagonal (A) and 15 Å hexagonal (B) windows of cages. d) ethylene diamine (ED) ligand used to functionalize the MIL-101.

Instead, MIL-101 (3D-$[Cr_3O(BDC)_3(F,OH)-(H_2O)_2]$ is a crystalline Cr-terephthalate with a framework made by two different kinds of cages with an internal free diameters of 29 and 34Å, and a prevolumes of 12 and 20Å, respectively. The smallest cages exhibit pentagonal windows with a free opening of 12 Å, while the larger cages possess both pentagonal and larger hexagonal windows of a 14.5 Å x 16 Å free aperture [97],[100] (Figure 5.2b). The MIL-101 used in this work is the ED-MIL-101 in which the co-ordinatively unsaturated metal sites were

functionalized with ethylene diamine ($NHCH_2CH_2NH_2$) (Figure 5.2d). The presence of co-ordinatively unsaturated metal sites could be used to induce regioselectivity and shape or size selectivity for the passage of specific gas.

### 5.2.2 Membrane preparation

The membranes used in the present chapter were provided by the School of Chemistry, University of Manchester (UK). To test the effect of substituent on the gas transport property different MOFs were embedded into the PIM-1 polymeric matrix: UiO-66 neat, UiO-66-$NH_2$, UiO-66-$(COOH)_2$, and ED-MIL-101. The membranes were prepared with the following method: the MOF particles were dispersed in anhydrous chloroform and stirred overnight in a vial. At the same time, PIM-1 was dissolved in anhydrous chloroform and stirred overnight in a vial. The particles were sonicated in an ultrasonic bath for 30 minutes before filtering the PIM-1 solution trough glass wool into the MOF suspension. The resulting dispersion was stirred overnight. The solution was then cast into a levelled flat-bottom glass petri-dish in a desiccator, and left to evaporate over 3-5 days. The amounts used for each membrane are given in Table 5.1.

Table 5.1. Composition of the membranes studied in the present chapter

| MOF type | *PIM-1:Filler* ratio | Amount of filler *(%wt)* |
|---|---|---|
| UiO-66 neat | 10:1 | 9 |
| | 10:2 | 71 |
| | 10:3 | 23 |
| | 10:4 | 29 |
| UiO-66-($NH_2$) | 10:1 | 9 |
| | 10:2 | 17 |
| | 10:3 | 23 |
| | 10:4 | 29 |
| UiO-66-$(COOH)_2$ | 10:1 | 9 |
| | 10:2 | 17 |
| | 10:3 | 23 |
| | 10:4 | 29 |
| ED-MIL-101 | 10:1 | 9 |
| | 10:2 | 17 |
| | 10:3 | 23 |
| | 10:4 | 29 |

### 5.2.3 Gas permeation measurements

The permeation experiments were performed on a fixed volume/pressure increase instrument constructed by GKSS (Geesthacht, Germany). The feed gas pressure was set at 1 bar (the actual value was read with a resolution of 0.1 mbar); the permeate pressure was measured in the range from 0 to maximum, 13.3 mbar, with a resolution of 0.001 mbar. The gases were always tested in the same order (He, $H_2$, $N_2$, $O_2$, $CH_4$, and $CO_2$), although it was verified by repeating a measurement cycle that if sufficiently long vacuum was applied to completely remove the previous gas, the measurement order for these materials was irrelevant. Feed pressure, permeate pressure, and temperature are continuously recorded during each measurement run. The temperature was controlled at a constant temperature of 25 ± 1 °C. Before the first measurement, the membrane cell was evacuated for sufficient time (at least 1 h) with a two-stage rotary pump. Between two subsequent measurements, the system was evacuated for a period of at least five times the time lag of the previous species in order to guarantee the complete removal of the previous gas. Circular membranes, with an effective exposed surface area of 2.14 $cm^2$ were used. The pressure increase on the permeate side was recorded as a function of time from the moment that the membrane was exposed to the feed gas. The whole permeation curve takes the following form:

$$p_t = p_0 + (d_p / d_t)_0 \cdot t + \frac{RT \cdot A \cdot \ell}{V_P \cdot V_m} \cdot p_f \cdot S\left( \frac{D \cdot t}{\ell^2} - \frac{1}{6} - \frac{2}{\pi^2} \sum_1^{\infty} \frac{(-1)^n}{n^2} \exp\left( - \frac{D \cdot n^2 \cdot \pi^2 \cdot t}{\ell^2} \right) \right) \quad \text{Eq. 5.1}$$

in which $p_t$ is the permeate pressure at time $t$ and $p_0$ is the starting pressure, typically less than 0.05 mbar. The baseline slope $(dp/dt)_0$ is usually negligible for a defect-free membrane. $R$ is the universal gas constant, $T$ is the absolute temperature, $A$ is the exposed membrane area, $V_P$ is the permeate volume, $V_m$ is the molar volume of a gas in standard conditions (0 °C and 1 atm), $p_f$ is the feed pressure, $S$ is the gas solubility, $D$ the gas diffusion coefficient, and $\ell$ the membrane thickness. The time lag method was applied to the recorded data to determine the gas diffusion coefficient (Figure 5.3, Figure 5.4) [100].

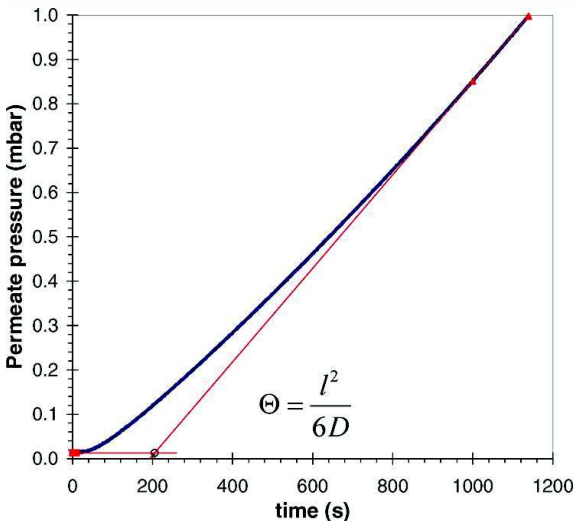


**Figure 5.3.** Schematic representation of a permeation measurement with the determination of the time lag from the tangent to the steady state pressure increase curve.

The permeability coefficient, *P*, is calculated from the following equation, describing the steady state permeation:

$$P_t = P_0 + (dp/dt)_0 \cdot t + \frac{RT \cdot A}{V_p \cdot V_m} \cdot \frac{p_f \cdot p}{\ell} \left( t - \frac{\ell^2}{6D} \right) \qquad \text{Eq. 5.2}$$

the last term in Equation (5.2) corrects for the so-called permeation time lag, $\Theta$, which is inversely proportional to the diffusion coefficient of the gas:

$$\Theta = \frac{\ell^2}{6D} \qquad \text{Eq. 5.3}$$

the gas solubility coefficient, S, was obtained indirectly as the ratio of the permeability to the diffusion coefficient by assuming the solution-diffusion transport mechanism:

$$S = P / D \qquad \text{Eq. 5.4}$$

Permeabilities are reported in Barrer [1 Barrer=$10^{-10}$ $cm^3$(STP) cm $cm^{-2}$ $s^{-1}$ cm $Hg^{-1}$].

A practical example of the permeate pressure increase measurement and the time lag determination is given in Figure 5.4

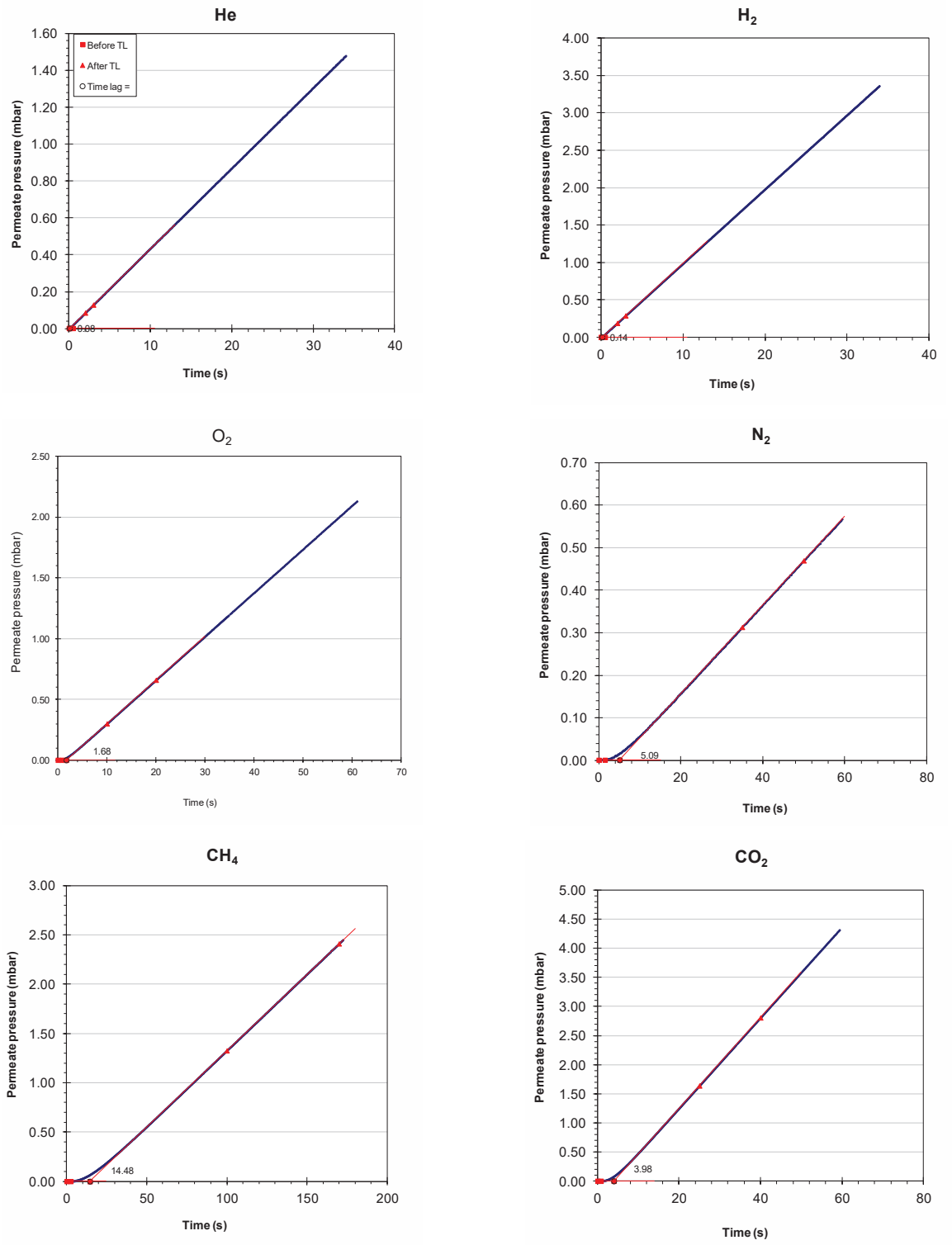


**Figure 5.4.** Example of the pressure increase curves with indication of the time lag determination for six permanent gases He, $H_2$, $N_2$, $O_2$, $CH_4$ and $CO_2$ in membrane Uio-66-$(COOH)_2$ 10:1

## 5.3 Results and discussion

### 5.3.1 Theory for gas transport in mixed-matrix membranes

The simplest model which is usually used to describe the gas transport in mixed matrix membranes is the Maxwell model [104]:

$$P_{MMM} = P_c \left| \frac{P_d + 2P_c - 2\Phi_d (P_c - P_d)}{P_d + 2P_c + \Phi_d (P_c - P_d)} \right| \qquad \text{Eq. 5.5}$$

Where the $P_{MMM}$ is the effective permeability of the mixed matrix membrane, $P_c$ and $P_d$ represent the gas permeabilities in the continuous and dispersed phase, respectively and $\Phi_D$ is the volume fraction of dispersed phase. The Maxwell model is applied to the systems containing spherical fillers with a relatively low loading [49]. The transport can occur in different ways depending on the types of nanoparticles dispersion. In fact, the incorporation of fillers into the polymer phase can significantly alter the transport properties of gases through the MMM. For this reason, the preparation of mixed matrix membranes with a polymer continuous phase is a crucial step that will influence the gas transport properties.

Several fundamentally different cases may occur, as displayed schematically in Figure 5.5.

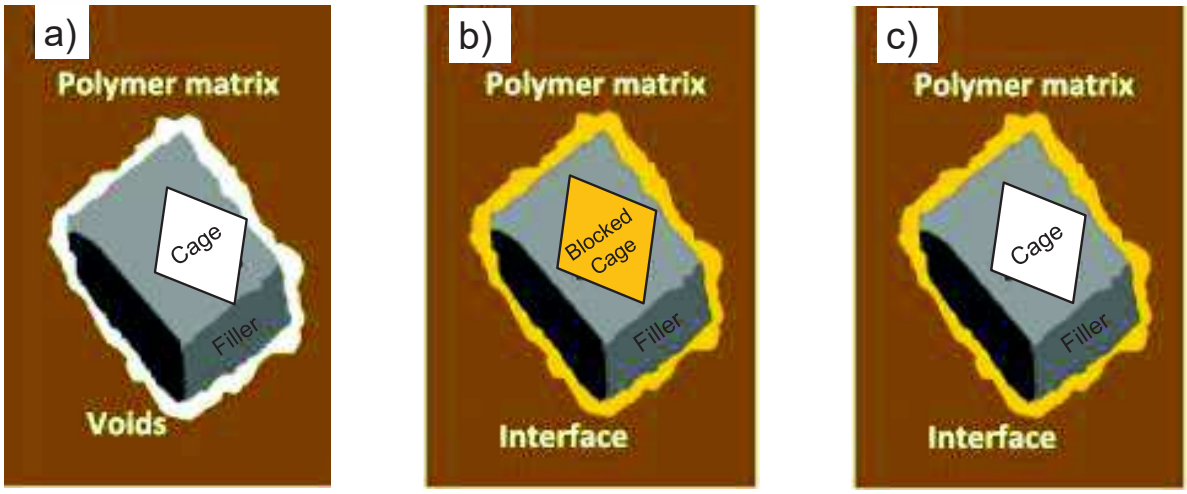


**Figure 5.5.** Schematic representation of the gas permeation trough the mixed-matrix membrane: a) According the first case $P_d \gg P_c$; b) According the second case $P_d \ll P_c$; c) According the Maxwell-model ($0 < Pd < \infty$) (figures adapted from [107]);

**First case**

This situation occurs when the interaction between the polymer and filler particles is bad, giving rise to the formation of undesirable channels between both phases. This occurs when the polymer chains do not completely adhere to the surface of the fillers (Figure 5.5a).

In this case, since the permeability of the gas in the dispersed phase and around the particles is much higher than that of the continuous phase, we find:

$$\boldsymbol{P_d \gg P_c} \qquad \text{Eq. 5.6}$$

Thus, $P_d$ can be considered infinite ($P_d \sim \infty$) and equation 5.5 then becomes:

$$P_{MMM} = P_c \left| \frac{1 + 2\Phi_d}{1 - \Phi_d} \right| \qquad \text{Eq. 5.7}$$

The formation of these non-selective voids at the interface allows bypassing of the gas around the fillers particles. At low filler loadings this results in a higher permeability but constant selectivity. At relatively high filler loadings, above the percolation threshold, continuous channels are formed across the membrane, which deteriorates the selectivity of the MMM, and thus the gas separation performance of the membrane [105].

**Second case**

Another phenomena that can happened during the MMM preparation is the partial or complete blockage of the MOF cage by the polymer phase (Figure 5.5b). In this situation the permeability of the gas in the dispersed phase is much lower than that of the continuous phase:

$$\boldsymbol{P_d \ll P_c} \qquad \text{Eq. 5.8}$$

The permeability of the dispersed phase can then be considered negligible (Pd ≈ 0) and equation 5.5 becomes:

$$P_{MMM} = P_c \left| \frac{2P_c - 2\Phi_d P_c}{2P_c + \Phi_d P_c} \right| \qquad \text{Eq. 5.9}$$

Thus, the fillers behave as impermeable obstacles to the transport and in this case no positive effects of the addition of fillers on the transport properties of the membrane will be observed [106].

**Third case**

Generally, the permeability of the gases through the dispersed phase is comprised between the two extreme cases discussed above, for which $P_d$=0 and $P_d$= ∞.

$$\mathbf{0 < P_d < \infty} \qquad \text{Eq. 5.10}$$

The fillers exhibit an intrinsic permeability. This permeability will be different from that of the polymer matrix and its behaviour must be described by the complete Maxwell equation (Eq. 5.5). This occurs when the MOFs are well distributed within the polymer matrix causing a greatly modification of the membrane free-volume (Figure 5.6).

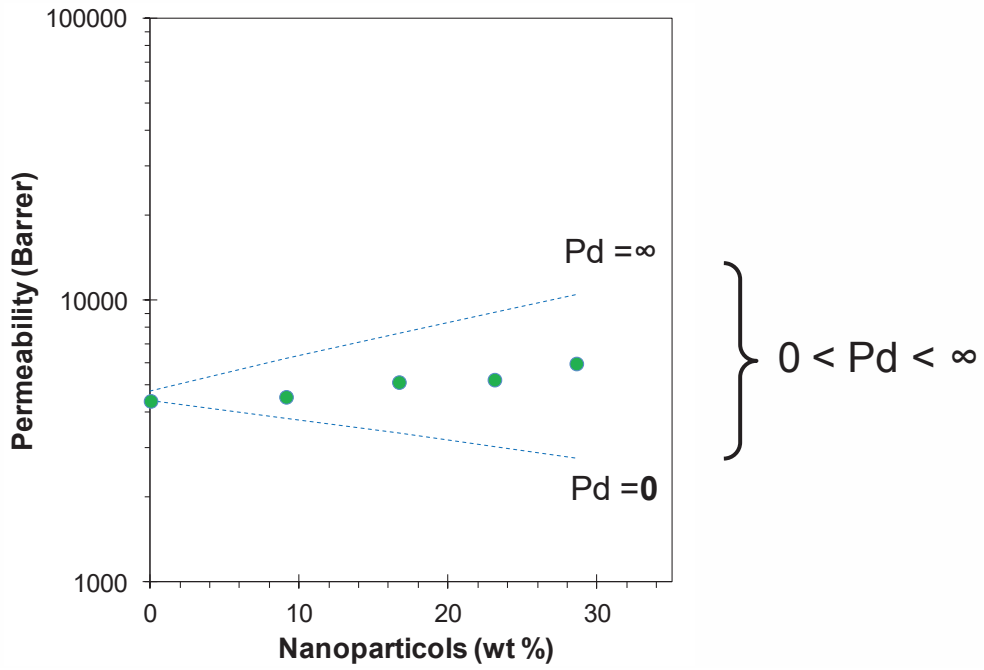


**Figure 5.6.** Graphic representation of gas transport properties of the previous cases for different filler concentrations. The dashed lines delimit the range of permeabilities predicted by the Maxwell model. The points indicate an example where the filler in the MMM slightly increases the permeability of the polymer matrix.

**Fourth case**

This is a special example of the previous situation, in which the permeability of the continuous phase is exactly equal to that of the dispersed phase:

$$P_c = P_d \qquad \text{Eq. 5.11}$$

Thus, equation 5.5 simplifies to:

$$P_{MMM} = P_c \qquad \text{Eq. 5.12}$$

This means that the presence of the nanoparticles has no influence on the gas transport properties of the membrane. If the polymer matrix is not otherwise affected, the filler should have no influence on the MMM permeability and selectivity with respect to the neat polymer. In this case, the mixed matrix membrane will show an identical permeability as the neat polymer membrane. This may be the case for one single gas, but rarely will it be the case for more gases of different size or solubility. Therefore, the selectivity of these membranes is likely to be affected by the filler, because in at least one of the gases of a gas pair $P_C \neq P_D$, and thus the selectivity will change.

These non-ideal effects in organic-inorganic materials for gas separation were also investigated by Koros et al. [105]. They described the relationship between mixed matrix membranes morphologies and transport properties for a number of different situations, shown in Figure 5.7.

Between the two limiting cases it is possible to recognize other specific nanoscale morphologies of the mixed matrix membranes that affect the gas transport properties of the membranes. Figure 5.7 shows the gas transport properties for five cases of different interface morphology. The complete Maxwell equation previously described corresponds to the “0 case” in which a good interface interaction was obtained with an ideal gas transport properties. In fact, the gas transport is characterized by a simultaneous rise in permeability and in selectivity of the MMMs respect to the neat membrane, due to the loading of the fillers. “Case I” corresponds to a region of the external rigidified polymer layer that causes a reduced permeability, but it maintains the positive effect on the selectivity. “Case II and III” present voids at the interface and case III is only a specific example of case II, where the effective void size is equal to the gas size. Cases IV and V are both characterized by a reduction of gas permeability due to a strong interaction of gases with the membrane matrix. In the specific situation of case IV, the gas is completely withheld by

the membrane and the permeability decreases without affecting the selectivity. Instead, for the V case the diffusion of the gas is slowed down due to the presence of an additional resistance at the interface inside the filler particle, making it even more selective. Thus, while the permeability decreases, the selectivity slightly increases.

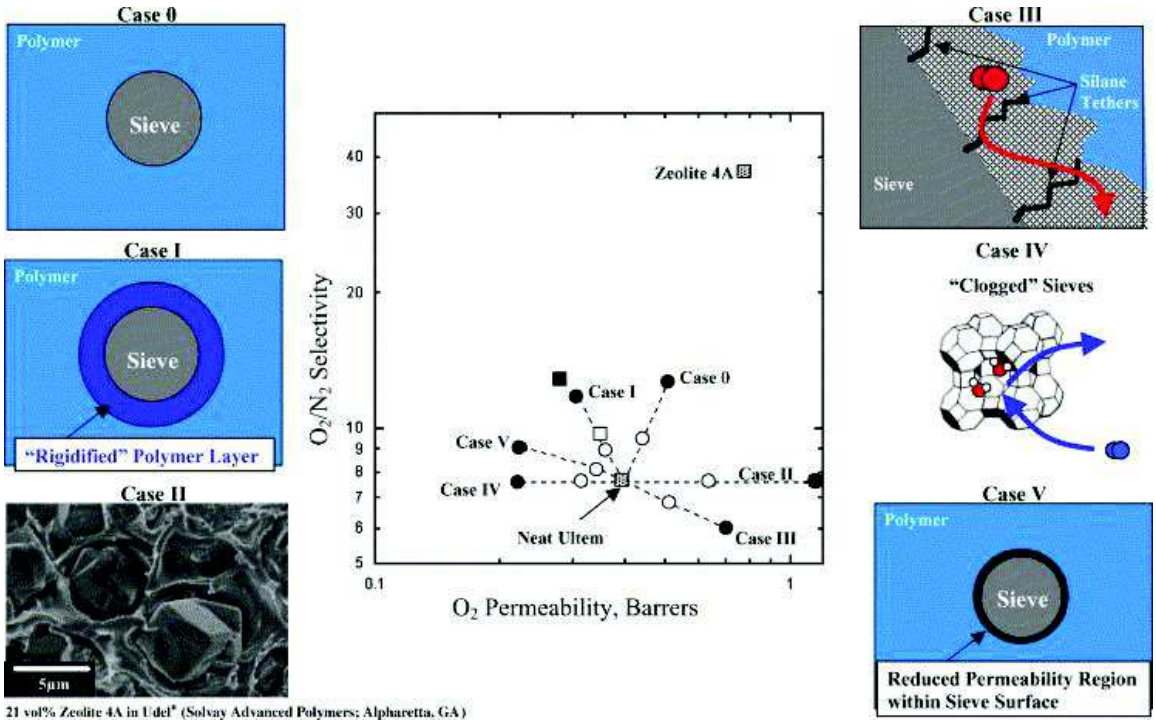


**Figure 5.7.** Summary of relationship between the morphology at the interface and gas transport properties of a generic mixed matrix membrane. Adapted from [105]

### 5.3.2 Gas permeation data

#### 5.3.2.1 MIL-101 based MMMs

The results of the permeability measurements for the "as cast" ED-MIL-101 MMMs are given in Figure 5.8a. The most permeable species is $CO_2$, confirming a solubility controlled transport for this gas, which is typical for $CO_2$ in PIMs. The permeation order of different gases is not affected by the MOFs addition ($CO_2$ > $H_2$ >He > $O_2$ > $CH_4$ > $N_2$). Although some of the permeabilities of MMMs are higher than that of neat PIM-1 for all gases, there is a clear trend of decreasing permeability with increasing filler content (Figure 5.8a). The reason for this discrepancy with the neat polymer is not fully understood, but it is might be due to minor differences in the membrane preparation protocol, which is known to influence the membrane properties for PIMs. The neat polymer solution is cast as such, just after its preparation, whereas

the solutions for the MMMs undergo sonication (of the fillers), mixing with the polymer solution, and more extended stirring of the particle suspension. Furthermore, it is known that any fillers in the PIM matrix may affect the free volume of the polymer itself [106]. The latter may have caused the step increase, while the further effect of the filler is a decrease. Nevertheless, the gas transport properties of the MMMs can be described satisfactorily with the Maxwell model (Eq. 5.5).

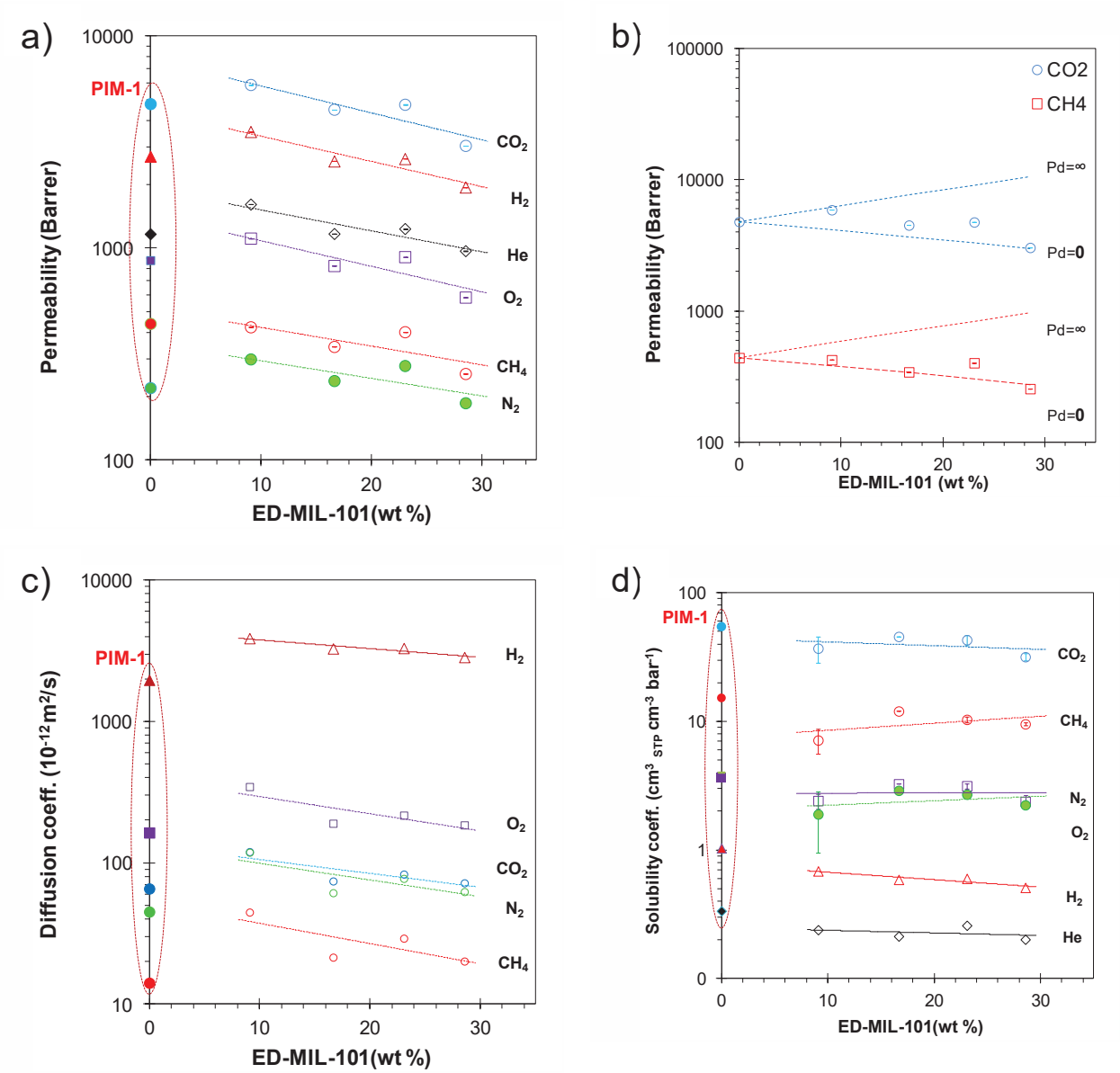


**Figure 5.8.** a) Permeabilities for $CO_2$, $H_2$, He, $O_2$, $CH_4$, $N_2$, of MMMs as a function of MOF ED-MIL-101 loading (wt%), compared to that of neat PIM-1; b) $CO_2$ and $CH_4$ permeabilities as a function of ED-MIL-101(wt %) concentration. The lines correspond to the fit of the experimental data with Maxwell equation for the lower limit and the upper limit with Pd=0 and Pd = ∞, respectively; c) Diffusion and d) Solubility coefficient as a function of the MOFs concentration. Except in figure b), the lines are solely reported ad a guide to the eye.

When plotting the permeabilities of the gas pair of major interest ($CO_2/CH_4$) as a function of MOFs concentration in the Maxwell windows for the two limit cases ($Pd$=0 and $Pd$=∞), the permeabilities of both gases are close to the lower limit, for which $Pd$=0 Figure 5.8b. This means that the fillers act on the MMM performance as obstacles with low permeability.

The decrease in permeability of the MMMs with increasing filler content reflects mostly the changes in the diffusion coefficient (Figure 5.8c). Remarkably, all MMMs present a higher diffusion coefficient compared to the neat membrane, highlighting a similar discontinuity in the trend as a function of the filler content as was already observed for the permeability.

On the other hand, the solubility hardly depends on the filler content (Figure 5.8d), confirming that the influence of the filler on the permeability is mostly related to how the diffusion path is affected.

#### 5.3.2.2 UiO-66 based MMMs

Instead, for three MOFs of the UiO family (UiO-66, UiO-66-$NH_2$, UiO-66-$(COOH)_2$) without functionalization, with amine functionalization and with acid functionalization, the related "As cast" MMMs showed different behaviour, as shown in Figure 5.9, Figure 5.10 and Figure 5.11, respectively. In all cases, the increasing weight percentage of UiO-66 tends to give more permeable membranes (Figure 5.9a, Figure 5.10a and Figure 5.11a). The higher permeability of the MMMs with respect to the neat membranes is due to the enhanced diffusivity of the gas through the definite size of the sieves MOFs (8-11 Å) (Figure 5.9c, Figure 5.10c and Figure 5.11c), which offer a favourable diffusion path. Also in this case, the solubility is hardly affected by the presence of the UiO fillers (Figure 5.9d, Figure 5.10d and Figure 5.11d)

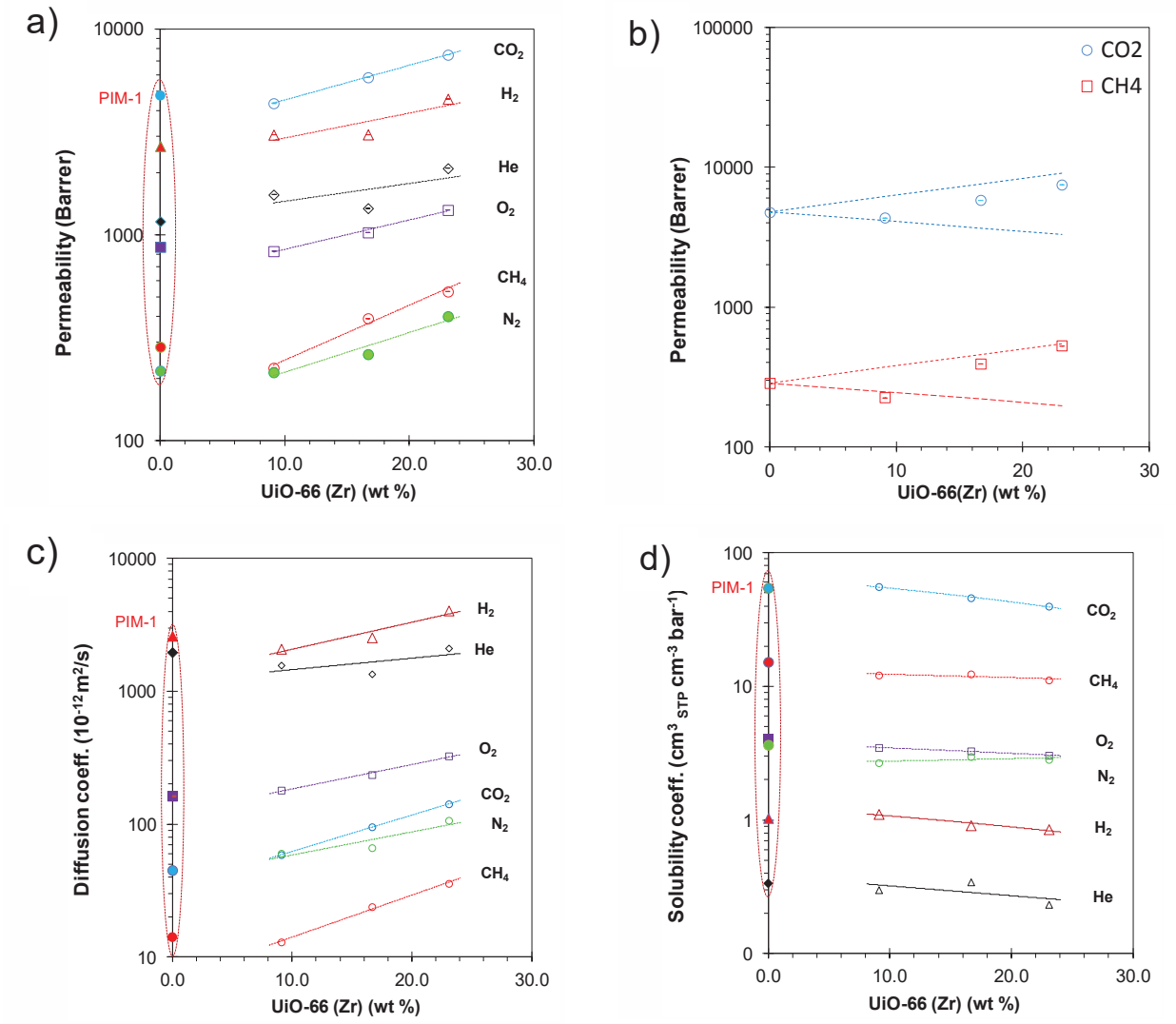


**Figure 5.9.** a) Permeabilities for $CO_2$, $H_2$, He, $O_2$, $CH_4$, $N_2$, of MMMs as a function of the UiO-66(Zr) loading (wt%), compared to that of neat PIM-1; b) $CO_2$ and $CH_4$ permeabilities as a function of the UiO-66(Zr) concentration. The lines correspond to the fit of the experimental data with Maxwell equation for the lower limit and the upper limit with Pd=0 and Pd = ∞, respectively; c) Diffusion and d) Solubility coefficient as a function of the MOFs concentration. The lines are solely reported ad a guide to the eye.

The positive effect of the UiO filler on the permeability of $CO_2$ and $CH_4$ is clearly seen when plotting the permeability together with the upper and lower limits defined by the Maxwell equation (Figure 5.9b, Figure 5.10b and Figure 5.11b), especially for the non-functionalized UiO-66-(Zr). As above, the position of neat PIM-1 with respect of the MMMs may slightly depend on the membrane preparation conditions. In all cases,the measured data fall within the window defined by the Maxwell equation, indicating that there ar no anomalies.

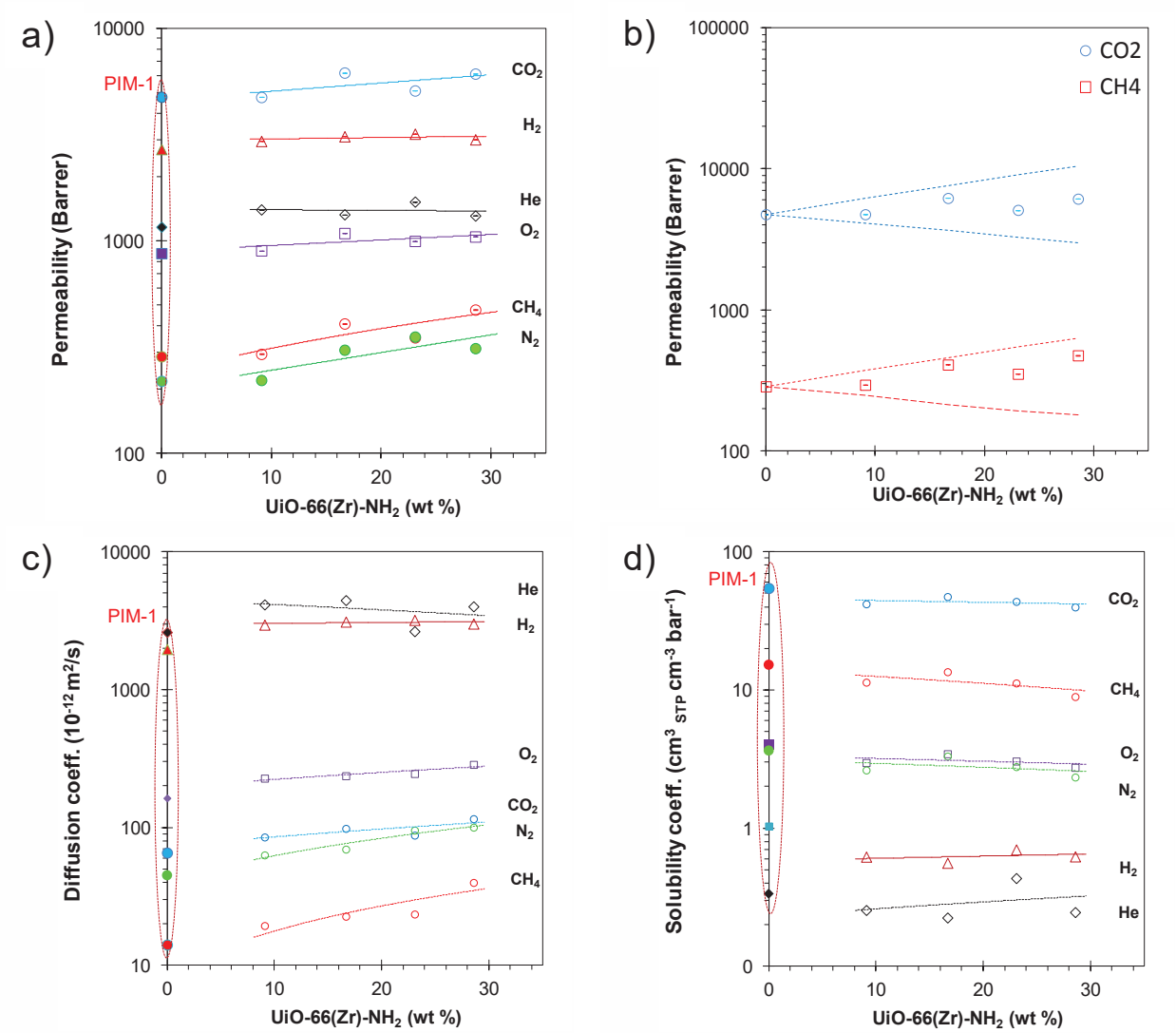


**Figure 5.10.** a) Permeabilities for $CO_2$, $H_2$, He, $O_2$, $CH_4$, $N_2$, of MMMs as a function of the UiO-66-$NH_2$ loading, compared to that of neat PIM-1; b) $CO_2$ and $CH_4$ permeabilities as a function of the UiO-66-$NH_2$ concentration. The lines correspond to the fit of the experimental data with Maxwell equation for the lower limit and the upper limit with Pd=0 and Pd = ∞, respectively; c) Diffusion and d) Solubility coefficient as a function of the MOFs concentration. The lines are solely reported ad a guide to the eye.

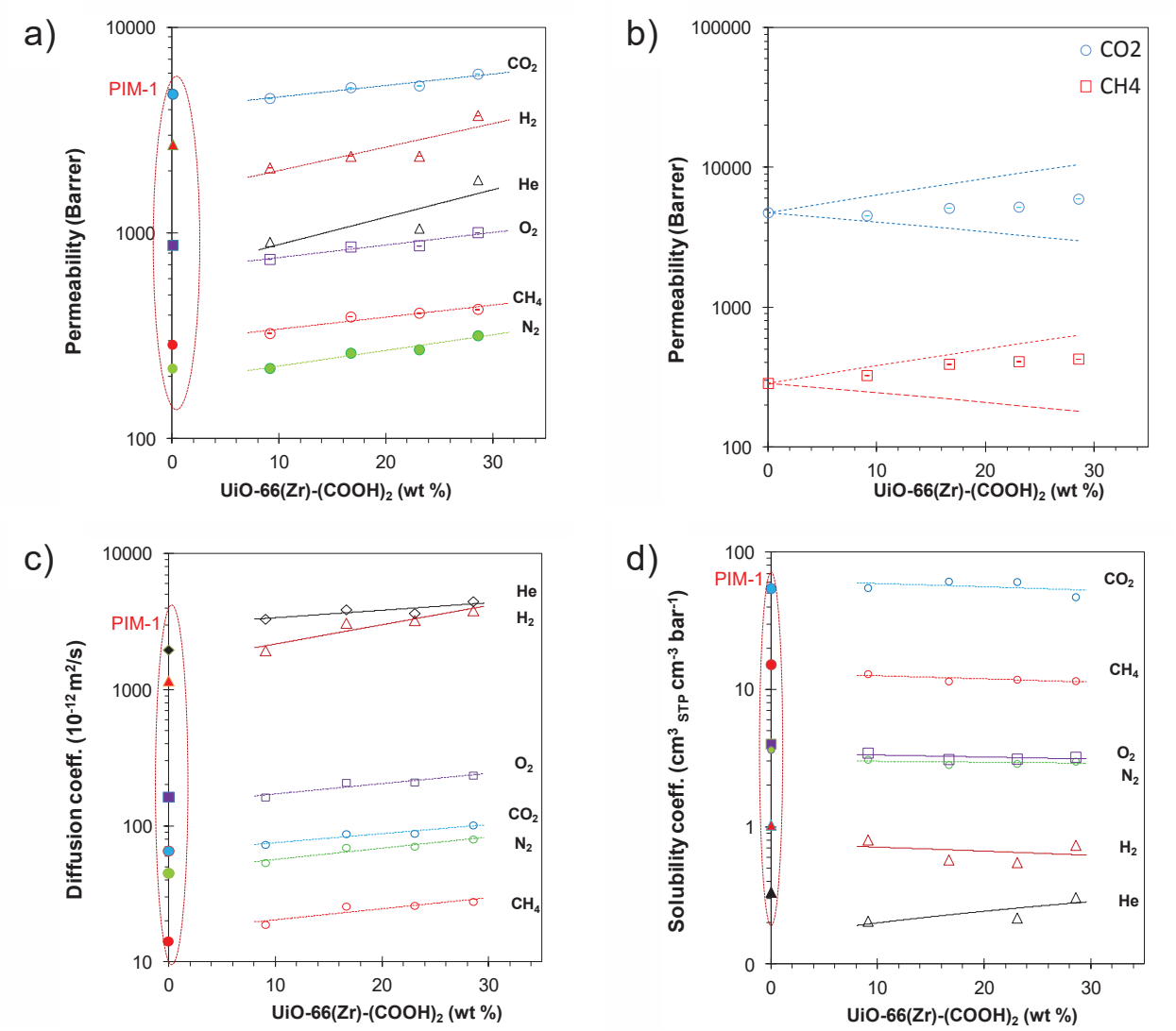


**Figure 5.11.** a) Permeabilities for $CO_2$, $H_2$, He, $O_2$, $CH_4$, $N_2$, of MMMs as a function of the UiO-66-$(COOH)_2$ loading (wt%), compared to that of neat PIM-1; b) $CO_2$ and $CH_4$ permeabilities as a function of the UiO-66-$(COOH)_2$ concentration. The lines correspond to the fit of the experimental data with Maxwell equation for the lower limit and the upper limit with Pd=0 and Pd = ∞, respectively; c) Diffusion and d) Solubility coefficient as a function of the MOFs concentration. The lines are solely reported ad a guide to the eye.

For those mixed matrix membrane that were not mechanically damaged during the testing, the gas measurements were carried out in "as cast" conditions and after methanol treatment of the membrane. It is known that high free volume of polymer as PIM-1 are sensitive to treatment with alcohols like methanol (MeOH) [105], which removes residual casting solvent and increases the free volume. Moreover, the alcohol-treatment of the membrane containing MOFs may serve to remove the residual casting solvent blocked inside the MOF cavities and to active the fillers [107]. The comparison of the $CO_2$ and $CH_4$ permeability in the "as cast" membranes and after

MeOH treatment is shown in Figure 5.12 for all four MOFs. In all cases, the permeabilities after alcohol-treatment are significantly higher than those of the "as cast" membranes. In most cases, the permeabilities after methanol-treatment show a more monotonous trend than the trend observed for the "as cast" membranes. This is because the methanol treatment cancels the differences in the casting history.

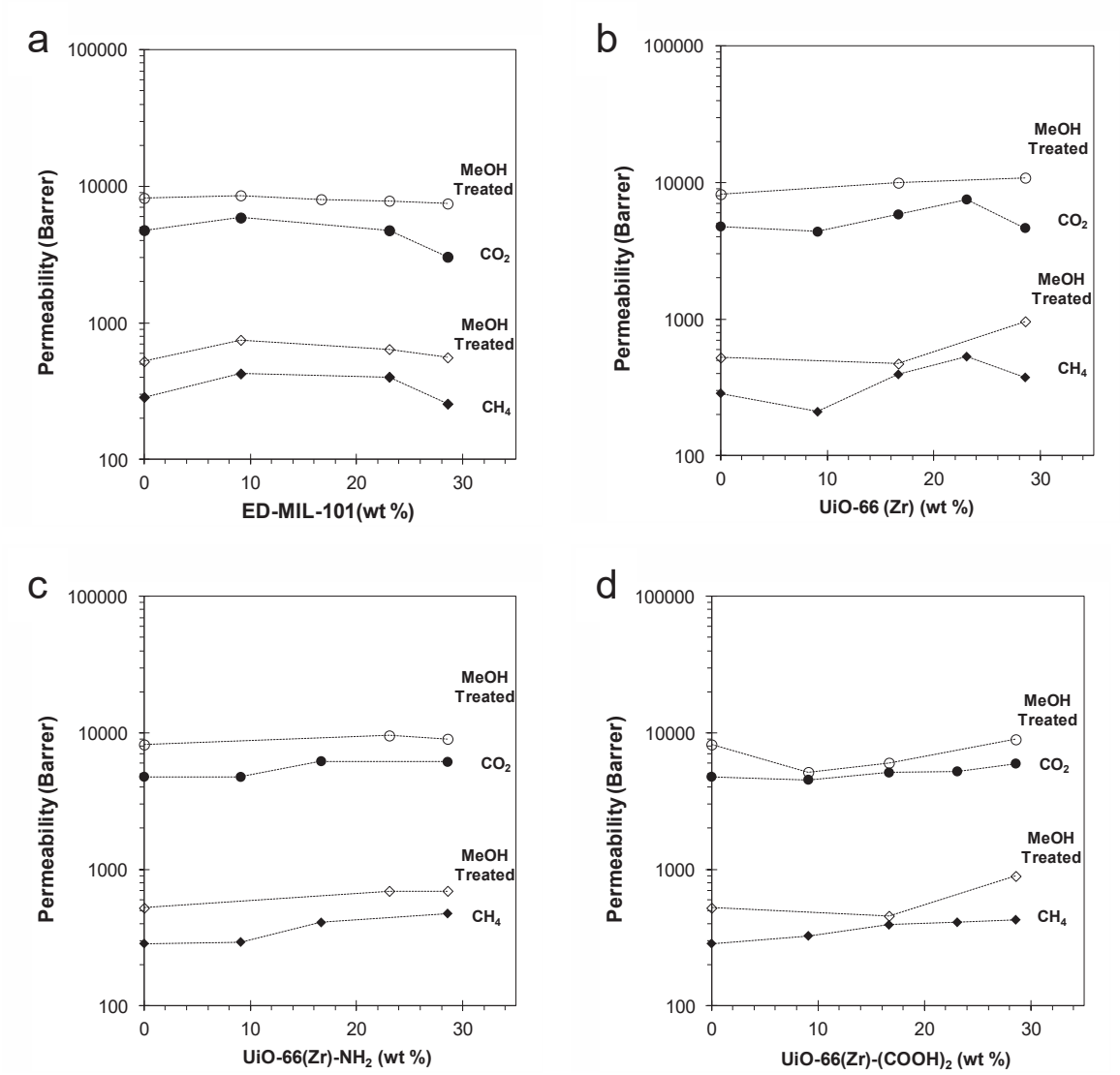


**Figure 5.12.** $CO_2$ and $CH_4$ permeability as cast (black) and MeOH (white). a) increasing the ED-MIL-101 loaded; b) increasing the UiO-66 loaded; c) increasing the UiO-66-($NH_2$) loaded; d) increasing the UiO-66-$(COOH)_2$ loaded.

For the ED-MIL-101 filler, the negative effect of the filler on the permeability is also confirmed after the MeOH treatment. Only for methane, the permeability in neat PIM is lower than that of the MMMs. This is most likely due to the formation of microfractures in the sample because of

the pressure of the sealing ring during the measurement of the as-cast membrane, which reduce the membrane selectivity. The UiO-based membranes confirm the strongest positive effect of the MOF on the permeability of the membrane for UiO-66-(Zr), whereas the $–NH_2$ functionalized UiO-66 seems to have only a slightly positive effect. The effect of the –COOH functionalized UiO-66 in absolute terms seems to be negative, but with increasing filler concentration there is clearly an increasing trend in permeability. Unfortunately, very small sample specimens were available for this work and only single measurements could be performed. Of course, duplo- or triplo- measurements would greatly enhance the reliability of the conclusions and perhaps finding more subtle changes rather than general trends.

### 5.3.3 Comparative study based on the Robeson diagram

The performance of MMMs, in comparison with polymeric membranes in general, is usually evaluated by looking at the position of the MMMs with respect to Robeson's upper bound [108,109]. A summary of the present results is given in Figure 5.13. The $CO_2/CH_4$ selectivity for the all MMMs overtake the upper bound in the region close to the neat PIM-1.
Figure 5.13a clearly shows the negative effect of the filler ED-MIL101 on the performance of PIM-1 membranes, because the filler causes a decrease in terms of selectivity and in terms of permeabiity. The data thus shift to the lower left corner of the Robeson diagram.

The reduction in terms of selectivity respect to the neat PIM-1 (moving from high to low into the Robeson's plot) can be described as a consequence of a bad dispersion of MOFs inside the matrix. Instead, the reduction in terms of permeability with respect to the neat polymer can be associated to the clogged sieve phenomena that occurs when the free volume of the polymer matrix is occupied by the fillers [86]. On the other hand, for the UiO-66-$NH_2$ and UiO-66 based MMMs an increase in the permeabilities with the MOFs concentration was observed and at the same time only a slight decrease of the $CO_2/CH_4$ selectivity took place, remaining nevertheless close to the value of neat PIM-1 Figure 5.13b and c. Finally, the Permeability of the membrane with UiO-66-$(COOH)_2$, increased slightly, but the selectivity remained more or less constant, close to that of neat PIM-1.

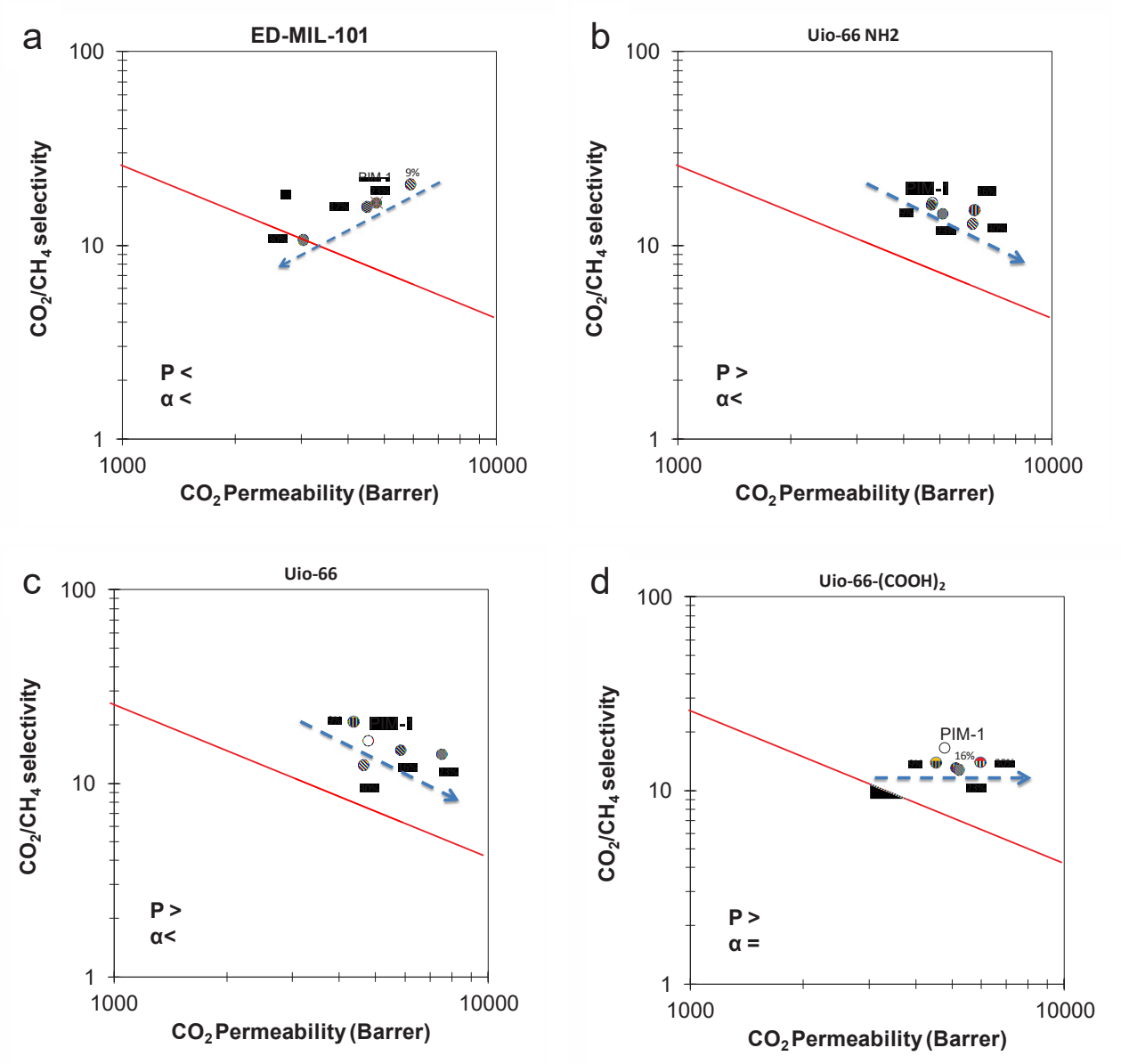


**Figure 5.13.** Robeson's plot of $CO_2/CH_4$ selectivity for a) ED-MIL101 b) UiO-66-($NH_2$) c) UiO-66 d) UiO-66-$(COOH)_2$/PIM-1 membranes with 9wt % (yellow), 17 wt% (blue), 23wt% (green), 30 wt% (red). PIM-1 data are reported for comparison (open symbols). The red line represents the Robeson 2008 upper bound [109].

## 5.4 Conclusions

This work reported the study of gas transport properties for Zr/Cr-based metal organic frameworks dispersed into the PIM-1 a polymer with high intrinsic microporosity. The studies show that the gas transport through the mixed matrix membranes could in most cases described effectively by the Maxwell model indicating a good dispersion of the fillers in the organic

polymer matrix. More specifically, the dispersion of Cr-based MOFs (ED-MIL-101) decreases the permeability of PIM-1 with increasing filler loading. Instead, all the Zr-based MOFs (UiO-66, UiO-66($NH_2$) and UiO-66$(COOH)_2$) increase the PIM-1 permeabilities with different effect on the ideal $CO_2/CH_4$ selectivity. For UiO-66 and UiO-66($NH_2$), the increasing $CO_2$ permeabilities are accompanied by a decrease of the ideal $CO_2/CH_4$ selectivity. Finally, the UiO-66-$(COOH)_2$ based MMMs improve the PIM-1 performance in terms of permeabilities overtaking the upper bound in the region of higher permeability and the ideal $CO_2/CH_4$ selectivity keeps the ideal value close to that of neat PIM-1. The methanol treatment seems to improve the permeability for all membranes but further investigation needs to understand if this effect is ascribed to the activation of MOFs or for the only benefits on the free volume of PIM-1. Unfortunately, very small sample specimens were available for this work and only single measurements could be performed. For future work, duplicate or triplicate measurements would greatly enhance the reliability of the measurements and their conclusions.

# Chapter 6. General Conclusions

The scope of this work was to study different kinds of membrane-based technology for the $CO_2/CH_4$ separation process for biogas upgrading, in order to understand their working principle in terms of gas transport properties and their limits and advantages for this use. Three different types of membranes were examined: Thin film composite Pebax®/PAN Hollow fibre membranes, membrane contactors for $CO_2/CH_4$ separation by facilitated $CO_2$ transport in ionic liquids, and Mixed Matrix Membranes based on the polymer of intrinsic microporosity PIM-1 and various metal organic framework fillers. The approaches used for each type of membrane and the associated problems were reviewed and discussed.

## 6.1 Advantages and limitations of Pebax®/PAN Hollow fibre membranes

The thin film composite Pebax®/PAN hollow fibre membranes were successfully tested for potential use in $CO_2/CH_4$ separation via preliminary studies of pure gas permeation. They present a lot of advantages respect to the other kinds of membranes, such as low cost, excellent mechanical stability at high pressure, high density of packaging and easy processability.

### 6.1.1 Cost of membrane and their marketing

The marketing of membrane systems for gas separation has reached in 2000 a total value of 160 million dollars, and according to some estimates it will reach 730 million dollars in 2020. Different systems for upgrading at small-scale were developed (Table 6.1), the first of which were introduced by Grace Membrane system, Separex and Cynara companies.

The cost of a membrane depends primarily on two factors: on the cost of the polymer needed for the manufacture and on the type of module design. The cost for the membrane made with 50g of polymer characterized by good separating properties and high cost is in the $\$50/m^2$-$500/m^2$ range (1$/g-10$/g of polymer). The Pebax/PAN composite hollow fibre made in this work present an active dense layer of 5 μm thick, so a smaller amount of polymer is required for the membrane preparation. Considering that the cost of this polymer is relatively low, the membrane manufacture for this kind of membrane can be done at relatively low cost, although the total membrane cost should of course also include the cost of the porous support material.

Table 6.1. Principal Suppliers of membrane natural gas separation system [111]

| *Company* | *Membrane material* | *Membrane module type* |
|---|---|---|
| Medal | polyimide | Hollow fibre |
| W.R.Grace | Cellulose acetate | Spiral-wound |
| Separex | Cellulose acetate | Spiral-wound |
| Cynara | Cellulose acetate | Hollow fibre |
| ABB/MTR | Perfluoro polymers<br>silicon rubbery | Spiral-wound |
| Permea | polysulfone | Hollow fibre |

### 6.1.2 Mechanical and performance stability

Regarding, the membrane stability in terms of mechanical resistance and performance in the time, the Pebax/PAN hallow fibre studied, showed a pressure resistance, up to at least 14 bar, which was the physical limit of the setup used. Moreover, the coating on the inner surface of the fibres avoids the negative effects such as sticking or accidental mechanical damages occurring in the case of external coating, ensuring a greater performance stability of membrane in the time and easier handling.

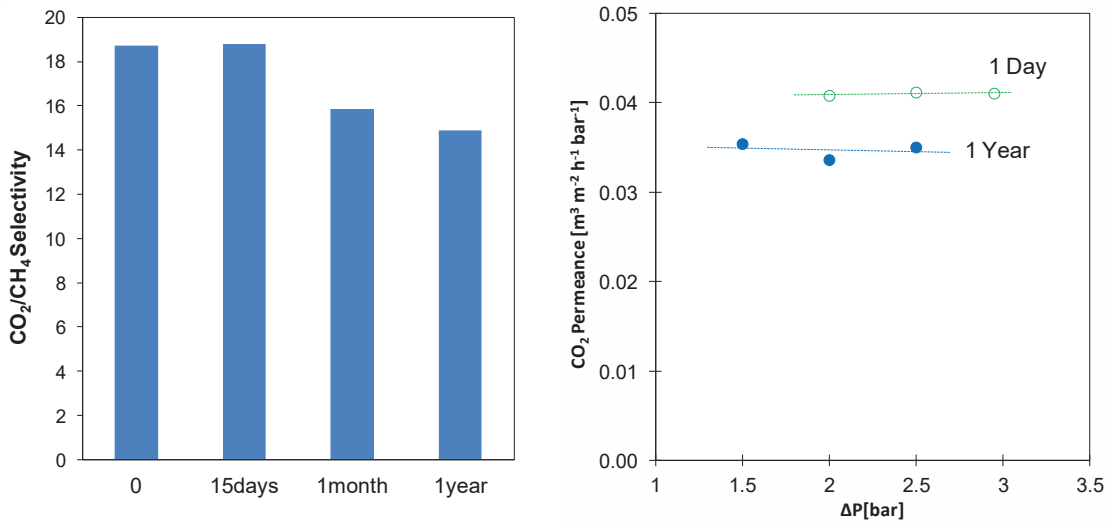


**Figure 6.1.** Aging effect on the a) $CO_2/CH_4$ selectivity and b) in the $CO_2$ permeance of Pebax/PAN hollow fibres.

In fact, Figure 6.1 shows that the selectivity and permeability slightly decrease after one year but they remain in the same order of magnitude, showing an excellent performance stability due to a good mechanical resistance.

### 6.1.3 Processability and scale-up

Generally, polymeric membranes offer an easy processability into different configurations, to both flat sheets and hollow fibres, and straightforward scalability. In this specific case, using a new coating method based on the cross flow filtration, it is possible to obtain the simultaneous coating of a large number of fibres. This facilitates the scale-up because the coating can be applied directly onto existing hollow fibre modules.

## 6.2 Advantages and limitations of membrane contactors for $CO_2/CH_4$ separation by facilitated $CO_2$ transport in ionic liquids

This work discussed the potential use of membrane contactors for the upgrading process in which facilitated transport of $CO_2$ takes place by means of a mobile carrier. Generally, the main limitation for long-term operation of facilitated transport membranes is the loss of carriers by evaporation of reactive media or solvent. In this work, the stability problem due to the evaporation of carrier was avoided, using as the solvent an ionic liquid, characterized by negligible vapour pressure at room temperature. Moreover, the carriers are contained inside the lumen of fibres to avoid its loss. However, for most of facilitated membrane feed precondition with water are necessary to increase the mobility of carrier or to accelerate the reaction rate. The advantage of this membrane for upgrading process is that the precondition with water is not necessary because the raw biogas contains at least 85% relative humidity. Another crucial point for membrane contactors for facilitated $CO_2$ transport in ionic liquids is the compatibility between the solvent (in this case ionic liquid) and hollow fibre material in order to avoid problems related to the solvent-induced deterioration, membrane wetting and pore blocking. The membrane contactor studied in this work showed no problems with operation stability over 2 hours and a good separation in time for the $CO_2/CH_4$ mixture. Obviously, long term tests are needed in future research on this topic. The $CO_2$ was adsorbed in greater quantities than methane with a solubility selectivity of 3. The study of the contactor performance with the Carbonic Anhydrase enzyme-doped ionic liquid provided the proof of principle for the potential use in the

upgrading of biogas, but for a better understanding of the entire process, this still needs further investigation. The goal is to develop a facilitated transport membrane that can maintain its permeability and selectivity without the loss of this performance in time. Moreover, the principle of separation for this type of membrane is based on a biocatalytic process and the $CO_2$ produced may have the requirements to be used in the food market. In order to use not only the methane from biogas as a source of energy but in order to recover also the $CO_2$ and to avoid its disposal into the atmosphere.

## 6.3 Advantages of mixed Matrix membranes

Mixed matrix membrane with Zr/Cr-based MOF dispersed in PIM-1 were prepared with the objective to increase the selectivity and/or the permeability of the organic polymer PIM-1. The MOFs can affect the membrane transport in two different ways: by acting as molecular sieves they can increase the selectivity, or by increasing the free volume of PIM-1 they can improve the permeability. The main limit for this kind of membrane is that the transport properties are strongly dependent on the morphology of the membrane. The interfacial contact zone appears to be equally important to achieve optimum transport properties. PIM-1 membranes exhibit very high permeability ($Pe_{CO2} \approx 4800$ Barrer) and a great $CO_2/CH_4$ selectivity ($\alpha = 17$). The MMM may further improve these two parameters depending on the MOF type and on the quality of the dispersion. The best improvement of the PIM-1 performance were obtained loading the UiO-66-$(COOH)_2$ based MOFs. In the case of UiO-66-$(COOH)_2$ is possible to obtain simultaneously an increase in permeability ($Pe_{CO2} \approx 6000$ Barrer) maintaining the $CO_2/CH_4$ selectivity close to that of neat polymer; The ED-MIL-101 decreases permeability and selectivity of PIM-1 probably due to the bad dispersion of fillers. On the other hand, the UiO-66 and UiO-66-$(NH_2)$ increase the $CO_2$ permeability decreasing the ideal $CO_2/CH_4$ selectivity. But further investigations are needed to activate and make accessible the cages with specific dimensions of MOFs.

## 6.4 Comparison between different kind of membranes and future directions

The energy consumption, permeability, selectivity, chemical absorbent, transport mechanism and cost for the different membranes types are compared in Table 6.2. This table shows an overview of the overall cost and performance of each membrane kind.

Table 6.2. Comparison of different types of membranes for $CO_2/CH_4$ separation adapted from [111]

| *Polymer type* | *Membrane type* | *Transport Mechanism* | *Energy consumption* | *Permeability* | *Selectivity* | *Chemical absorbent* | *Cost* |
|---|---|---|---|---|---|---|---|
| Polymeric | Composite hollow fibres | Solution-diffusion | Low | Good | Good | No | Low |
| Polymeric ionic liquid | Membrane contactor | Facilitated transport | High | Low | Good | Yes | Medium to high |
| Hybrid: Polymeric + MOFs | Mixed matrix membranes | Solution-Diffusion with Maxwell model | Medium | High | Good | No | Medium to high |

The Pebax®/PAN hollow fibres modules allow large areas of membrane to be packaged into compact membrane modules with respect to the membrane contactor and flat mixed matrix membranes. Moreover, the cost of the polymer is much lower than the material cost for the fabrication of other kinds of membranes. The PAN porous support and the thin selective Pebax layer are made with low cost polymers ($50/m$^2$-500/m$^2$) [110]. Instead, the cost of ionic liquid for the facilitated transport membrane contactor and of the enzyme are higher (1$/g and 0.1$/g). The highest cost of material is for the mixed matrix membranes: MOFs (30-80$/g) and unknown for PIM-1 (being a material of new synthesis). However, the cost of membranes used in gas separation processes is a relatively small fraction of the final membrane process cost. The cost depend primarily on the equipment, such as pressure vessels, pipes, flanges, and valves that are required. One possible way to reduce membrane skid cost is to increase the permeance of the membranes, allowing a smaller membrane area to be used to treat the same volume of gas. For this reason, the mixed matrix membrane can represent a valid solution to this problem with a good trade-off between the material cost for membrane fabrication and membrane performance. In fact, these membranes present a good $CO_2/CH_4$ selectivity (α 17-20), similar to the Pebax®/PAN hollow fibres (α = 18), but with a much higher $CO_2$ permeability with respect to the Pebax composite membranes. In conclusion, this work demonstrated that:

1. Composite Pebax® /PAN hollow fibre membranes can be successfully prepared by means of a dynamic cross-flow filtration coating method. The membranes show a high $CO_2/CH_4$ selectivity = 18, with a good $CO_2$ permeability (76.2 barrer).
2. A good sorption selectivity ($\alpha_s$= 3) was obtained for the $CO_2/CH_4$ mixture with the membrane contactor of PAN hollow fibres and ionic liquid [BMIM][OTf]. This membrane does not require water removal before gas separation step and the separation principle is based on a process of biocatalysis that requires further investigation to understand its full potential.

3. Zr/Cr-based MOFs, dispersed into the PIM-1 for the fabrication of mixed matrix membranes show excellent gas transport properties. The addition of fillers can increase this performance depending on the MOF type. Zr-based MOFs of the UiO-66 family increases permeability of PIM-1 decreasing selectivity. Instead, Cr-based MOFs of the MIL-101 family decrease the PIM-1 permeability with increasing filler concentration. The best improvement of the PIM-1 performance was obtained with the UiO-66-$(COOH)_2$ dispersion which yielded a simultaneous increase in permeability ($Pe_{CO2} \approx 6000$ Barrer), maintaining the $CO_2/CH_4$ selectivity close to that of neat polymer.

Definitely, the membrane technology offers a potentially valid alternative to the traditional techniques of $CO_2/CH_4$ separation in from various points of view. Nevertheless, each of the systems studied in the present work still needs further investigation to evaluate the performance under real operating conditions.

# Bibliography

[1] K.C. Surendra, D. Takara, A.G. Hashimoto, S.K. Khanal, Biogas as a sustainable energy source for developing countries: Opportunities and challenges, Renew. Sustain. Energy Rev. 31 (2014) 846–859. doi:10.1016/j.rser.2013.12.015.

[2] K. Stamatelatou, G. Antonopoulou, G. Lyberato, Production of biogas via anaerobic digestion, Elsevier, 2010. doi:10.1533/9780857090492.2.266.

[3] A. Petersson, J.B. Holm-nielsen, D. Baxter, Biogas upgrading technologies – developments and innovations, IEA Bioenergy. (2009).

[4] P. Kaparaju, J. Rintala, Generation of heat and power from biogas for stationary applications: biolers, gas engines and turbines, combined heat and power (CHP) plants and fuel cells, Elsevier, 2013. doi:10.1533/9780857097415.3.404.

[5] D. Divya, L.R. Gopinath, P. Merlin Christy, A review on current aspects and diverse prospects for enhancing biogas production in sustainable means, Renew. Sustain. Energy Rev. 42 (2015) 690–699. doi:10.1016/j.rser.2014.10.055.

[6] C. Mao, Y. Feng, X. Wang, G. Ren, Review on research achievements of biogas from anaerobic digestion, Renew. Sustain. Energy Rev. 45 (2015) 540–555. doi:10.1016/j.rser.2015.02.032.

[7] H. Yang, H. Ye, S. Zhai, G. Wang, Leak detection of gas transport pipelines based on wigner distribution, 2011 Int. Symp. Adv. Control Ind. Process. 7 (2011) 258–261. doi:10.1002/apj.

[8] J.B. Holm-Nielsen, T. Al Seadi, P. Oleskowicz-Popiel, The future of anaerobic digestion and biogas utilization, Bioresour. Technol. 100 (2009) 5478–5484. doi:10.1016/j.biortech.2008.12.046.

[9] M.G. Mengistu, B. Simane, G. Eshete, T.S. Workneh, A review on biogas technology and its contributions to sustainable rural livelihood in Ethiopia, Renew. Sustain. Energy Rev. 48 (2015) 306–316. doi:10.1016/j.rser.2015.04.026.

[10] M. Ferreira, I.P. Marques, I. Malico, Biogas in Portugal: Status and public policies in a European context, Energy Policy. 43 (2012) 267–274. doi:10.1016/j.enpol.2012.01.003.

[11] Y. He, D.M. Bagley, K.T. Leung, S.N. Liss, B.-Q. Liao, Recent advances in membrane technologies for biorefining and bioenergy production, Biotechnol. Adv. 30 (2012) 817–858. doi:10.1016/j.biotechadv.2012.01.015.

[12] T.T.T. Cu, P.H. Cuong, L.T. Hang, N. Van Chao, L.X. Anh, N.X. Trach, et al., Manure management practices on biogas and non-biogas pig farms in developing countries - using livestock farms in Vietnam as an example, J. Clean. Prod. 27 (2012) 64–71. doi:DOI 10.1016/j.jclepro.2012.01.006.

[13] O. Chasnyk, G. Sołowski, O. Shkarupa, Historical, technical and economic aspects of biogas development: Case of Poland and Ukraine, Renew. Sustain. Energy Rev. 52 (2015) 227–239. doi:10.1016/j.rser.2015.07.122.

[14] M. Larsson, S. Grönkvist, P. Alvfors, Upgraded biogas for transport in Sweden – effects of policy instruments on production, infrastructure deployment and vehicle sales, J. Clean.

Prod. (2015). doi:10.1016/j.jclepro.2015.08.056.

[15] S. Rasi, J. Läntelä, J. Rintala, Trace compounds affecting biogas energy utilisation - A review, Energy Convers. Manag. 52 (2011) 3369–3375. doi:10.1016/j.enconman.2011.07.005.

[16] K. Stamatelatou, G. Antonopoulou, G. Lyberato, Production of biogas via anaerobic digestion, Elsevier, 2010. doi:10.1533/9780857090492.2.266.

[17] R.P.J.M. Raven, K.H. Gregersen, Biogas plants in Denmark: successes and setbacks, Renew. Sustain. Energy Rev. 11 (2007) 116–132. doi:10.1016/j.rser.2004.12.002.

[18] S. Basu, A.L. Khan, A. Cano-Odena, C. Liu, I.F.J. Vankelecom, Membrane-based technologies for biogas separations., Chem. Soc. Rev. 39 (2010) 750–768. doi:10.1039/b817050a.

[19] M. Scholz, T. Melin, M. Wessling, Transforming biogas into biomethane using membrane technology, Renew. Sustain. Energy Rev. 17 (2013) 199–212. doi:10.1016/j.rser.2012.08.009.

[20] E. Ryckebosch, M. Drouillon, H. Vervaeren, Techniques for transformation of biogas to biomethane, Biomass and Bioenergy. 35 (2011) 1633–1645. doi:10.1016/j.biombioe.2011.02.033.

[21] R.W. Baker, Membrane Technology and Applications, John Wiley & Sons, Ltd, Chichester, UK, 1985. doi:10.1016/S0376-7388(00)83139-7.

[22] A. Marković, D. Stoltenberg, D. Enke, E.-U. Schlünder, A. Seidel-Morgenstern, Gas permeation through porous glass membranes, J. Memb. Sci. 336 (2009) 32–41. doi:10.1016/j.memsci.2009.02.030.

[23] J.C. Jansen, M. Macchione, E. Drioli, High flux asymmetric gas separation membranes of modified poly(ether ether ketone) prepared by the dry phase inversion technique, J. Memb. Sci. 255 (2005) 167–180. doi:10.1016/j.memsci.2005.01.032.

[24] P. Bernardo, J.C. Jansen, F. Bazzarelli, F. Tasselli, A. Fuoco, K. Friess, et al., Gas transport properties of Pebax®/room temperature ionic liquid gel membranes, 2012. doi:10.1016/j.seppur.2012.02.041.

[25] Y. Zhang, J. Sunarso, S. Liu, R. Wang, Current status and development of membranes for CO2/CH4 separation: A review, Int. J. Greenh. Gas Control. 12 (2013) 84–107. doi:10.1016/j.ijggc.2012.10.009.

[26] C.A. Scholes, S. Kanehashi, G.W. Stevens, S.E. Kentish, Water permeability and competitive permeation with CO2 and CH4 in perfluorinated polymeric membranes, Sep. Purif. Technol. 147 (2015) 203–209. doi:10.1016/j.seppur.2015.04.023.

[27] I. Pinnau, L.G. Toy, Gas and vapor transport properties of amorphous perfluorinated copolymer membranes based on 2,2-bistrifluoromethyl-4,5-difluoro-1,3-dioxole/tetrafluoroethylene, J. Memb. Sci. 109 (1996) 125–133. doi:10.1016/0376-7388(95)00193-X.

[28] K.C. Khulbe, G. Chowdhury, B. Kruczek, R. Vujosevic, T. Matsuura, G. Lamarche, Characterization of the PPO dense membrane prepared at different temperatures by ESR, atomic force microscope and gas permeation, J. Memb. Sci. 126 (1997) 115–122. doi:10.1016/S0376-7388(96)00278-5.

[29] M. Pourafshari Chenar, M. Soltanieh, T. Matsuura, A. Tabe-Mohammadi, K.C. Khulbe, The effect of water vapor on the performance of commercial polyphenylene oxide and

Cardo-type polyimide hollow fiber membranes in CO2/CH4 separation applications, J. Memb. Sci. 285 (2006) 265–271. doi:10.1016/j.memsci.2006.08.028.

[30] M. Macchione, J.C. Jansen, E. Tocci, E. Drioli, Influence of residual solvent on the gas transport properties of dense Hyflon® AD 60X gas separation membranes, Desalination. 200 (2006) 49–51. doi:10.1016/j.desal.2006.03.238.

[31] A. Morisato, I. Pinnau, Synthesis and gas permeation properties of poly(4-methyl-2-pentyne), J. Memb. Sci. 121 (1996) 243–250. doi:10.1016/S0376-7388(96)00183-4.

[32] J.G.W.R.W. Baker, The solution-diffusion model : a review, J. Memb. Sci. 107 (1995) 1–21. doi:10.1016/0376-7388(95)00102-I.

[33] L. Ansaloni, Y. Zhao, B.T. Jung, K. Ramasubramanian, M.G. Baschetti, W.S.W. Ho, Facilitated transport membranes containing amino-functionalized multi-walled carbon nanotubes for high-pressure CO2 separations, J. Memb. Sci. 490 (2015) 18–28. doi:10.1016/j.memsci.2015.03.097.

[34] W. He, Z. Wang, W. Li, S. Li, Z. Bai, J. Wang, et al., Cyclic tertiary amino group containing fixed carrier membranes for CO2 separation, J. Memb. Sci. 476 (2015) 171–181. doi:http://dx.doi.org/10.1016/j.memsci.2014.11.039.

[35] A. Mondal, M. Barooah, B. Mandal, Effect of single and blended amine carriers on CO2 separation from CO2/N2 mixtures using crosslinked thin-film poly(vinyl alcohol) composite membrane, Int. J. Greenh. Gas Control. 39 (2015) 27–38. doi:10.1016/j.ijggc.2015.05.002.

[36] X. He, M.-B. Hägg, Energy Efficient Process for CO2 Capture from Flue gas with Novel Fixed-site-carrier Membranes, Energy Procedia. 63 (2014) 174–185. doi:10.1016/j.egypro.2014.11.018.

[37] Y.T. Zhang, L. Zhang, H.L. Chen, H.M. Zhang, Selective separation of low concentration CO2 using hydrogel immobilized CA enzyme based hollow fiber membrane reactors, Chem. Eng. Sci. 65 (2010) 3199–3207. doi:10.1016/j.ces.2010.02.010.

[38] M. Saeed, L. Deng, CO2 facilitated transport membrane promoted by mimic enzyme, J. Memb. Sci. 494 (2015) 196–204. doi:http://dx.doi.org/10.1016/j.memsci.2015.07.028.

[39] D.R. Paul, D.R. Kemp, The diffusion time lag in polymer membranes containing adsorptive fillers, 2007. doi:10.1002/polc.5070410109.

[40] A. Ebadi Amooghin, M. Omidkhah, A. Kargari, The effects of aminosilane grafting on NaY zeolite–Matrimid®5218 mixed matrix membranes for CO2/CH4 separation, J. Memb. Sci. 490 (2015) 364–379. doi:10.1016/j.memsci.2015.04.070.

[41] R. Swaidan, X. Ma, E. Litwiller, I. Pinnau, High pressure pure- and mixed-gas separation of CO2/CH4 by thermally-rearranged and carbon molecular sieve membranes derived from a polyimide of intrinsic microporosity, J. Memb. Sci. 447 (2013) 387–394. doi:10.1016/j.memsci.2013.07.057.

[42] L. Deng, M.-B. Hägg, Carbon nanotube reinforced PVAm/PVA blend FSC nanocomposite membrane for CO2/CH4 separation, Int. J. Greenh. Gas Control. 26 (2014) 127–134. doi:10.1016/j.ijggc.2014.04.018.

[43] Z. Sedláková, G. Clarizia, P. Bernardo, J. Jansen, P. Slobodian, P. Svoboda, et al., Carbon Nanotube- and Carbon Fiber-Reinforcement of Ethylene-Octene Copolymer Membranes for Gas and Vapor Separation, Membranes (Basel). 4 (2014) 20–39. doi:10.3390/membranes4010020.

[44] T.C. Merkel, Ultrapermeable, Reverse-Selective Nanocomposite Membranes, Science (80-. ). 296 (2002) 519–522. doi:10.1126/science.1069580.

[45] R. Pal, Permeation models for mixed matrix membranes, J. Colloid Interface Sci. 317 (2008) 191–198. doi:10.1016/j.jcis.2007.09.032.

[46] J.D. Felske, Effective thermal conductivity of composite spheres in a continuous medium with contact resistance, Int. J. Heat Mass Transf. 47 (2004) 3453–3461. doi:10.1016/j.ijheatmasstransfer.2004.01.013.

[47] S. a. Hashemifard, a. F. Ismail, T. Matsuura, Prediction of gas permeability in mixed matrix membranes using theoretical models, J. Memb. Sci. 347 (2010) 53–61. doi:10.1016/j.memsci.2009.10.005.

[48] E.A. Feijani, H. Mahdavi, A. Tavasoli, Poly(vinylidene fluoride) based mixed matrix membranes comprising metal organic frameworks for gas separation applications, Chem. Eng. Res. Des. 96 (2015) 87–102. doi:10.1016/j.cherd.2015.02.009.

[49] E.L. Cussler, Membranes containing selective flakes, J. Memb. Sci. 52 (1990) 275–288. doi:10.1016/S0376-7388(00)85132-7.

[50] A.G. Chmielewski, A. Urbaniak, K. Wawryniuk, Membrane enrichment of biogas from two-stage pilot plant using agricultural waste as a substrate, Biomass and Bioenergy. 58 (2013) 219–228. doi:10.1016/j.biombioe.2013.08.010.

[51] P. Bernardo, E. Drioli, G. Golemme, Membrane gas separation: A review/state of the art, Ind. Eng. Chem. Res. 48 (2009) 4638–4663. doi:10.1021/ie8019032.

[52] P. Dolejš, V. Poštulka, Z. Sedláková, V. Jandová, J. Vejražka, E. Esposito, et al., Simultaneous hydrogen sulphide and carbon dioxide removal from biogas by water–swollen reverse osmosis membrane, Sep. Purif. Technol. 131 (2014) 108–116. doi:10.1016/j.seppur.2014.04.041.

[53] S. Sridhar, R. Suryamurali, B. Smitha, T.M. Aminabhavi, Development of crosslinked poly(ether-block-amide) membrane for CO2/CH4 separation, Colloids Surfaces A Physicochem. Eng. Asp. 297 (2007) 267–274. doi:10.1016/j.colsurfa.2006.10.054.

[54] C.E. Powell, G.G. Qiao, Polymeric CO2/N2 gas separation membranes for the capture of carbon dioxide from power plant flue gases, J. Memb. Sci. 279 (2006) 1–49. doi:10.1016/j.memsci.2005.12.062.

[55] V.I. Bondar, B.D. Freeman, I. Pinnau, Gas sorption and characterization of poly(ether-b-amide) segmented block copolymers, J. Polym. Sci. Part B Polym. Phys. 37 (1999) 2463–2475. doi:10.1002/(sici)1099-0488(19990901)37:17<2463::aid-polb18>3.0.co;2-h.

[56] F. Tasselli, F. Bazzarelli, P. Bernardo, J.C. Jansen, G. Clarizia, PEBAX–based Composite Hollow Fibre Membranes for Gas Separation, Procedia Eng. 44 (2012) 710–711. doi:10.1016/j.proeng.2012.08.540.

[57] K. Kim, P.G. Ingole, J. Kim, H. Lee, Separation performance of PEBAX/PEI hollow fiber composite membrane for SO2/CO2/N2 mixed gas, Chem. Eng. J. 233 (2013) 242–250. doi:10.1016/j.cej.2013.08.030.

[58] X. Ren, J. Ren, H. Li, S. Feng, M. Deng, Poly (amide-6-b-ethylene oxide) multilayer composite membrane for carbon dioxide separation, Int. J. Greenh. Gas Control. 8 (2012) 111–120. doi:10.1016/j.ijggc.2012.01.017.

[59] L. LIU, A. CHAKMA, X. FENG, Preparation of hollow fiber poly(ether block amide)/polysulfone composite membranes for separation of carbon dioxide from nitrogen,

Chem. Eng. J. 105 (2004) 43–51. doi:10.1016/j.cej.2004.08.005.

[60] J. Guo, G. Zhang, W. Wu, S. Ji, Z. Qin, Z. Liu, Dynamically formed inner skin hollow fiber polydimethylsiloxane/polysulfone composite membrane for alcohol permselective pervaporation, Chem. Eng. J. 158 (2010) 558–565. doi:10.1016/j.cej.2010.01.053.

[61] S.H. Choi, F. Tasselli, J.C. Jansen, G. Barbieri, E. Drioli, Effect of the preparation conditions on the formation of asymmetric poly(vinylidene fluoride) hollow fibre membranes with a dense skin, Eur. Polym. J. 46 (2010) 1713–1725. doi:10.1016/j.eurpolymj.2010.06.001.

[62] C. Macosko, Rheology: Principles, Measurements and Applications, 1996. doi:10.1016/S0032-5910(96)90008-X.

[63] F. Tasselli, J.C. Jansen, F. Sidari, E. Drioli, Morphology and transport property control of modified poly(ether ether ketone) (PEEKWC) hollow fiber membranes prepared from PEEKWC/PVP blends: Influence of the relative humidity in the air gap, J. Memb. Sci. 255 (2005) 13–22. doi:10.1016/j.memsci.2005.01.014.

[64] F. Tasselli, J.C. Jansen, E. Drioli, PEEKWC ultrafiltration hollow-fiber membranes: Preparation, morphology, and transport properties, J. Appl. Polym. Sci. 91 (2004) 841–853. doi:10.1002/app.13207.

[65] J.C. Chen, I.R. Harrison, Modification of polyacrylonitrile (PAN) carbon fiber precursor via post-spinning plasticization and stretching in dimethyl formamide (DMF), Carbon N. Y. 40 (2002) 25–45. doi:10.1016/S0008-6223(01)00050-1.

[66] F. Bazzarelli, P. Bernardo, F. Tasselli, G. Clarizia, V.G. Dzyubenko, P. Vdovin, et al., Multilayer composite SBS membranes for pervaporation and gas separation, Sep. Purif. Technol. 80 (2011) 635–642. doi:10.1016/j.seppur.2011.06.025.

[67] B. Al-Shammari, T. Al-Fariss, F. Al-Sewailm, R. Elleithy, The effect of polymer concentration and temperature on the rheological behavior of metallocene linear low density polyethylene (mLLDPE) solutions, J. King Saud Univ. - Eng. Sci. 23 (2011) 9–14. doi:10.1016/j.jksues.2010.07.001.

[68] H.H. Winter, Can the gel point of a crosslinking polymer be detected by the G'-G" crossover?, Polym. Eng. Sci. 27 (1987) 1698–1702. doi:10.1002/pen.760272209.

[69] D.L. Meixner, P.N. Dyer, Characterization of the transport properties of microporous inorganic membranes, J. Memb. Sci. 140 (1998) 81–95. doi:10.1016/S0376-7388(97)00268-8.

[70] J.C. Jansen, M. MacChione, C. Oliviero, R. Mendichi, G. a. Ranieri, E. Drioli, Rheological evaluation of the influence of polymer concentration and molar mass distribution on the formation and performance of asymmetric gas separation membranes prepared by dry phase inversion, Polymer (Guildf). 46 (2005) 11366–11379. doi:10.1016/j.polymer.2005.10.041.

[71] K. Huang, X.-M. Zhang, Y.-X. Li, Y.-T. Wu, X.-B. Hu, Facilitated separation of CO2 and SO2 through supported liquid membranes using carboxylate-based ionic liquids, J. Memb. Sci. 471 (2014) 227–236. doi:10.1016/j.memsci.2014.08.022.

[72] Z. Dai, R.D. Noble, D.L. Gin, X. Zhang, L. Deng, Combination of ionic liquids with membrane technology: A new approach for CO2 separation, J. Memb. Sci. 497 (2016) 1–20. doi:10.1016/j.memsci.2015.08.060.

[73] W.M. McDanel, M.G. Cowan, N.O. Chisholm, D.L. Gin, R.D. Noble, Fixed-site-carrier

facilitated transport of carbon dioxide through ionic-liquid-based epoxy-amine ion gel membranes, J. Memb. Sci. 492 (2015) 303–311. doi:10.1016/j.memsci.2015.05.034.

[74] S. Zhang, N. Sun, X. He, X. Lu, X. Zhang, Physical properties of ionic liquids: Database and evaluation, J. Phys. Chem. Ref. Data. 35 (2006) 1475–1517. doi:10.1063/1.2204959.

[75] C. Cadena, J.L. Anthony, J.K. Shah, T.I. Morrow, J.F. Brennecke, E.J. Maginn, Why Is CO2 So Soluble in Imidazolium-Based Ionic Liquids?, J. Am. Chem. Soc. 126 (2004) 5300–5308. doi:10.1021/ja039615x.

[76] H. Zhao, Methods for stabilizing and activating enzymes in ionic liquids - A review, J. Chem. Technol. Biotechnol. 85 (2010) 891–907. doi:10.1002/jctb.2375.

[77] H. Ying, R.E. Baltus, Experimental measurement of the solubility and diffusivity of CO 2 in room-temperature ionic liquids using a transient thin-liquid-film method, Ind. Eng. Chem. Res. 46 (2007) 8166–8175. doi:10.1021/ie070501u.

[78] L.A. Neves, C. Afonso, I.M. Coelhoso, J.G. Crespo, Integrated CO2 capture and enzymatic bioconversion in supported ionic liquid membranes, Sep. Purif. Technol. 97 (2012) 34–41. doi:10.1016/j.seppur.2012.01.049.

[79] Crank_1975_Diffusion.pdf, (n.d.).

[80] W. Wang, Y. Wu, M. Rong, L. Éhn, I. Černušák, Theoretical computation of thermophysical properties of high-temperature $F_2$, $CF_4$, $C_2F_2$, $C_2F_4$, $C_2F_6$, $C_3F_6$ and $C_3F$, J. Phys. D. Appl. Phys. 45 (2012) 285201. doi:10.1088/0022-3727/45/28/285201.

[81] J.E. Bara, T.K. Carlisle, C.J. Gabriel, D. Camper, A. Finotello, D.L. Gin, et al., Guide to CO 2 Separations in Imidazolium-Based Room-Temperature Ionic Liquids, Ind. Eng. Chem. Res. 48 (2009) 2739–2751. doi:10.1021/ie8016237.

[82] R. Fortunato, M.J. González-Muñoz, M. Kubasiewicz, S. Luque, J.R. Alvarez, C. a M. Afonso, et al., Liquid membranes using ionic liquids: The influence of water on solute transport, J. Memb. Sci. 249 (2005) 153–162. doi:10.1016/j.memsci.2004.10.007.

[83] N.B. McKeown, Polymers of Intrinsic Microporosity, ISRN Mater. Sci. 2012 (2012) 1–16. doi:10.5402/2012/513986.

[84] P.M. Budd, N.B. McKeown, B.S. Ghanem, K.J. Msayib, D. Fritsch, L. Starannikova, et al., Gas permeation parameters and other physicochemical properties of a polymer of intrinsic microporosity: Polybenzodioxane PIM-1, J. Memb. Sci. 325 (2008) 851–860. doi:10.1016/j.memsci.2008.09.010.

[85] J. Ahn, W.-J. Chung, I. Pinnau, J. Song, N. Du, G.P. Robertson, et al., Gas transport behavior of mixed-matrix membranes composed of silica nanoparticles in a polymer of intrinsic microporosity (PIM-1), J. Memb. Sci. 346 (2010) 280–287. doi:10.1016/j.memsci.2009.09.047.

[86] A.F. Bushell, M.P. Attfield, C.R. Mason, P.M. Budd, Y. Yampolskii, L. Starannikova, et al., Gas permeation parameters of mixed matrix membranes based on the polymer of intrinsic microporosity PIM-1 and the zeolitic imidazolate framework ZIF-8, J. Memb. Sci. 427 (2013) 48–62. doi:10.1016/j.memsci.2012.09.035.

[87] A. Karmakar, A. V. Desai, S.K. Ghosh, Ionic metal-organic frameworks (iMOFs): Design principles and applications, Coord. Chem. Rev. (2015). doi:10.1016/j.ccr.2015.08.007.

[88] P. Llewellyn, G. Maurin, J. Rouquerol, Adsorption by Metal-Organic Frameworks,

Elsevier, 2014. doi:10.1016/B978-0-08-097035-6.00014-0.

[89] B. Zornoza, C. Tellez, J. Coronas, J. Gascon, F. Kapteijn, Metal organic framework based mixed matrix membranes: An increasingly important field of research with a large application potential, Microporous Mesoporous Mater. 166 (2013) 67–78. doi:10.1016/j.micromeso.2012.03.012.

[90] E. Adatoz, A.K. Avci, S. Keskin, Opportunities and challenges of MOF-based membranes in gas separations, Sep. Purif. Technol. 152 (2015) 207–237. doi:10.1016/j.seppur.2015.08.020.

[91] O.G. Nik, X.Y. Chen, S. Kaliaguine, Functionalized metal organic framework-polyimide mixed matrix membranes for CO 2/CH 4 separation, J. Memb. Sci. 413-414 (2012) 48–61. doi:10.1016/j.memsci.2012.04.003.

[92] D. Wu, G. Maurin, Q. Yang, C. Serre, H. Jobic, C. Zhong, Computational exploration of a Zr-carboxylate based metal–organic framework as a membrane material for $CO_2$ capture, J. Mater. Chem. A. 2 (2014) 1657–1661. doi:10.1039/C3TA13651E.

[93] H. Jeazet, T. Koschine, C. Staudt, K. Raetzke, C. Janiak, Correlation of Gas Permeability in a Metal-Organic Framework MIL-101(Cr)–Polysulfone Mixed-Matrix Membrane with Free Volume Measurements by Positron Annihilation Lifetime Spectroscopy (PALS), Membranes (Basel). 3 (2013) 331–353. doi:10.3390/membranes3040331.

[94] J.H. Cavka, S. Jakobsen, U. Olsbye, N. Guillou, C. Lamberti, S. Bordiga, et al., A new zirconium inorganic building brick forming metal organic frameworks with exceptional stability, J. Am. Chem. Soc. 130 (2008) 13850–13851. doi:10.1021/ja8057953.

[95] J. Hajek, M. Vandichel, B. Van De Voorde, B. Bueken, D. De Vos, M. Waroquier, et al., Mechanistic studies of aldol condensations in UiO-66 and UiO-66-NH 2 metal organic frameworks, J. Catal. 331 (2015) 1–12. doi:10.1016/j.jcat.2015.08.015.

[96] F. Vermoortele, M. Vandichel, B. Van De Voorde, R. Ameloot, M. Waroquier, V. Van Speybroeck, et al., Electronic Effects of Linker Substitution on Lewis Acid Catalysis with Metal – Organic Frameworks ** Angewandte, Angew. Chem. Int. Ed. Engl. 4 (2012) 4887–4890. doi:10.1002/anie.201108565.

[97] D.Y. Hong, Y.K. Hwang, C. Serre, G. Férey, J.S. Chang, Porous chromium terephthalate MIL-101 with coordinatively unsaturated sites: Surface functionalization, encapsulation, sorption and catalysis, Adv. Funct. Mater. 19 (2009) 1537–1552. doi:10.1002/adfm.200801130.

[98] J.C. Jansen, K. Friess, E. Drioli, Organic vapour transport in glassy perfluoropolymer membranes: A simple semi-quantitative approach to analyze clustering phenomena by time lag measurements, J. Memb. Sci. 367 (2011) 141–151. doi:10.1016/j.memsci.2010.10.063.

[99] G. Ferey, A Chromium Terephthalate-Based Solid with Unusually Large Pore Volumes and Surface Area, Science (80-. ). 309 (2005) 2040–2042. doi:10.1126/science.1116275.

[100] Q. Yang, A.D. Wiersum, P.L. Llewellyn, V. Guillerm, C. Serre, G. Maurin, Functionalizing porous zirconium terephthalate UiO-66(Zr) for natural gas upgrading: a computational exploration., Chem. Commun. (Camb). 47 (2011) 9603–9605. doi:10.1039/c1cc13543k.

[101] S. a. Hashemifard, a. F. Ismail, T. Matsuura, A new theoretical gas permeability model using resistance modeling for mixed matrix membrane systems, J. Memb. Sci. 350 (2010) 259–268. doi:10.1016/j.memsci.2009.12.036.

[102] E. V. Perez, K.J. Balkus, J.P. Ferraris, I.H. Musselman, Mixed-matrix membranes containing MOF-5 for gas separations, J. Memb. Sci. 328 (2009) 165–173. doi:10.1016/j.memsci.2008.12.006.

[103] T.-S. Chung, L.Y. Jiang, Y. Li, S. Kulprathipanja, Mixed matrix membranes (MMMs) comprising organic polymers with dispersed inorganic fillers for gas separation, Prog. Polym. Sci. 32 (2007) 483–507. doi:10.1016/j.progpolymsci.2007.01.008.

[104] R. Mahajan, W.J. Koros, Factors Controlling Successful Formation of Mixed-Matrix Gas Separation Materials, Ndustrial Eng. Chem. Res. 39 (2000) 2692–2696. doi:10.1021/ie990799r.

[105] T.T. Moore, W.J. Koros, Non-ideal effects in organic–inorganic materials for gas separation membranes, J. Mol. Struct. 739 (2005) 87–98. doi:10.1016/j.molstruc.2004.05.043.

[106] K. Althumayri, W.J. Harrison, Y. Shin, C. Casiraghi, P.M. Budd, P. Bernardo, et al., Article Title : The influence of few-layer graphene on the gas permeability of the high-free-volume polymers of intrinsic microporosity-1, Phil. Trans. R. Soc. . A 20150031 (n.d.) in press. doi:10.1098/rsta.2015.0031.

[107] A.J. Hill, S.J. Pas, T.J. Bastow, M.I. Burgar, K. Nagai, L.G. Toy, et al., Influence of methanol conditioning and physical aging on carbon spin-lattice relaxation times of poly(1-trimethylsilyl-1-propyne), J. Memb. Sci. 243 (2004) 37–44. doi:10.1016/j.memsci.2004.06.007.

[108] L.M. Robeson, Correlation of separation factor versus permeability for polymeric membranes, J. Memb. Sci. 62 (1991) 165–185. doi:10.1016/0376-7388(91)80060-J.

[109] L.M. Robeson, The upper bound revisited, J. Memb. Sci. 320 (2008) 390–400. doi:10.1016/j.memsci.2008.04.030.

[110] R.W. Baker, K. Lokhandwala, Natural Gas Processing with Membranes: An Overview, Ind. Eng. Chem. Res. 47 (2008) 2109–2121. doi:10.1021/ie071083w.

# Acknowledgements

**Chapter. 3.** The work leading to these results has received funding from the Italian national research program "Programma Operativo Nazionale Ricerca e Competitività 2007-2013, project PON01_01840 MicroPERLA". The financial support from the Czech Science Foundation by the project No. 14-12695S is also acknowledged. Dr. C. Cantoni (Arkema, Italy) is gratefully acknowledged for providing the Pebax®1657 samples. F. Lupi and D. Gabriele are gratefully acknowledged for their assistance with rheological experiments.

**Chapter. 4.** The work leading to these results has received funding from the University of Calabria, International mobility program, "Fondi 5 per mille".

**Chapter. 5.** Prof. Peter Budd and Muhanned Khdhayyer of the University of Manchester are gratefully acknowledged for providing the mixed matrix membranes

# Personal Acknowledgements

I came to the end of this long and exciting journey and as the end of a long trip, I look back and I realize that there are many people who have come into my life in these three years. To all of you, and forgive me if I do not mention one by one a sincere thanks.

I would like to say thanks to Dr. Lidietta Giorno for giving me the opportunity to carry out my PhD thesis at the ITM-CNR, point of excellence at international level, where I could compare myself with great minds and guys from around the world, teaching me that when the reason to drive an idea, no matter the place of origin or their religion. The "other" becomes a value added and differences can coexist in a dynamic and harmonious way.

Thanks to Dr. Jansen for his daily presence, for his teachings, for help me to grow professionally and to stimulate and encourage me to exceed my limits.

Thanks also to Prof. Curcio for its expertise and its continued availability.

Thank to Eng. P. Bernardo, Eng. G. Clarizia and Dr. Tasselli for having followed in these three years and for their constant teachings.

Thanks also to Prof. J. Crespo and Prof. I. Coelhoso for giving me the opportunity to spend part of my PhD at the Universidade de Lisboa. Thanks for putting at my disposal your knowledge.

I would like to say a big thanks to Ing. Carla Martins for its preparation, for his patience and for the comprehension… that's not all! Thanks for the tips, advice and above all for the immense laughter between a cigarette and the other ☺

I would like to say thanks to my fellow travelers, thanks Mariella for sharing joys and pains "Portuguese";

But, above all, thanks to Gisella unsurpassed friend and roommate. Thank you for having relieved the "saudade" of home with a good bottle of wine and a piece of Parmigiano cheese. Thanks for the songs that we sing with out loud, for sharing with me and Romeo your bed in the cold Lisbon nights... I love you and I'll always love you.

Speaking of friends, I must thank Giulia and Serena, they are my constant "... cause it never Began for us

It'll never end for us ... "

Thanks to Valentina, for your sincerity and spontaneity, for having supported me in difficult times, let me never abandoned.

Thanks to all my friends of Fagnano, sorry if I do not appoint one by one, but know that you are my safe haven where I can always take refuge with all my weaknesses and follies.

Now comes the hard part ...

Thanks to my parents for conveying to me the important values such as honesty and humility, thank you for your sacrifices that have allowed me to achieve all my aspiration. Thanks for teaching me that happiness lies in small things...

Thanks to my sister Enrica and my brother in law Giulio, thank you for your continued support, for your advice in the worst moments of affliction, thanks to keep always me close to you, I love you.

And finally, I would like to thank myself, that I do not ever give up and I accept ever new challenges. Thanks to my rational part and to my being "tramp" that prefers the trees and caves respect to the tables and chairs because is the way to rest close to the cheek of God.

# Ringraziamenti

Sono giunta alla fine di questo lungo e avvincente percorso e come alla fine di ogni lungo viaggio volgo lo sguardo su ciò che è stato e mi accorgo che molte sono le persone che sono entrate nella mia vita e mi hanno accompagnato in questi tre anni. A tutti voi e mi perdonerete se non vi citerò uno per uno va un sentito grazie.

Inizio con il rivolgere un sentito grazie alla Gent.ma Dottoressa Lidietta Giorno per avermi concesso la possibilità di svolgere la mia tesi di Dottorato presso l'ITM-CNR punto di eccellenza a livello internazionale, luogo in cui ho potuto confrontarmi con menti eccelse e ragazzi provenienti da tutto il mondo, insegnandomi che quando è la ragione a guidare un'idea, non ha importanza il luogo di provenienza o la propria religione. Il "diverso" diventa un valore aggiunto e le differenze possono coesistere in modo dinamico e armonioso.

Desidero ringraziare il Dott. Jansen per la sua quotidiana presenza, per i suoi insegnamenti, per avermi stimolato a crescere professionalmente e incoraggiata a superare i miei limiti.

Un ringraziamento va anche al Prof. Curcio per le sue competenze e la sua continua disponibilità.

Ringrazio l'Ing. P. Bernardo, l'Ing. G. Clarizia e il Dott. Tasselli per avermi seguita in questi tre anni e per i loro costanti insegnamenti.

Grazie anche al Prof. J. Crespo e alla Prof.ssa I. Coelhoso per avermi concesso la possibilità di trascorrere parte del mio dottorato presso l'Universidade de Lisboa. Grazie per aver messo a mia completa disposizione le vostre conoscenze.

Voglio dire un enorme grazie all'Ing. Carla Martins per la sua preparazione, per la sua grande pazienza e comprensione…non è tutto! Grazie per i suggerimenti, i consigli e soprattutto per le immense risate tra una sigaretta e l'altra ☺.

Un sentito grazie va ai miei compagni di viaggio, grazie Mariella per aver condiviso gioie e dolori alla "portoghese";

Ma soprattutto grazie a Gisella insuperabile amica e coinquilina. Grazie per aver alleviato le nostalgie di casa con una buona bottiglia di vino e un pezzo di parmigiano. Grazie per le canzoni gridate a squarciagola, per aver condiviso con me e Romeo il tuo lettino nelle freddi notti di Lisbona, figuracce, ma anche esperienze veramente indimenticabili…ti voglio bene e te ne vorrò sempre.

A proposito di amiche devo ringraziare Giulia e Serena, siete le mie costanti "…cause it never began for us

It'll never end for us…"

Grazie a Valentina, per la tua sincerità e spontaneità, per avermi sostenuta nei momenti più difficili, per non avermi abbandonata mai.
Grazie a tutti i miei amici di Fagnano, scusate se non vi nomino uno per uno, ma sappiate che siete il mio porto sicuro dove posso sempre rifugiarmi con tutte le mie debolezze e follie.
Ora arriva la parte più difficile…
Grazie ai miei genitori per avermi trasmesso valori importanti come l'onestà e l'umiltà, grazie per i vostri sacrifici che mi hanno permesso di realizzare ogni mia aspirazione. Grazie per avermi insegnato che la felicità sta nelle piccole cose…
Grazie a mia sorella Enrica e a mio cognato Giulio, grazie per il continuo sostegno, per i vostri consigli nei momenti di peggiore sconforto, grazie per essermi sempre vicini, vi voglio bene.
E infine voglio ringraziare me stessa, che non mi arrendo mai e non mi do mai per vinta accettando ogni nuova sfida. Grazie alla mia parte razionale e al mio essere "vagabondo" che alle tavole e alle sedie preferisce gli alberi e le caverne perché lì sento di potermi poggiare alla guancia di Dio.